

**THE IMPACT OF BIOCHAR SURFACE PROPERTIES ON SAND AND ON  
SANDY LOAM REGARDING WATER REPELLENCY, WATER RETENTION,  
AND GAS TRANSMISSIVITY**

by

Susan Chin Yi

A dissertation submitted to the Faculty of the University of Delaware in partial fulfillment of the requirements for the degree of Doctor of Philosophy in Civil Engineering

Spring 2018

© 2018 Susan Yi  
All Rights Reserved

**THE IMPACT OF BIOCHAR SURFACE PROPERTIES ON SAND AND ON  
SANDY LOAM REGARDING WATER REPELLENCY, WATER  
RETENTION, AND GAS TRANSMISSIVITY**

by

Susan Chin Yi

Approved: \_\_\_\_\_  
Sue McNeil, Ph.D.  
Chair of the Department of Civil & Environmental Engineering

Approved: \_\_\_\_\_  
Babatunde Ogunnaike, Ph.D.  
Dean of the College of Engineering

Approved: \_\_\_\_\_  
Ann L. Ardis, Ph.D.  
Senior Vice Provost for Graduate and Professional Education

I certify that I have read this dissertation and that in my opinion it meets the academic and professional standard required by the University as a dissertation for the degree of Doctor of Philosophy.

Signed:

---

Paul T. Imhoff, Ph.D.  
Professor in charge of dissertation

I certify that I have read this dissertation and that in my opinion it meets the academic and professional standard required by the University as a dissertation for the degree of Doctor of Philosophy.

Signed:

---

Pei Chiu, Ph.D.  
Member of dissertation committee

I certify that I have read this dissertation and that in my opinion it meets the academic and professional standard required by the University as a dissertation for the degree of Doctor of Philosophy.

Signed:

---

Mingxin Guo, Ph.D.  
Member of dissertation committee

I certify that I have read this dissertation and that in my opinion it meets the academic and professional standard required by the University as a dissertation for the degree of Doctor of Philosophy.

Signed:

---

Yan Jin, Ph.D.  
Member of dissertation committee

## ACKNOWLEDGMENTS

I am personally grateful to Dr. Imhoff, my advisor, for giving me the opportunity to obtain a doctorate under him, for his consistent mentoring, advice, his brilliant suggestions, and patience. I appreciate all the feedback and his exceptional mentorship during my doctorate studies. I hope to emulate the valuable skills I've learned.

I also thank my dissertation committee members: Dr. Pei Chiu for helping with my first manuscript and sharing his insights, Dr. Mingxin Guo for contributing his biochar knowledge and research supplies, and Dr. Yan Jin for sharing her ideas regarding soil mechanisms and their physical properties. I would also like to acknowledge Dr. Bob Hill from the University of Maryland for lending me his instruments. Without Dr Hill's help, obtaining critical data for chapter 3 would have been impossible.

My personal gratitude is sent to Dr. Rovshan Mahmudov and Michael Davidson with their help and sharing their technical expertise, and the friends I made during the PhD program: Dr. Erfan Mostafid, Dr. Solmaz Marzooghi, Inyoung Kim, Dr. Soohoon Choi, and Dr. Minho Maeng.

I would like to show my great appreciation to the United States Department of Education for the financial support through the Graduate Assistance in Areas of National Need (GAANN) fellowship and other scholarships awarded to me during my entire academic career to achieve these pursuits. I also like to thank all the people in the past and now who kept on encouraging me to continue with academia.

Lastly, I would like express my love and gratitude to my family members: my brother Dr. Woong Yi and my lovely mother Myong Hee Youn. Thank you for

everything. Best of all, thank you for teaching me how to overcome all obstacles in life. I will always remember to be healthy, happy, and always have gratitude as I live my life.

## TABLE OF CONTENTS

LIST OF TABLES .....	x
LIST OF FIGURES .....	xi
ABSTRACT.....	xv

### Chapter

1	INTRODUCTION .....	1
1.1	Significance of Work .....	1
1.2	Dissertation outline .....	2
2	THE ORIGIN AND REVERSIBLE NATURE OF POULTRY LITTER BIOCHAR HYDROPHOBICITY .....	5
2.1	Background .....	5
2.2	Materials and Methods.....	8
2.2.1	Poultry litter biochar production.....	8
2.2.2	Hypothesis testing with poultry litter biochar pyrolyzed at 400°C .....	8
2.2.3	Effect of pyrolysis temperature.....	10
2.2.4	Effect of contact time with water.....	10
2.2.5	Rinsate analyses .....	11
2.2.6	Effect of mixing with sand.....	12
2.3	Results and Discussion .....	13
2.3.1	Post-treatment effects on poultry litter biochar hydrophobicity ..	13
2.3.2	Effect of pyrolysis temperature.....	14
2.3.3	Effect of contact time with water.....	15
2.3.4	Rinsate analyses .....	17
2.3.5	Effect of mixing with sand.....	20
2.4	Conclusions and Implications .....	22

3	SOIL-WATER RETENTION CURVE MODELS FOR BIOCHAR AMENDED SOILS .....	30
3.1	Background.....	30
3.2	Theory.....	35
3.2.1	Intrapore adsorbed and capillary water ( $pF > 3.85$ ) .....	35
3.2.2	Intrapore water ( $pF < 3.85$ ).....	36
3.2.3	Interpore water .....	37
3.2.4	Models for water retention in biochar-amended media .....	42
3.3	Materials and Methods.....	43
3.3.1	Biochars .....	43
3.3.2	Biochar particle density, surface area, and intrapore volume .....	45
3.3.3	Particle-size distribution .....	46
3.3.4	Intrapore adsorbed and capillary water ( $pF > 3.85$ ) .....	46
3.3.5	Interpore capillary water ( $pF < 3.85$ ).....	48
3.4	Results & Discussion .....	49
3.4.1	Particle density.....	49
3.4.2	Biochar specific surface area .....	50
3.4.3	Biochar intrapore volume .....	50
3.4.4	Particle size distribution.....	51
3.4.5	Porosity .....	52
3.4.6	Water retention $pF > 3.85$ .....	53
3.4.7	Soil water characteristic.....	55
3.4.7.1	PLBC in sand .....	55
3.4.7.2	SRBC in sand.....	56
3.4.7.3	PLBC in sandy loam .....	57
3.4.7.4	SRBC in sandy loam.....	58
3.4.7.5	Available water capacity.....	59
3.5	Conclusions.....	60
4	THE EFFECTS OF BIOCHAR ON GAS TRANSPORT IN VARIABLY SATURATED SAND AND SANDY LOAM SOIL.....	76
4.1	Background.....	76
4.2	Materials and Methods.....	80
4.2.1	Sample preparation .....	80

4.2.2	Air-filled porosity .....	83
4.2.3	Gas diffusion .....	85
4.2.4	Gas diffusion models .....	87
4.2.5	Air permeability .....	90
4.2.6	Statistical analysis of gas diffusion.....	91
4.3	Results & Discussion .....	92
4.3.1	Air-filled porosity .....	92
4.3.2	Biochar intrapores .....	93
4.3.3	Gas diffusion.....	95
4.3.4	Gas diffusion models .....	98
4.3.5	Gas permeability .....	104
4.4	Conclusions.....	105
5	FUTURE WORK.....	117
5.1	Biochar on soil-water repellency .....	117
5.2	Biochar impact on soil-water retention.....	119
5.3	Biochar impact on soil-gas transport .....	120
	REFERENCES .....	121
Appendix		
A	THE ORIGIN AND REVERSIBLE NATURE OF POULTRY LITTER BIOCHAR HYDROPHOBICITY.....	138
A-1	Properties of poultry litter.....	139
A-2	Contact angle stability .....	140
A-3	Effect of leached compounds on air-water interfacial tension .....	142
A-4	Rinsate analyses.....	145
B	SOIL-WATER RETENTION CURVE MODELS FOR BIOCHAR AMENDED SOILS .....	151
B-1	Sample information and uncertainty.....	152
B-2	Total water potential of WP4C and osmotic potential.....	155
B-3	Biochar SEM images .....	158
B-4	Soil water retention data .....	159
B-4	Nomenclature .....	163
B-5	Arya model derivation .....	165
B-6	SWRC Model.....	169

C	THE EFFECTS OF BIOCHAR ON GAS TRANSPORT IN VARIABLY SATURATED SAND AND SANDY LOAM SOIL.....	170
	C-1 Schematic of diffusion apparatus.....	171
	C-2 Schematic of air permeability apparatus.....	173
	C-3 Photographs of biochars.....	174
D	PERMISSIONS.....	175

## LIST OF TABLES

Table 2-1: Water drop penetration time of poultry litter and fresh and treated poultry litter biochar produced at 400°C.....	24
Table 3-1: Biochar specific surface area, intrapore volume, intrapore air-entry pressure, and biochar densities .....	63
Table 3-2: Porosities and dry bulk density of samples with different biochar mass fractions .....	64
Table 3-3: Root-mean-square errors of biochar water retention models .....	65
Table 4-1: Summary of air-filled porosities and dry bulk density of samples.....	108
Table 4.2: Root mean square error (RMSE) of gas diffusion models evaluated using total porosity and the fitted parameters.....	109
Table 4-3: Root mean square error (RMSE) of gas diffusion models evaluated using interpore porosity and the fitted parameters .....	110
Table A1: Properties of poultry litter prior to pyrolysis <sup>a</sup> .....	139
Table A2: Air-water interfacial tensions of water solutions mixed with PLBC400 and t-test results .....	144
Table A3: Properties of water extractable organic carbons detected from PLBC300 rinsate using GC-MS .....	147
Table A4: Properties of water extractable organic compounds from PLBC600 rinsate using GC-MS .....	148
Table B1: The number of data collected per individual sample using WP4C to obtain water sorption data.....	152
Table B2: Estimates of uncertainty of biochar in sand samples used in soil-water retention characteristic curves .....	153
Table B3: Estimates of uncertainty of biochar in sandy loam (SL) samples used in soil-water retention characteristic curves .....	154

## LIST OF FIGURES

Figure 2-1: Mean contact angles (CAs) of poultry litter biochar (PLBCs) produced at varying pyrolysis temperatures. Error bars represent $\pm 1$ SEM. Mean CA for sand shown with upper and lower bound of the SE of the sample mean. Relative humidity, $17.4 \pm 0.42\%$ ; temperature, $20.5^\circ\text{C}$ .	25
Figure 2-2: Mean contact angles of poultry litter biochar at $300^\circ\text{C}$ (PLBC300) and heated PLBC300 at $105^\circ\text{C}$ for 12 h (HT-PLBC300) after they were submerged in deionized water for different times. Error bars represent $\pm 1$ SEM. Relative humidity, $54.8 \pm 2.9\%$ ; temperature, $21.0^\circ\text{C}$ .	26
Figure 2-3: Total organic carbon (TOC) leached from poultry litter biochar (PLBC) produced at $300^\circ\text{C}$ and $600^\circ\text{C}$ when rinsed in deionized (DI) water at 1:200 solid to liquid mass ratio for 24 h (PLBC300 and PLBC600, respectively). Error bars represent $\pm 1$ SEM.	27
Figure 2-4: Mean contact angles of poultry litter biochar (PLBC)–sand mixtures (w/w) for PLBC pyrolyzed at 300 (PLBC300), 350 (PLBC350), and $600^\circ\text{C}$ (PLBC600). Error bars represent $\pm 1$ SEM. Relative humidity, $17.7 \pm 1.5\%$ ; temperature, $20.3^\circ\text{C}$ .	28
Figure 2-5: Surface geometry of (a) sand, (b) poultry litter biochar (PLBC) pyrolyzed at $300^\circ\text{C}$ (PLBC300), (c) PLBC at $350^\circ\text{C}$ (PLBC350), and (d) PLBC at $600^\circ\text{C}$ (PLBC600). All particles collected between #30 (0.595mm opening) and #35 sieves (0.5-mm opening).	29
Figure 3-1: Intrapore volumes from mercury intrusion porosimetry: (a) cumulative intrapore volumes from duplicate measurements of poultry litter biochar (PLBC) (●/○) or Soil Reef™ biochar (SRBC) (■/□), where $pF$ for mercury-air system are converted to $pF$ for air-water system; and (b) pore volume distribution of PLBC and SRBC.	66
Figure 3-2. Particle size distribution by mass (a, b) and volume (c, d) of PLBC in sandy loam (SL) and SRBC in sandy loam at 2% and 7% by weight, respectively.	67

Figure 3-3. Water sorption data for biochar: (a) total and matric potential measurements for PLBC, and (b) total potential measurements for SRBC where osmotic effects were negligible. ....	68
Figure 3-4. Water sorption data for PLBC/sediment mixtures and model predictions: (a) 2 and 7% (w/w) PLBC in sand, (b) 2% PLBC in sandy loam (SL), and (c) 7% (w/w) PLBC in SL. Solid lines in (b) and (c) are best-fits to SL data. ....	69
Figure 3-5. Water sorption data for SRBC/sediment mixtures and model predictions: (a) 2 and 7% (w/w) SRBC mixtures in sand, (b) 2% SRBC in sandy loam (SL), and (c) 7% (w/w) SRBC in SL. Solid lines in (b) and (c) are best-fits to SL data. ....	70
Figure 3-6. Soil water retention data and model predictions for mixtures of PLBC and sand. Data collected from tension table (TT), pressure plate extractor (PPE), or dew point tensiometer (WP4C). (a) Model 1, reference soil; (b) Model 2, reference soil + intrapores $pF > 3.85$ ; and (c) Model 3, reference soil + all intrapores.....	71
Figure 3-7. Soil water retention data and model predictions for mixtures of SRBC and sand. (a) Model 1, reference soil; (b) Model 2, reference soil + intrapores $pF > 3.85$ ; and (c) Model 3, reference soil + all intrapores. ..	72
Figure 3-8. Soil water retention data and model predictions for mixtures of PLBC and SL. (a) Model 1, reference soil; (b) Model 2, reference soil + intrapores $pF > 3.85$ ; and (c) Model 3, reference soil + all intrapores; and (d) Model 4, reference soil + all intrapores + changes in interpores.	73
Figure 3-9. Soil water retention data and model predictions for mixtures of SRBC and SL. (a) Model 1, reference soil; (b) Model 2, reference soil + intrapores $pF > 3.85$ ; and (c) Model 3, reference soil + all intrapores; and (d) Model 4, reference soil + all intrapores + changes in interpores.	74
Figure 3-10. Average measured and model-predicted changes in available water capacity with biochar addition. ....	75

- Figure 4-1: Mercury intrusion porosimetry and water retention data from Chapter 3 were used to plot % water filled in intrapores and the volumetric water content (VWC) of the intrapores (in red) as a function of total air-filled porosity in (a) for sand mixtures and (c) for sandy loam (SL) mixtures. The % water filled in intrapores and the VWC are plotted as a function of pressure ( $pF = -\log |h, cm-H_2O|$ ) in (b) for sand mixtures and in (d) for SL mixtures. Sand and sandy loam were not plotted since they were assumed to have negligible intrapores. .... 111
- Figure 4-2: Relative gas diffusivity ( $D_p/D_o$ ) as a function of total air-filled porosity ( $\epsilon$ ) where (a) includes sand mixtures, and (c) is of mixtures in sandy loam (SL). The plots  $D_p/D_o$  as a function of air-filled porosity from interpores ( $\epsilon^{inter}$ ) are shown in (b) for sand mixtures and in (d) for SL mixtures. Plots (a) and (c) show the % porosity contribution from interpores of PLBC and SRBC mixtures in red. .... 112
- Figure 4-3: Relative gas diffusivity ( $D_p/D_o$ ) as a function of total air-filled porosity ( $\epsilon$ ) where plots are of: (a) Sand, (b) 7% PLBC-Sand, (c) 7%SRBC-Sand, (d) sandy loam, (e) 7%PLBC-SL, and (f) 7%SRBC-SL. The lines are the comparison of the Buckingham model, Penman-Call (PC) model, Millington-Quirk (MQ) model, Penman-Millington-Quirk (PMQ) model, and the Variable Inactive Pore Space (VIPS) model. .... 113
- Figure 4-4: Relative gas diffusivity ( $D_p/D_o$ ) as a function of air-filled porosity from interpores ( $\epsilon^{inter}$ ) where the plots are: (a) 7% PLBC-Sand, (b) 7%SRBC-Sand, (c) 7%PLBC-SL, and (d) 7%SRBC-SL. The lines are the comparison of the Buckingham model, Penman-Call (PC) model, Millington-Quirk (MQ) model, Penman-Millington-Quirk (PMQ) model, and the Variable Inactive Pore Space (VIPS) model. .... 114
- Figure 4-5: Fitted Archie's law model plots of relative gas diffusivity ( $D_p/D_o$ ) as a function of total air-filled porosity ( $\epsilon$ ) in (a) for sandy loam, (b) for 7%PLBC-SL, and (d) for 7%SRBC-SL. Plots of  $D_p/D_o$  as a function air-filled porosity from interpores ( $\epsilon^{inter}$ ) are in (c) for 7%PLBC-SL and (e) for 7%SRBC-SL. Sand mixtures were not plotted since the particle size distribution was not affected. .... 115
- Figure 4-6: Plots of gas permeability ( $k_a$ ) as a function of total air-filled porosity ( $\epsilon$ ) in (a) for sand mixtures, and (c) for sandy loam (SL) mixtures. The gas permeability plotted as a function of air-filled porosity from intrapores ( $\epsilon^{inter}$ ) are in (b) for sand mixtures, and in (d) for sandy loam mixtures. Vertical lines indicate logarithmic intrapore air-entry pressure for PLBC (black line) and SRBC (red dotted line). .... 116

Figure A1: Time-dependent contact angle of water droplets place on PLBC300 and PLBC600. ....	141
Figure A2: FTIR spectra of water extractable compounds from PLBC at 300°C (PLBC300), PLBC at 300°C heated for 12 h at 105°C (HT-PLBC300), and PLBC at 600°C (PLBC600). Highlighted region is spectral region 2800 - 3020 cm <sup>-1</sup> . ....	149
Figure A3: Baseline corrected GCMS spectrogram of water extractable organic compounds from biochar produced at pyrolysis temperatures 300°C and 600°C (PLBC300 and PLBC600, respectively). Peaks below the absorbance of 3000 were ignored for chemical identification. ....	150
Figure B1: (a) Total water potential versus gravimetric moisture content (MC) of PLBC. Solid line indicates where osmotic effects dominate total potential. (b) PLBC data linearly regressed for MC > 0.40. (c) Corrected water potential of PLBC for $pF > 3.85$ at MC < 0.3. ....	157
Figure B2: SEM images of rinsed PLBC (a, b, and c) and SEM images of rinsed SRBC (d, e, and f). ....	158
Figure B3: Soil water retention data and Model 3 prediction of PLBC in Sand at 2% and 7% ....	159
Figure B4: Soil water retention data and Model 3 prediction of SRBC in Sand at 2% and 7% ....	160
Figure B5: Soil water retention data and Model 4 prediction of PLBC in sandy loam (SL) at 2% and 7% ....	161
Figure B6: Soil water retention data and Model 4 prediction of SRBC in sandy loam (SL) at 2% and 7% ....	162
Figure C1: Schematic of diffusion apparatus. ....	171
Figure C2: Schematic of diffusion apparatus intact. ....	172
Figure C3: Schematic of air permeability apparatus intact. ....	173
Figure C4: Photographs of rinsed and sieved biochars where (a) is poultry litter biochar (PLBC) and (b) is Soil Reef biochar (SRBC). ....	174

## ABSTRACT

Biochar is a carbon-rich material produced from heating biomass in an anoxic environment and used as a soil amendment. Biochar amendment to soils has shown many added benefits. It can reduce greenhouse gas emissions, increase soil fertility, reduce stormwater runoff, enhance soil-microbial activities, and mitigate soil contamination. Furthermore, the carbon in biochar is environmentally recalcitrant and may persist in soils for hundreds to thousands of years, providing an alternative soil carbon sequestration strategy.

Because of these recognized benefits, the interest in using biochar for soil reclamation and soil fertility enhancement has been rising over the past decade. This then requires a better understanding of the effects of biochar on soil properties to optimize their use. Delineating the influence of biochar on soil physical properties will facilitate modeling efforts and provide a strategy to expediently assess soil property changes in large-scale biochar applications. Therefore, experiments were conducted to elucidate the effects of biochar amendment to sand and sandy loam on water repellency, water retention, and gas transmissivity.

In Chapter 2, the effects of biochar amendment on soil water repellency was investigated using poultry litter biochar (PLBC) in a series of experiments testing the existence, persistence, and the solubility of organics covering the PLBC surfaces. The hydrophobicity of PLBCs produced at pyrolysis temperatures ranging from 300-600°C was characterized by measuring the contact angle with deionized water. Results showed

that the hydrophobicity of PLBC increased with increasing pyrolysis temperature. The biochars that were the most and the least hydrophobic were then tested to confirm the hypothesis that organic vapors condensed on biochar surfaces during pyrolysis caused biochar hydrophobicity. Furthermore, the chapter shows PLBC surface roughness contributed to a measurable contact angle that may impart hydrophobic characteristics to mixtures with sand at 2 – 5 % mass biochar amendment rates.

The experiments discussed in Chapters 3 and 4 were then conducted using PLBC produced from 300°C and commercially available Soil Reef™ pinewood-derived biochar (SRBC). The biochars were rinsed, oven-dried, and sieved to ~0.545 mm to reduce the impact of organic vapor coatings on biochar particles that may complicate the results of water retention and gas transmissivity experiments. The effects of post-treated biochars (PLBC and SRBC) were then assessed on sand and sandy loam at variable saturation conditions to identify the mechanisms responsible for altering soil-water retention and gas transport.

In Chapter 3, a predictive model, based on particle pore spaces (pores between the particles and pores within biochar) and adsorption onto particles, was developed and tested for the sand and sandy loam receiving 2 and 7% by mass of either PLBC or SRBC amendment.

The last set of experiments in Chapter 4 evaluated the gas transport parameters, gas diffusivity ( $D_p/D_o$ ) and air-permeability ( $k_a$ ), of sand and sandy loam at variable saturated conditions with 7% by mass biochar amendment. Both biochars were post-treated PLBC and SRBC. Biochar increased gas diffusion in sandy loam, but not in sand. However, biochar did decrease air-permeability in both sand and sandy loam.

## Chapter 1

### INTRODUCTION

#### 1.1 Significance of Work

Biochar production and its application to agricultural soils is gaining interest from several sectors of society in both developing and developed countries [Lehmann, 2007; Lehmann and Joseph, 2009; Lehmann et al., 2011]. Past studies have shown that biochar can sequester carbon and reduce greenhouse gas emissions [Clough et al., 2010; Rogovska et al., 2011], increase soil pH [Zhang et al., 2010], and improve crop production [Lehmann et al., 2011]. Furthermore, studies have suggested biochar's role in removing heavy metals from the environment [Lehmann and Joseph, 2009; Singh et al., 2010a; Beesley et al., 2011; Cao et al., 2011; Fellet et al., 2011; Uchimiya et al., 2012]. Converting biomass residues to biochar can additionally reduce landfill wastes and provide energy sources through the production of bio-oils and syngas [Laird et al., 2009; Nanda et al., 2013]. Biochars are useful in society and may solve many resource-related issues.

Biochar is a carbon-enriched black solid material produced by heating biomass under anoxic conditions. When biochar is added to soils, physical, chemical, and biological interactions occur through which the overall soil quality is generally improved [Lehmann and Joseph, 2009; Pereira et al., 2011]. Biochar properties and the soil improvement effects are dependent on the parent material of the biochar, pyrolysis conditions, especially temperature [Ahmad et al., 2012; Kinney et al., 2012; Song and Guo, 2012], soil properties [Luz Cayuela et al., 2013], and environmental conditions

[*Joseph et al.*, 2010; *Singh et al.*, 2010b]. Because of the number of influencing factors and their complex interactions, a scientific understanding of the effects biochar has on soil is currently limited, particularly regarding soil property improvements in unsaturated regions.

Natural soil exchanges gases with the atmosphere and interacts with water and microorganisms. Various soil properties affect the transport of fluids and contaminants in the subsurface. Because biochar amendment alters soil by introducing new components, it is necessary to evaluate and quantify the physiochemical changes of biochar-amended soil. Understanding biochar-soil interactions will determine large-scale agricultural and environmental implications.

Hence, the goal of this thesis research was to understand the underlying soil processes in the variably saturated regions of biochar-amendment soils, with a focus on soil water repellency, soil water retention, and gas transport.

## **1.2 Dissertation outline**

In Chapter 2, a study is reported that describes the role of biochar on soil water repellency; it is important to establish this relationship due to soil water repellency's influence on hydrology, geomorphology, and soil erosion [*Wallis et al.*, 1993; *Doerr et al.*, 2000; *Bauters et al.*, 2000a; *Arye et al.*, 2007]. Soil water repellency is an issue in natural systems. Soil infiltration rates are generally altered in response to changes in water repellency. Water repellent soils can enhance overland flow [*Savage*, 1974], promote preferential flow patterns that allow faster transport of contaminants through the subsurface [*Granged et al.*, 2011], and impact agricultural production [*Doerr et al.*, 2000].

Soil water repellency is a dynamic phenomenon often related to organic matter interacting with water molecules, where the attraction between solid and liquid phase is weak [Leelamanie and Karube, 2007]. If attraction between air and water exceeds that between solid and water, repellency occurs [Israelachvili, 1991]. This phenomenon affects both soil hydraulic and soil gas properties [Jury *et al.*, 1991].

Soil water behavior is often understood at macroscopic scales based on soil water content and matric potential; however, soil water behavior is controlled by microscopic and pore scale processes that are often overlooked in numerical models and up-scaling procedures [Jury *et al.*, 1991; Diamantopoulos *et al.*, 2013]. Because of the potential impact of biochar on soil water repellency and the importance of soil water repellency in affecting soil hydrology, the effects of poultry litter biochar on soil water repellency were explored and the work is presented in Chapter 2.

Chapter 3 is a study of biochar's impact on soil water retention. Soil water retention plays a significant role in the environment, as it drives many environmental processes. It is a major soil hydraulic property that is important in many disciplines, e.g., agronomy, climatology, hydrology, ecology, and environmental engineering [Rawls *et al.*, 2003]. Soil water retention controls the amount of water available for plants and soil microbes. Soil water can also influence soil thermal energy and heat capacity [Bear *et al.*, 1991] and determine vapor exchange with the atmosphere [Conklin, 2005]. The amount of water retained in soil affects transport of contaminants in the subsurface [Liu and Bodvarsson, 2001] and atmospheric greenhouse gas emissions from soils [Moldrup *et al.*, 2005b]. The soil water characteristic curve (SWC) is used to describe soil water retention as a function of soil water pressure or matric potential and is used in models for soil strength and air permeability [Rajkai *et al.*,

2004]. Hence, SWCs of soils amended with biochar were measured and a model was developed to help understand the impact of biochar on water retention and the mechanisms causing changes in water retention. This work is described in Chapter 3.

Chapter 4 describes work evaluating how gas flow and gas diffusion change with biochar amendment. It is accepted that biochars often promote microbial activities that reduce greenhouse gas (GHG) emissions [Spokas *et al.*, 2012b]. To understand gas flux in biochar-amended soils, the effective diffusion coefficient ( $D_p$ ) and air permeability ( $k_a$ ) were quantified in sand and in sandy loam with and without biochar amendment. These two gas transport parameters are needed to model soil aeration [Poulsen *et al.*, 2006]. They are dependent on the volumetric water content and air filled porosity [Poulsen and Blendstrup, 2008], which are in turn influenced by SWC.

Molecular diffusion is the mechanism of gas transport that is driven by gas concentration gradients, where  $D_p$  accounts for resistances in the soil as well as molecular structure of the diffusing compound [Jury *et al.*, 1991]. When the bulk gas phase moves in response to pressure gradients, a Darcy-type equation is used to describe gas transport and  $k_a$  is the parameter accounting for resistance associated with the pore structure and water distribution [Kawamoto *et al.*, 2006a].

The relationships between  $D_p$  and pore structure and  $k_a$  and pore structure can be vastly different since gas diffusion can occur in pore systems with disconnected gas pores while gas advection requires connected gas pore space [Eden *et al.*, 2012]. Here, gas species may partition into water blocking pores, diffuse through the water, and then partition back into the gas phase. These two gas parameters were measured and compared with published works in Chapter 4.

## Chapter 2

### THE ORIGIN AND REVERSIBLE NATURE OF POULTRY LITTER BIOCHAR HYDROPHOBICITY

#### 2.1 Background

Thermochemical conversion (pyrolysis) of biomass produces bioenergy and solid byproduct, called biochar, which can be added to soils to sequester carbon to mitigate climate change [Lehmann and Joseph, 2009; Clough *et al.*, 2010; Rogovska *et al.*, 2011], enhance soil fertility [Novak *et al.*, 2009; Uzoma *et al.*, 2011; Spokas *et al.*, 2012a], and increase crop production [Atkinson *et al.*, 2010; Jeffery *et al.*, 2011]. Conversion of excess biomass residues to biochar may reduce large volumes and disposal costs of agricultural wastes. For example, the US poultry industry generates 10.9 million dry t of poultry litter (PL) annually and may benefit from this approach [Song and Guo, 2012]. However, there is uncertainty about the long-term improvement in soil properties from any type of biochar addition [Spokas *et al.*, 2014]. A majority of previous laboratory and field studies were conducted using fresh biochar [Spokas, 2013]. As biochar ages, abiotic surface reactions alter surface group chemistry by reducing pH, oxidizing biochar surfaces, and increasing cation exchange capacity [Cheng *et al.*, 2006; Cheng *et al.*, 2008; Cheng and Lehmann, 2009; Joseph *et al.*, 2010; Spokas *et al.*, 2014], which in turn influence soil biology, mineralogy, nutrient retention, and hydrology of biochar-amended media.

An important biochar property receiving recent attention is wettability. Although the hydrophobicity of fresh biochar pyrolyzed at low temperatures is recognized [Laird *et al.*, 2009; Sohi *et al.*, 2010], few have characterized this hydrophobicity as a function of pyrolysis conditions or have elucidated the origin of this hydrophobicity. Freshly created biochar from corn stover, magnolia leaf, and apple wood were found to be

hydrophobic when pyrolyzed at ~300 to 400°C but hydrophilic at pyrolysis temperatures of 500 to 600°C [Kinney *et al.*, 2012]. The pyrolysis temperature ranges for the creation of hydrophobic or hydrophilic biochar may not be universal because biochar produced from wood and bark at 500 to 600°C were hydrophobic [Smetanova *et al.*, 2013].

Hydrophobic biochar particles mixed with soil are expected to alter the distribution of water and air and to affect water infiltration. For example, mixtures of hydrophilic sand with identically sized hydrophobic sand particles resulted in significant changes in water imbibition [Bauters *et al.*, 2000b]: the matric potential at which water entered initially dry sand decreased by a factor of four when the percentage of hydrophobic particles increased from 0 to 3.1% [Bauters *et al.*, 2000b]. In addition to its direct effect on the infiltration and distribution of water in soil, hydrophobicity can affect microbial growth, with higher microbial counts found in wettable zones than in water-repellent regions [Bruun, 2011]. Although hydrophobic biochar may alter water distribution in soil, water repellency may be transient. Kinney *et al.* [2012] found that sonicating hydrophobic biochar particles for 1 h in ultrapure water reduced the molarity of an ethanol drop (MED) index, an indirect measure of wettability, from 15 to 10 [Kinney *et al.*, 2012]. Water repellency has been studied for decades by soil scientists (see reviews by [DeBano, 1981; DeBano, 2000; Doerr *et al.*, 2000; Diehl, 2013]), and processes influencing water repellency of soils (e.g., soil moisture) are also expected to affect the water repellency of soils amended with hydrophobic biochar particles. Thus, the hydrophobicity of some biochar may be an important factor influencing transient changes in plant fertility, nutrient cycling, and greenhouse gas production in biochar-amended soils by changing water distribution and flow.

Several factors may influence biochar hydrophobicity. Surface roughness, which is correlated with  $N_2$ -Brunauer-Emmett-Teller (BET) surface area, may affect surface wetting [Wenzel, 1936; Cassie and Baxter, 1944; Valipour *et al.*, 2014]. Thus, the high BET surface areas associated with many biochar [Brown *et al.*, 2006; de la Rosa *et al.*, 2014] may influence their wettability. Mineralogical and chemical studies of biochar surfaces indicate the presence of fine biochar particles and salts [Spokas *et al.*, 2014], which may be removed with exposure to water opening up new pores and thus altering surface roughness and wettability [Spokas *et al.*, 2014]. For poultry litter, polar oxygen- and nitrogen-containing functional groups in the litter (e.g., as water, ammonia, and CO) may be lost during pyrolysis creating a C-rich hydrophobic poultry litter biochar surface. Finally, volatile organic compounds are produced during the production of biochar [Olsson *et al.*, 2003], and these compounds may condense onto biochar surfaces [Spokas *et al.*, 2011] and alter wettability. The composition of such sorbed compounds varies with parent material and pyrolysis temperature [Spokas *et al.*, 2011]. The chemical constituents of heavy bio-oils produced from chicken manure with a calorific value of 27.9 MJ kg<sup>-1</sup> consisted mostly of aliphatic carbons (53.5% of total C) and aromatic carbons (39.9% of total C) [Schnitzer *et al.*, 2007a].

In this chapter, the hydrophobicity of biochar produced from poultry litter was characterized, extending a previous study on the wettability of biochar from plant-based feedstocks [Kinney *et al.*, 2012]. Similar to the results of Kinney *et al.* [2012], PLBC produced by pyrolysis at low temperatures were found to be hydrophobic. Three hypotheses about the cause of PLBC hydrophobicity were tested: (i) increased surface roughness from pyrolysis, (ii) loss of polar oxygen- and nitrogen-containing functional groups in PL (e.g., as water, ammonia, CO, and small alcohol and amine vapors) during

pyrolysis resulting in a C-rich hydrophobic surface, and (iii) condensation of organic vapors created during pyrolysis covering biochar surfaces. The reversible nature of this hydrophobicity was assessed under controlled laboratory conditions. Finally, the influence of PLBC hydrophobicity on macroscopic soil behavior (i.e., contact angle of PLBC–sand mixtures) was evaluated for a range of PLBC mass fractions because the impact of biochar particles on soil wettability is expected to vary with biochar content.

## **2.2 Materials and Methods**

### **2.2.1 Poultry litter biochar production**

Poultry litter pellets were purchased from Perdue AgriRecycle, LLC, which processes wastes collected from chicken farms into pellets by drying at 80 to 110°C and pelleting. The pellets were < 4 mm and contained 7.7% gravimetric moisture content. The dried mass consisted of 71.5% organic matter and 28.5% mineral ash. The organic carbon (OC) content of PL pellets was  $335.1 \pm 3.2 \text{ g kg}^{-1}$  (mean  $\pm$  SEM) [Song and Guo, 2012]. The elemental composition of poultry litter is presented in Appendix A, Table A1.

Poultry litter biochar was created by slow pyrolysis following the procedures of Song and Guo [2012]. Seven pyrolysis temperatures were used, ranging from 300 to 600°C at 50°C increments. Details of the pyrolysis procedure and properties of PLBC (e.g., nutrient content) and  $N_2$ -BET surface area are summarized in publication by Song and Guo [2012] [Song and Guo, 2012].

### **2.2.2 Hypothesis testing with poultry litter biochar pyrolyzed at 400°C**

Measurements were first conducted to establish PLBC's water repellency and to test hypotheses about the cause of hydrophobicity. Poultry litter biochar pyrolyzed at

400°C (PLBC400) was selected for initial testing. The hydrophobicity of PL pellets before pyrolysis was also assessed.

The water drop penetration time (WDPT) [Dekker and Ritsema, 2000; Letey *et al.*, 2000; Bachmann *et al.*, 2003] was used to determine particle hydrophobicity. Uniform PL pellet or biochar particles (5 g) sieved between 1.8 and 2 mm mesh openings were placed in a 25 mL dish. In the initial tests, WDPT did not vary between 10, 30, and 50  $\mu$ L droplets, so 10  $\mu$ L deionized (DI) water droplets were used. For each sample, 5 to 10 droplets were sequentially placed on dry regions of the sample, and the time to completely penetrate the sample surface was recorded. The particles were classified as follows: WDPT < 5 s, wettable (nonrepellent); WDPT 5 to 60 s, slightly repellent; WDPT 60 to 600 s, strongly repellent; WDPT 600 to 3600 s, severely repellent; and WDPT > 3600 s, extremely repellent [DeBano, 1981; Dekker and Jungerius, 1990]. The air temperature was 22.5°C, and the relative humidity (RH) was 50% for all measurements.

Preliminary results indicated that PLBC400 was hydrophobic. To test three hypotheses about the cause of this hydrophobicity, a series of WDPT tests were conducted on PLBC400 subjected to (i) vacuum treatment in which PLBC400 was placed in a vacuum at -20 inch *Hg* pressure for 24 h to remove high volatile compounds; (ii) vacuum/water treatment in which vacuum-treated PLBC400 was rinsed in deionized (DI) water for 24 h at 1:200 mass-to-liquid ratio to remove water-extractable compounds (the water-rinsed biochar was decanted and dried in a desiccator for 48 h); (iii) vacuum/heat treatment, in which vacuum-treated PLBC400 was heated at 105°C for 24 h to remove water and low volatile organic compounds; and (iv) heat treatment (HT), in which PLBC400 heated at 105°C for 1, 2, 3, or 24 h.

### **2.2.3 Effect of pyrolysis temperature**

The impact of pyrolysis temperature on the hydrophobicity of biochar was assessed by contact angle (CA) measurements. Unlike WDPT and MED tests, which are indirect measurements of soil wettability [Bachmann *et al.*, 2000; Kinney *et al.*, 2012], CA measurements directly quantify the influence of solid surface properties on the distribution and morphology of water in porous media.

Contact angles were measured on PLBC produced at 300, 350, 400, 450, 500, 550, 600°C and on a pure quartz sand (30/40 Accusand, Unimin Co.) using the sessile drop method [Bachmann *et al.*, 2000]. During these measurements, RH was 17 to 18%, and temperature ranged from 20.3 to 20.9°C. To prepare CA test samples, microscope slides were washed with 1% nitric acid, dried at 105°C, and cooled to room temperature. A double-sided adhesive tape (Scotch Removable Double Sided Tape, 3M Co.) with an area of approximately 6 cm<sup>2</sup> was placed on each slide to affix the particles. Biochar and the reference sand were sieved between #30 (0.595 mm opening) and #35 (0.5 mm opening) mesh to a geometric mean diameter of 0.545 mm, which reduced effects associated with variable particle sizes. Particles were placed on adhesive tape following standard procedures [Bachmann *et al.*, 2000]. Three slides were prepared per sample, and CA was measured at the three-phase contact line on five to six water droplets on each slide using a goniometer fitted to a microscope (NRL CA Goniometer model no. 100-00-155, Ramé-hart, Inc.). A water drop size of 10 µL was selected after verifying the stability of CA for different water volumes.

### **2.2.4 Effect of contact time with water**

The wettability of two biochar was evaluated as a function of water contact time: PLBC pyrolyzed at 300°C (PLBC300) and PLBC300 heated for 12 h at 105°C

(HT-PLBC300). Approximately 30 g of each biochar were sieved between #30 and #35 mesh and added to degassed DI water at a mass ratio of 1.13:1 (biochar:DI) in 250 mL amber bottles. At this ratio, biochar were submerged with approximately 1 cm water covering the particles. After 24 h, 2.0 – 2.4 g of mass (biochar + DI water) was removed from each bottle and placed in a desiccator for 24 to 96 h until the biochar was visibly dry. Deionized water was added to each bottle to maintain 1 cm water covering the particles. Sampling was repeated at 48 and 72 h.

All samples were prepared in triplicate, and CAs measured following the methods described above on dried biochar at RH to 51 to 57% and temperatures of 20.6 to 21.6°C.

### **2.2.5 Rinsate analyses**

Triplicate samples were prepared using sterilized flasks, each containing 1 g of PLBC300 or PLBC600 (each sieved between #30 and #35 mesh) and 200 mL of DI water. Samples were agitated at 200 rpm, and 17 mL of the extraction supernatant were removed at 1, 2, 4, 6, 19, and 24 h. Total organic carbon (TOC) of the decanted and filtered (pore size, 0.45  $\mu\text{m}$ ) (Cellulose Nitrate Membrane Filter, Whatman Ltd.) extract samples were measured with an Apollo 9000 TOC analyzer (Teledyne Tekmar). From these samples the mass of water-extractable organic carbon was determined as a function of time. The filtered solutions from PLBC300 and PLBC600 collected at 24 h were further analyzed using dichloromethane ( $\text{CH}_2\text{Cl}_2$ ) extraction (7 g of extract solution to 4 g  $\text{CH}_2\text{Cl}_2$  shaken in 50-mL vials) and analyzed by gas chromatography–mass spectrometry (GC–MS) (5973N Network Mass Selective Detector Gas Chromatograph, Agilent). Peaks from the GC–MS spectra were identified using the MSD ChemStation NIST 2000 library (Agilent).

To identify which functional groups in the water-extractable organics were causing hydrophobicity, triplicate samples were prepared for PLBC300, PLBC600, and HT-PLBC300 (15 g of biochar added to 10 g of DI water in 50-mL bottles). The samples were agitated for 24 h at 200 rpm. A decanted droplet (0.1 mL) from each sample was transferred onto a zinc selenide (*ZnSe*) polarizer (cat. no. 602L08, RJ Spectroscopy Co.) and dried in a desiccator overnight at room temperature, leaving a thin film of precipitate. The *ZnSe* polarizer was placed in a Fourier transform infrared spectrometer (Nexus 670 Thermo Nicolet, Thermo Scientific Instruments Co.), and the spectrum was recorded from 500 to 4000  $\text{cm}^{-1}$  with a 4  $\text{cm}^{-1}$  resolution using 64 scans.

Finally, the air–water interfacial tension of the biochar rinsates was measured to assess the effect of leached compounds (details and results are found in Appendix A).

### **2.2.6 Effect of mixing with sand**

To investigate the effect of biochar particles on soil wettability at various mass fractions, PLBC300, PLBC350, and PLBC600 were sieved between #30 and #35 mesh and added to cleaned 30/40 Accusand (sand) at 0, 2, 5, 15, 30, 60, 80, and 100% (w/w). Following the procedures described above, CAs were measured on these PLBC–sand mixtures at RH of 14.7 to 21.8% and temperature between 20.0 to 20.7°C. The effects of biochar mass fractions on the mixture CAs for the three biochar types were evaluated using one-way ANOVA and Tukey–Kramer post-hoc comparison tests.

## 2.3 Results and Discussion

### 2.3.1 Post-treatment effects on poultry litter biochar hydrophobicity

Non-pyrolyzed poultry litter pellets had an average WDPT of 20 s, making this material slightly water repellent (Table 2.1). After pyrolysis at 400°C, the average WDPT increased to > 3600 s (extremely water repellent).

This hydrophobicity was unaffected by exposing biochar to a vacuum of -20 inch *Hg* for 24 h. Vacuum treatment followed by rinsing with DI water for 24 h removed the hydrophobicity with mean WDPT < 1 s; the water-rinsed biochar was even more water-wetting than the feedstock. Similarly, vacuum treatment followed by heating at 105°C for 24 h eliminated the hydrophobicity, with average WDPT < 1 s. When PLBC400 was heated to 105°C for 1, 2, 3, and 24 h, hydrophobicity disappeared: mean WDPT was 240 s for 1 and 2 h of heating and decreased to <1 s for the 3- and 24-h treatments (Table 2.1).

Song and Guo [2012] reported an increase in  $N_2$ -BET surface area from 0.90 m<sup>2</sup> g<sup>-1</sup> for PL pellets to 3.94 m<sup>2</sup> g<sup>-1</sup> for PLBC400 after PL pyrolysis [Song and Guo, 2012]. Surface roughness increases with  $N_2$ -BET surface area [Hodson *et al.*, 1997; Hsieh *et al.*, 2005], and increases in surface roughness may increase hydrophobicity [Wenzel, 1936; Cassie and Baxter, 1944; Valipour *et al.*, 2014]. Spokas *et al.* [2014] recently demonstrated that PL biochar produced at 350°C and rinsed with distilled water for 24 h (1:20 w/w) released inorganic salts and very fine biochar particles from the biochar surface, which could open pores and increase surface roughness. Because heat treatment should not have removed these salts or biochar fines but removed PLBC400 hydrophobicity, change in surface roughness was unlikely to be the primary cause of this hydrophobicity, invalidating the first hypothesis.

The second hypothesis can also be ruled out because, although it is possible that pyrolysis resulted in the loss of polar oxygen-containing functional groups on biochar surfaces making the surface hydrophobic, rinsing with water should not have rendered the surface more hydrophilic if these functional groups were absent.

The third hypothesis assumed the hydrophobicity was caused by organic vapors condensing on biochar surfaces while cooling near the end of pyrolysis. Results from all PLBC400 treatments were consistent with this third hypothesis and indicated that these organic compounds (i) were not sufficiently volatile to be removed by vacuum, (ii) had high vapor pressures to volatilize at 105°C within a few hours, and (iii) were altered or perhaps removed by water rinsing within 24 h. These results are consistent with other studies, where organic compounds accumulating on soil particles are widely accepted to be the origin of water repellency in many soils [Doerr and Thomas, 2000; Diehl, 2013].

### **2.3.2 Effect of pyrolysis temperature**

Figure 2-1 shows the CAs of sieved fresh biochar particles at pyrolysis temperatures between 300 and 600°C. Contact angles were measured within 60 s of water droplet placement on rough grain surfaces: preliminary tests indicated that CA was invariant with time for measurements < 60 s (Appendix A, Figure A1). The CA was  $101.1 \pm 2.9^\circ$  for 300°C biochar and decreased with pyrolysis temperature to  $20.6 \pm 1.0^\circ$  for 600°C biochar. The most precipitous drop occurred between 350 and 450°C. Biochar pyrolyzed at 450°C and above were only slightly more water repellent than pure quartz sand. These data are consistent with the hypothesis that hydrophobicity was caused by condensed organic vapors: when pyrolysis ceased and samples cooled, concentrations of organic vapors in the pyrolyzer headspace would be lower at higher

pyrolysis temperatures, yielding smaller mass of surface condensates and hence lower hydrophobicity and smaller CAs.

### **2.3.3 Effect of contact time with water**

Charcoal produced during wildfires is a black carbon material similar to biochar. However, charcoal is neither produced under engineered conditions nor intentionally added to soil [Smetanova *et al.*, 2013]. Because of the low-oxygen content near the ground surface during wildfires [Bryant *et al.*, 2005], pyrolytic conditions occur and fresh hydrophobic charcoals are produced [Briggs *et al.*, 2012]. Hydrophobicity of soil affected by wildfire may be significantly weakened after 2 to 3 mo [Huffman *et al.*, 2001; Hubbert and Oriol, 2005] or may last for as long as 6 yr [Dyrness, 1976]. Weakening of soil-water repellency has been attributed to soil moisture, and the reduction of hydrophobicity depends on the moisture content threshold that varies from severely burned to weakly burned soils [Doerr and Thomas, 2000; Doerr and Thomas, 2003; MacDonald and Huffman, 2004]. Hydrophobicity can return when soil moisture content falls below a threshold level [MacDonald and Huffman, 2004] and may vary seasonally [Taumer *et al.*, 2005]. Given these observations, the time scale for the duration of hydrophobic surfaces for charcoal particles in nature is uncertain.

In this study, biochar stored in air-tight containers at ambient conditions maintained their hydrophobicity for at least 10 mo. However, as PLBCs were exposed to heat or water, abiotic processes altered biochar hydrophobicity, as summarized for PLBC400 in Table 2-1. Because hydrophobic conditions are removable, the influence of biochar's wettability on water infiltration and distribution will be dynamic and may change after soil application. To evaluate the persistence of biochar hydrophobicity, a third set of experiments was conducted where hydrophobic PLBC300 and HT-

PLBC300 were allowed to sit in stagnant DI water over time. The changing CAs with time are plotted in Figure 2-2. Initially, CAs decreased from  $85.8 \pm 0.9^\circ$  at 0 h to  $28.4 \pm 5.8^\circ$  at 24 h. The rate of change in CAs decreased on subsequent sampling days, with CAs of  $4.5 \pm 2.3^\circ$  at 72 h. Thus, it would appear that the organic compounds causing hydrophobicity gradually dissolved, resulting in a decrease in CAs over a 3 d period. It is also possible, however, that water, rather than organic coating dissolution, gradually penetrated the matrices of this coating and was not completely removed in the drying period, resulting in an increase in wettability. Although it is difficult to estimate how long the change from hydrophobic to hydrophilic conditions might take for PLBC in natural soils, these data suggest that the transition could occur more quickly in wet environments.

It is interesting to compare the CA of fresh PLBC300 with that of heat-treated PLBC300 that was subjected to an identical DI water treatment. The CAs of HT-PLBC300 at 1, 2, and 3 d were approximately  $0^\circ$ . Thus, heating PLBC300 made this initially hydrophobic biochar instantaneously wettable and more water wetting than even PLBC produced at a pyrolysis temperature of  $600^\circ\text{C}$  where CAs were  $20.6 \pm 1.0^\circ$  (Figure 2-1), again supporting the third hypothesis.

Biochar hydrophobicity can be removed by water rinsing or heating, as demonstrated above. This transition may occur naturally over time in fire-affected soils [DeBano, 2000]. For example, hydrophobicity was removed over a 1 yr period by an in situ aging process associated with physical and biological processes [MacDonald and Huffman, 2004]. However, hydrophobicity might be re-established if dissolved organic C leaching from decomposed plant material sorbs to biochar surfaces [Kaszi *et al.*,

2010; Lamparter *et al.*, 2014]. Thus, although initial application of biochar may result in hydrophobic biochar surfaces, this hydrophobicity is expected to be transient.

#### 2.3.4 Rinsate analyses

The organic compounds causing PLBC hydrophobicity may be transferred to the aqueous rinsate. Therefore, analyses were performed to quantify the organic carbon leached from PLBC. Leached TOC is plotted versus time in Figure 2-3 and reached a plateau of  $71.7 \pm 2.3 \text{ mg L}^{-1}$  at 24 h for PLBC300, but for PLBC600 the TOC leached was minor ( $2.3 \pm 0.4 \text{ mg L}^{-1}$ ). The fraction of TOC leached over 24 h was 3.77% for PLBC300 and 0.11% for PLBC600. These leachable organics may include the water-extractable organic coating responsible for biochar hydrophobicity.

Ma'shum *et al.* [1988] reported that several layers of hydrophobic compounds were required to cover a sand particle to induce severe water repellency, whereas Zisman [1964] noted that even a single layer of hydrophobic substance on a hydrophilic soil particle can render it water repellent [Zisman, 1964; Ma'shum *et al.*, 1988]. Using the measured TOCs for PLBC300 and PLBC600, the surface coverage by organic condensates was estimated with

$$\# \text{ of carbon monolayers} = N_A \frac{\pi r^2 C}{MA} \quad [2-1]$$

where  $N_A$  is Avogadro number ( $6.022 \times 10^{23} \text{ mol}^{-1}$ ),  $r$  is van der Waals radius of carbon ( $1.7 \times 10^{-10} \text{ m}$ ),  $C$  is TOC leached ( $\text{g g}^{-1}$ ),  $M$  is atomic mass of carbon ( $12 \text{ g mol}^{-1}$ ), and  $A$  is the  $N_2$ -BET of biochar ( $\text{m}^2 \text{ g}^{-1}$ ). For 1 g of biochar produced at 300 and 600°C, the cumulative amounts of carbon released into water after 24 h were 14.34 and 0.46 mg, and their  $N_2$ -BET surface areas were 2.68 and  $5.79 \text{ m}^2 \text{ g}^{-1}$ , respectively [Song and Guo,

2012]. Using these values in Eq. [2-1], the TOC mass released within 24 h from PLBC300 provides 24.4 layers of carbon coverage, whereas TOC from PLBC600 provides only 0.4 layers. These calculations on carbon coverages are consistent with trends for CA reported in Figure 2-1 for PLBC300 and PLBC600: 24 OC layers increased the CAs to 101.1° (PLBC300), whereas a 0.4 layer of OC increased CAs from 6.6 to 20.6° (PLBC600).

The GC–MS analyses of TOC solutions from PLBC300 and PLBC600 extracted with  $CH_2Cl_2$  and Fourier transform infrared spectroscopy (FTIR) analyses of precipitates from rinsates of PLBC300, PLBC600, and HT-PLBC300 are discussed in detail in the online supplement. From GC–MS analyses, with > 95% match, 1,3-bis(1,1-dimethylethyl)benzene and 2,5-bis(1,1-dimethylethyl)-phenol were identified from both biochar, whereas tetradecane was detected in the PLBC300 rinsate but not in PLBC600. A small amount of octacosane was identified in the rinsate for PLBC600 at a 90% match that was not observed on PLBC300. These compounds all have alkyl *C-H* bonds that have been associated with soil organic matter producing hydrophobicity [DeBano, 1981; Capriel *et al.*, 1995; Ellerbrock *et al.*, 2005]. Although these four compounds coat biochar surfaces and may be associated with PLBC hydrophobicity, other compounds that are removable by water but that are either not extractable by  $CH_2Cl_2$  or are not analyzable by GC–MS (e.g., long-chain fatty acids) could also contribute to the observed hydrophobicity.

Spokas *et al.* [2011] identified volatile organic compounds sorbed on 77 biochar by thermal desorption and head space analysis with GC–MS. Consistent with this study, tetradecane, substituted benzenes, and other alkyl groups were sorbed onto biochar [Spokas *et al.*, 2011]. Spokas *et al.* [2011] concluded that there was a stronger linkage

between sorbed organic compounds and biochar production conditions linked with postproduction handling and processing than biochar feedstock. Similar to this study, when pyrolysis temperature was varied systematically using the same feedstock (cottonseed hulls) and slow pyrolysis unit, sorbed organic compounds decreased with increasing pyrolysis temperature from 200 to 800°C [Spokas *et al.*, 2011], consistent with the CA measurements in Figure 2-1 and the rinsate TOC trends in Figure 2-2. Organic compounds found in biochar, light bio-oil, and heavy bio-oil derived from poultry manure using a fast pyrolysis unit were identified [Schnitzer *et al.*, 2007a; Schnitzer *et al.*, 2007b] and included *N*-heterocyclics, substituted furans, substituted phenols, substituted benzenes, carbocyclics, and aliphatics, which include the compounds identified in PLBC organic coatings in this study.

The FTIR spectra of precipitates from hydrophobic PLBC300 showed small peaks between 3020 and 2800 cm<sup>-1</sup> (Appendix A, Figure A2), indicating *C-H* stretching from alkyl groups that have been associated with organic matter coatings causing hydrophobicity in soil [Capriel *et al.*, 1995; Doerr *et al.*, 2005; Ellerbrock *et al.*, 2005; Ellerbrock and Gerke, 2013]. More recently, FTIR peak areas in this region correlated well with the hydrophobicity of plant-derived biochar [Kinney *et al.*, 2012]. These peaks were much smaller for precipitates from hydrophilic PLBC600 and HT-PLBC300. Thus, the presence (PLBC300) or absence (PLBC600 and HT-PLBC300) of the hydrophobic *CH* groups in the 3020 to 2800 cm<sup>-1</sup> wavelength range is consistent with CAs measured for PLBC300, PLBC600, and HT-PLBC300. This suggests that alkyl compounds found in the OC coating on PLBC300 were the cause of hydrophobicity.

Leached compounds might accumulate at the air–water interface, altering the air–water interfacial tension and thus CAs. Data indicated that this effect was small and did not influence CAs measured within 60 s (see Appendix A, Figure A1). Furthermore, PLBC600 was more recalcitrant to OC leaching over the 24-h rinsing period than PLBC300; therefore, PLBC600 might be used for applications where OC loading must be minimized.

### **2.3.5 Effect of mixing with sand**

Biochar is typically added to soil at mass fractions ranging from 0.5 to 9% to increase soil fertility [Rondon *et al.*, 2007; Kinney *et al.*, 2012; Mukherjee *et al.*, 2014], although mass fractions up to 100% may be used for media in other settings (e.g., stormwater treatment) [Tian *et al.*, 2014]. Contact angles for mixtures of fresh PLBC (pyrolyzed at 300, 350, or 600°C) and quartz sand, all sieved to uniform particle size before mixing, are plotted in Figure 2-4. Contact angles increased from 6.6° for sand to 20.2° for 2%PLBC300, 30.1° for 2%PLBC350, and 26.6° for 2%PLBC600 biochar–sand mixtures. Using ANOVA, the mean CA of each biochar–sand mixture is dependent on biochar pyrolysis temperature for each biochar mass fractions ( $p < 0.05$ ). Tukey–Kramer post-hoc comparison of 2 and 5% PLBC–sand mixtures indicate a difference between PLBC300–Sand and PLBC350–Sand CAs ( $p < 0.05$ ) but not between PLBC300–Sand and PLBC600–Sand ( $p > 0.1$ ) or PLBC350–Sand and PLBC600–Sand ( $p > 0.5$ ). As the biochar mass fractions increase from 15 to 100%, the Tukey–Kramer post-hoc comparisons indicate that mean CAs for each pyrolysis temperature at each mass fraction are statistically different ( $p < 0.0001$ ). For the PLBC300–Sand and PLBC350–Sand mixtures, CAs increased linearly as biochar mass fractions increased from 5 to 100%, with CAs of approximately  $103.5 \pm 1.6^\circ$  for 100%

PLBC. Contact angles for PLBC600–Sand varied only slightly over the 5 to 100% biochar mass fraction range. In general, the overall trends in CAs for biochar–sand mixtures are consistent with CAs for individual PLBC shown in Figure 2-1: PLBC300 and PLBC350 increase hydrophobicity in a similar fashion, whereas PLBC600 affects CAs less. The less influence of a fewer hydrophobic particles on CAs of biochar–sand mixtures is consistent with other work examining the influence of a small number of hydrophobic grains in an otherwise hydrophilic medium [Bauters *et al.*, 2000a].

At 2 and 5% mass fractions, though, the addition of hydrophobic (PLBC300 or PLBC350) or hydrophilic (PLBC600) biochar particles resulted in similar increases in CA. For these small yet significant biochar mass fractions, increased CA may not be associated with the wetting characteristics of biochar surfaces, but an increase in surface roughness caused by the topology of biochar particles. Bachmann and McHale [2009] developed a model to predict the combined effects of the Young's Law CA, which is due to interfacial forces and is measured with droplets on planar surfaces, and packing roughness, caused not by intrinsic surface properties but by the curvature and spacing of layered particle grains [Bachmann and McHale, 2009]. Their model is based on the Wenzel [1936] and Cassie and Baxter [1944] models, assumes identically sized spherical particles packed on a planar surface, and was validated with data from glass beads, sand, clay and clay loam [Wenzel, 1936; Cassie and Baxter, 1944; Bachmann and McHale, 2009]. The Bachmann and McHale model indicates that CA on a rough grain surface is usually larger than Young's Law CA for the same surface material but is sensitive to particle packing. As shown in Figure 2-5, PLBC300, PLBC350, and PLBC600 have similar topology but are much more angular than the quartz sand. Thus, one plausible explanation for the similar effect of these three biochar on CAs at 2 and

5% mass fractions is that the predominant factor affecting CA is macroscopic surface roughness associated with grain spacing/particle packing between sand and PLBC rather than differences in OC surface coatings on particles. At larger biochar mass fractions, though, the effect of Young's Law CA, which varies with OC coatings, played a more dominant role than macroscopic surface roughness. Thus, at small biochar mass fractions, the effect of biochar on wettability may be a strong function of biochar particle size and topology and their relationship to particle size and topology of native soil grains. The influence of biochar surface properties (e.g., OC coating) may be more pronounced at larger biochar mass fractions. Future research might explore this relationship for different soils and biochar.

#### **2.4 Conclusions and Implications**

Three different mechanisms causing biochar hydrophobicity were postulated: (i) increases in surface roughness, (ii) loss of surface polar compounds, and (iii) condensation of organic compounds on biochar surfaces. Using the WDPT test on PLBC400 subjected to various treatments, the first two hypotheses were invalidated. The severity of biochar hydrophobicity was further evaluated using CA measurements to quantify its dependence on pyrolysis temperature. The organic coatings on poultry litter biochar contained alkyl groups that have been linked to hydrophobicity in plant-derived biochar [Kinney *et al.*, 2012], charcoals [Briggs *et al.*, 2012], ashes [Dlapa *et al.*, 2013], and soils altered by wildfires [DeBano, 2000]. The release of aliphatic compounds from PLBC could promote microbial activity [Lehmann *et al.*, 2011], which in some cases may be desirable, particularly the hydrophobic compounds could be easily removed by water rinsing. Alternatively, it may be preferable to use PLBC

pyrolyzed at sufficiently high temperatures to reduce transient effects associated with organic coating leaching.

Even if PLBC hydrophobicity is transient or if hydrophilic PLBC are used, depending on the native soil particle size distribution and particle topology, addition of PLBC could alter soil texture and roughness of granular surfaces, which may result in much smaller but longer-lasting changes in CA. Both hydrophobic and hydrophilic PLBC increased CAs by similar magnitudes at 2 and 5% mass fractions. Poultry litter biochar pyrolyzed at temperatures  $<400^{\circ}\text{C}$  and mixed with sediment at rates  $\geq 15\%$  (w/w) may increase sediment CAs by  $>30^{\circ}$ , as shown. Such changes for subcritical CA ( $< 90^{\circ}$ ) may reduce infiltration rates [Lamparter *et al.*, 2006] and alter water distribution during infiltration events through preferential fingered flows [Wallach *et al.*, 2013]. Additional study is necessary to quantify the impact of PLBC addition on water retention and infiltration in PLBC-amended media. Such studies should examine temporal effects because pyrolyzed PLBC is expected to become more hydrophilic with time through either leaching of organic coatings or gradual penetration of water into surface coating matrices.

Table 2-1: Water drop penetration time of poultry litter and fresh and treated poultry litter biochar produced at 400°C.

<b>Samples<sup>†</sup></b>	<b>Average WDPT<sup>‡</sup></b>	<b>Water repellency</b>
	seconds	
Poultry litter pellets	20	slightly repellent
PLBC400	>3600	extremely repellent
PLBC400, VT for 24 h	>3600	extremely repellent
PLBC400, VT for 24 h and HT for 24 h	<1	nonrepellent
PLBC400, HT for 1 h and 2 h	240	strongly repellent
PLBC400, HT for 3 h and 24 h	<1	nonrepellent
PLBC400, VT for 24 h, WR, and AD	<1	nonrepellent

<sup>†</sup> Treatment parameters: pyrolysis temperature = 400°C; heating temperature = 105°C; vacuum treatment pressure = -20 in *Hg*; air temperature = 22.5°C, and relative humidity % = 50%. AD, air dried in desiccator; HT, heat treatment; PLBC400, poultry litter biochar produced at 400°C; VT, vacuum treated; WR, rinsed in deionized water. <sup>‡</sup> Water drop penetration time.

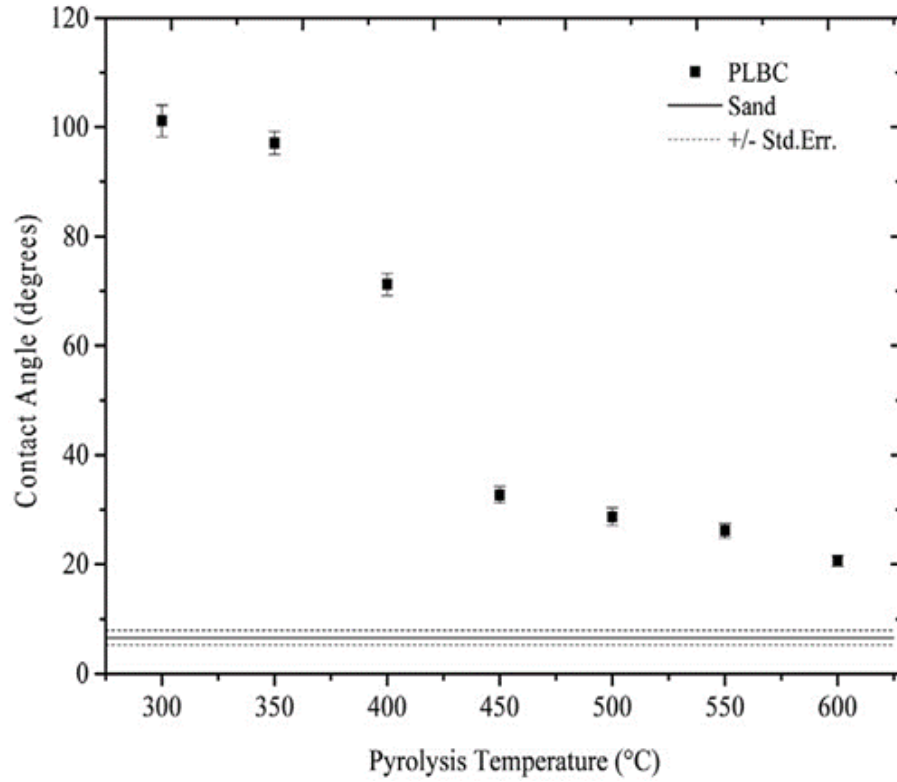


Figure 2-1: Mean contact angles (CAs) of poultry litter biochar (PLBCs) produced at varying pyrolysis temperatures. Error bars represent  $\pm 1$  SEM. Mean CA for sand shown with upper and lower bound of the SE of the sample mean. Relative humidity,  $17.4 \pm 0.42\%$ ; temperature,  $20.5^\circ\text{C}$ .

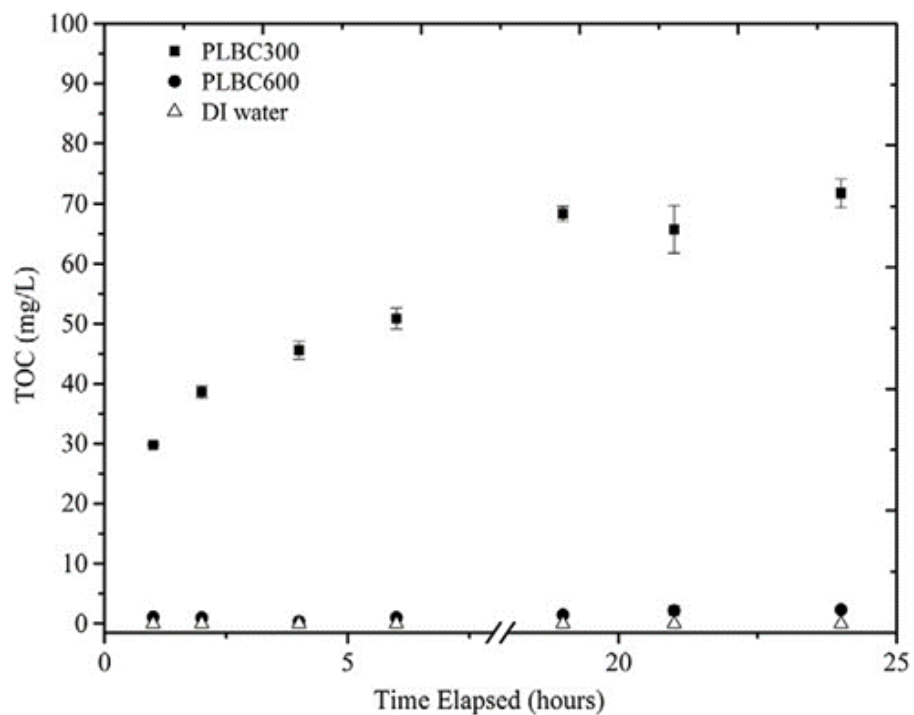


Figure 2-2: Mean contact angles of poultry litter biochar at 300°C (PLBC300) and heated PLBC300 at 105°C for 12 h (HT-PLBC300) after they were submerged in deionized water for different times. Error bars represent  $\pm 1$  SEM. Relative humidity,  $54.8 \pm 2.9\%$ ; temperature,  $21.0^\circ\text{C}$ .

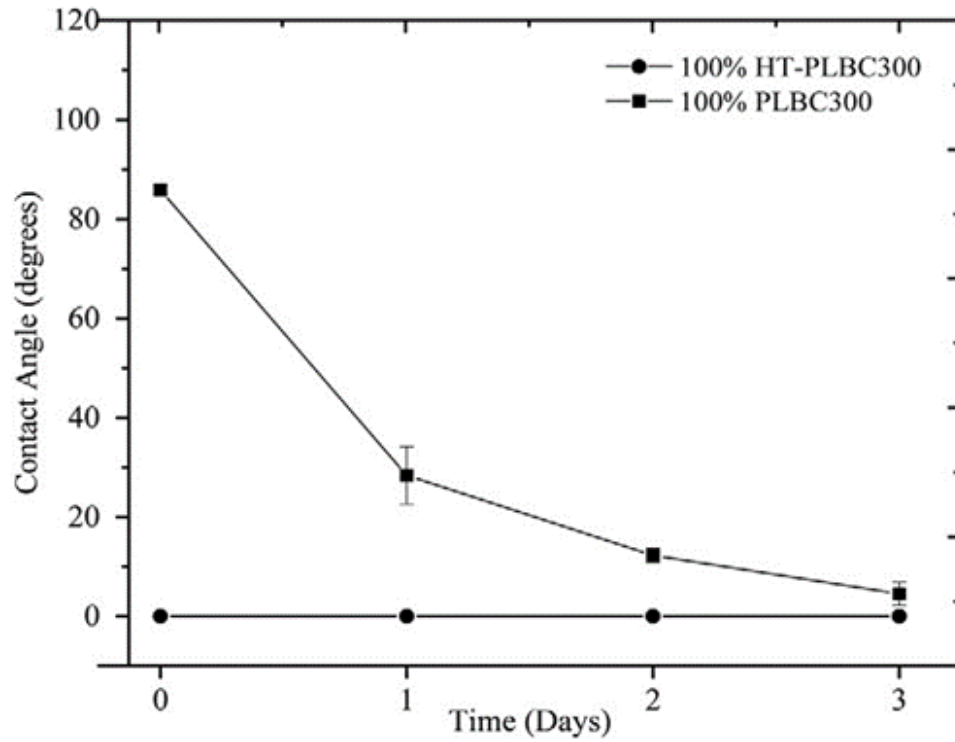


Figure 2-3: Total organic carbon (TOC) leached from poultry litter biochar (PLBC) produced at 300°C and 600°C when rinsed in deionized (DI) water at 1:200 solid to liquid mass ratio for 24 h (PLBC300 and PLBC600, respectively). Error bars represent  $\pm 1$  SEM.

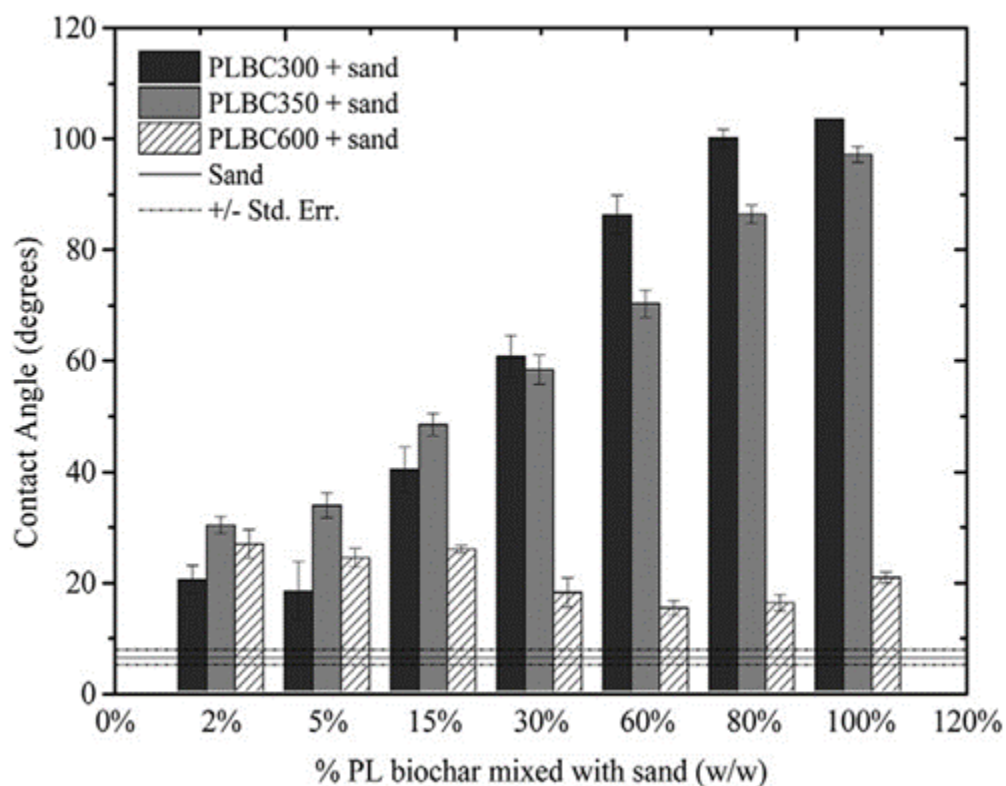


Figure 2-4: Mean contact angles of poultry litter biochar (PLBC)-sand mixtures (w/w) for PLBC pyrolyzed at 300 (PLBC300), 350 (PLBC350), and 600°C (PLBC600). Error bars represent  $\pm 1$  SEM. Relative humidity,  $17.7 \pm 1.5\%$ ; temperature,  $20.3^\circ\text{C}$ .



Figure 2-5: Surface geometry of (a) sand, (b) poultry litter biochar (PLBC) pyrolyzed at 300°C (PLBC300), (c) PLBC at 350°C (PLBC350), and (d) PLBC at 600°C (PLBC600). All particles collected between #30 (0.595mm opening) and #35 sieves (0.5-mm opening).

## Chapter 3

### SOIL-WATER RETENTION CURVE MODELS FOR BIOCHAR AMENDED SOILS

#### 3.1 Background

Biochar is a carbon-rich solid produced by pyrolysis of organic materials, often waste biomass. Biochar has been proposed as a soil amendment to increase water retention and soil fertility [Lehmann, 2007; Novak *et al.*, 2009]. When amended to stormwater treatment media, such as greenroofs or biofiltration media, biochar may increase water retention [Beck *et al.*, 2011; Tian *et al.*, 2014] and pollutant removal. Increases in water retention favor plant growth (greenroofs) and pollutant retention (biofiltration media). However, predicting these effects in soil or stormwater treatment media is difficult. Varying with organic feedstock and pyrolysis conditions, biochars possess different particle size distribution [Cetin *et al.*, 2004; Liu *et al.*, 2016], internal pore volume [Brewer *et al.*, 2014], surface area [Zabaniotou *et al.*, 2008; Song and Guo, 2012], and other properties that affect water retention. Thus, the influence on water retention will vary for each biochar/media combination.

The impact of a conifer and hardwood biochar on water retention in a sand, loam, and clay at  $pF = 6.8$  ( $pF = \log |h|$ ;  $h$  = matric potential or capillary pressure head in cm-H<sub>2</sub>O or 100 Pa) showed 15% (v/v) conifer biochar amendment to sand increased volumetric water content by 6% but caused no measureable change in loam and a 7% reduction in clay [Tryon, 1948]. Tryon [1948] postulated that clays sorbed water 5.6 – 12% more than biochar; thus, adding biochar reduced water retention in biochar-clay mixtures at  $pF = 6.8$ . Amendments with hardwood biochar retained 2.5 – 11.5% more water than conifer biochar, and fine sized biochar (< 1 mm) retained 10 – 20% more water than coarse biochar (2 – 5 mm).

Abel et al. [2013] amended five soils, two sands and three loamy sands with maize biochar at 1, 2.5, and 5% (w/w). Available water capacity, defined as water retained between  $pF$  1.8 (field capacity) to 4.2 (wilting point), showed significant improvement with increasing biochar content: available water capacity doubled at 5% (w/w) biochar amendment in sands, and increased by 50-70% at the same application rate in two of the loamy sands. However, for the loamy sand with initial organic matter (OM) content of 9.1%, almost eight times larger than the other loamy sands, biochar amendment slightly reduced available water capacity [Abel et al., 2013]. These data are consistent with the findings of Tryon [1948]: when soils have high initial available water holding capacity, caused by clay [Tryon, 1948] or organic matter [Abel et al., 2013], biochar amendment reduces this function. In these soils with initially high available water capacity, biochar retains water less efficiently than the native soil it replaced.

In a more recent study, water retention at the dry-end of the soil water characteristic (SWC) ( $5 < pF < 6.8$ ) was measured using a vapor sorption analyzer for sandy loam (~ 10% clay) amended with birch wood biochar and pig manure [Arthur et al., 2015]. For field-aged samples with pig manure amendment of 21 – 42 Mg ha<sup>-1</sup>, biochar amendment increased gravimetric water contents for  $5.5 < pF < 6.6$ . Arthur et al. [2015] attributed the increased water sorption to increases in specific surface area (SSA) resulting from biochar amendment. However, in a related study amendment of 20 Mg ha<sup>-1</sup> of the same biochar to sandy loam (16% clay) resulted in no increase in water sorption or SSA [Sun et al., 2013]. One explanation for these data was that for the sandy loam with the higher clay content, 16% versus 10%, the ability of biochar amendment to significantly increase SSA and thus water sorption was diminished [Arthur et al.,

2015]. This reasoning is similar to that provided by Abel et al. [2013]: if biochar replaces soil components that retain water equal to or better than biochar, water retention will not be improved.

In an effort to elucidate the mechanisms by which biochar alters soil water retention, Liu et al. [2017] conducted laboratory experiments where Mesquite biochar pyrolyzed at 400°C was amended to silica sand at 2% (w/w) [Liu et al., 2017]. The biochar and sand were sieved to three particle size ranges (<0.251, 0.251 - 0.853, and 0.853 - 2.00 mm), and water retention measurements made for various sand/biochar combinations. By quantifying the intrapores of the biochar (pores within the envelope of biochar particles and connected to external pores) and the interpores of the biochar/sand mixtures (larger pores between the exterior particle surfaces), Liu et al. [2017] were able to differentiate the influence of biochar on intrapore and interpore spaces. As matric potential decreased from  $pF \sim 6$  to  $pF \sim 3$ , Mesquite biochar increased water retention by adding intrapore spaces not present in 100% sand samples. With further decreases in matric potential, the elongated shapes of biochar particles increased the interpore volumes and thus water retention. Liu et al. [2017] suggested that for sandy soils, available water capacity would be enhanced most by biochars with high intrapores and irregular shapes.

The intrapores in biochars are formed during biochar production and are affected by the pyrolysis temperatures and the parent source materials [Brewer et al., 2014]. Intrapores may range in size from sub-nanometer to micrometer [Briggs et al., 2012; Hardie et al., 2014], and may provide significant intrapore volumes. Porosity of biochar particles have been measured from 50 to 85%, and intrapore volumes up to 3 cm<sup>3</sup> g<sup>-1</sup> for grass biochars [Brewer et al., 2014]. Scanning electron microscope (SEM)

images of acacia wood biochar produced in a continuous flow kiln at 550°C for 30 – 40 min showed that intrapores were elliptical in shape with an average minimum pore diameter ~ 0.1 μm and 95% of all pores < 22 μm [Hardie *et al.*, 2014].

The Young-Laplace equation can be used to understand the relationship between the radius of a cylindrical pore and capillary pressure that drains at this pressure

$$\Delta P = \frac{2\sigma \cos\theta^\circ}{r_p} \quad [3-1]$$

where  $\Delta P$  is the capillary pressure and is the difference between gas ( $P_g$ ) and water ( $P_w$ ) pressure,  $\sigma$  is the interfacial tension of air-water,  $\theta^\circ$  is the contact angle between the wetting fluid and the solid, and  $r_p$  is the pore radius. If soil pores are represented as a collection of cylindrical pores, biochar amendment may alter  $r_p$  due to rearrangement of biochar-soil particles (interpores) or the addition of pores within biochar particles (intrapores). In addition, biochar may affect air-water interfacial tension and the contact angle.

About 70 varieties of biochar produced at low temperature ( $\leq 350$  °C) were shown to release short chained organics (aldehydes, furans, and ketones), aromatic compounds, and large organic carbons [Spokas *et al.*, 2011]. These compounds may affect the air-water interfacial tension and the soil liquid contact angles [Savage, 1974; Beatty and Smith, 2010; Atanassova and Doerr, 2011]. The presence of alkyl groups on biochar surfaces have been linked to hydrophobicity in plant derived biochars [Kinney *et al.*, 2012], but a complicating factor is the organic compounds on biochar surfaces may be removed through heating or dissolution into water, resulting in increasingly hydrophilic surfaces as biochars age in the field [Ojeda *et al.*, 2015; Yi *et al.*, 2015]. Thus, because biochar amendment may alter  $r_p$ ,  $\sigma$ , and  $\theta^\circ$ , when a given capillary

pressure is applied to a soil-biochar mixture biochar may influence water retention through several mechanisms.

Finally, intrapores and interpores created or altered from biochar amendment may change over time [Liu *et al.*, 2016]. Biochars produced at lower temperatures (< 500°C) are susceptible to breakage, and over 50% biochar mass can be lost through weathering [Spokas *et al.*, 2014]. Despite the possible transient changes in air-water interfacial tension, contact angle, and intrapores/interpores with biochar amendment, models are needed to predict changes in water retention with biochar amendment, even if these changes may be altered in time. Many studies demonstrate the influence of biochar amendment on water retention, and some have fitted van Genuchten models to describe these data [Abel *et al.*, 2013; Liu *et al.*, 2017]. However, we are aware of no model that can predict the impact of biochar amendment on water retention, as most studies have been observational.

The purpose of this study was to develop a predictive biochar-soil SWC model that describes the influence of biochar amendment on water retention by accounting for biochar's influence on intrapores and interpores. The model excludes biochar impact on air-water interfacial tension and contact angle. In this model, volumetric water content retained in a biochar-amended soil at each capillary pressure step is determined by summing the volumetric water content from: 1) the native soil without biochar addition ( $\theta^s$ ), 2) the change in intrapore water for  $3.85 < pF < 6.8$  due to the changes in adsorbed and capillary water when soil is replaced with biochar ( $\Delta\theta^{ads}$ ), 3) the additional intrapore capillary water within biochar for  $pF < 3.85$  ( $\Delta\theta^{intra}$ ), and 4) the change in water stored in interpores ( $\theta^{inter}$ ). This model was developed as follows.

## 3.2 Theory

### 3.2.1 Intrapore adsorbed and capillary water ( $pF > 3.85$ )

The Kelvin equation describes the relationship between total water potential,  $\Psi$ , which is the sum of the osmotic and the matric potential, and water vapor pressure,  $P$  [Jury *et al.*, 1991; Dane and Topp, 2002; Decagon Devices, 2013]:

$$pF = \log |\Psi| = \log \left| 0.0102 \frac{RT}{M} \rho_w \ln \left( \frac{P}{P_0} \right) \right| \quad [3-2]$$

where  $R$  is the universal gas constant ( $\text{J mol}^{-1} \text{ } ^\circ\text{K}^{-1}$ ),  $T$  is the absolute temperature ( $^\circ\text{K}$ ),  $M$  is the molecular mass of water ( $\text{g mol}^{-1}$ ),  $\rho_w$  is density of water ( $\text{g m}^{-3}$ ), and  $P_0$  is the saturated water vapor pressure at sample temperature ( $^\circ\text{K}$ ). Water retention in the highly dry region of the SWC is controlled by relative humidity ( $P/P_0$ ). The chilled mirror dew point technique may be used to measure  $\Psi$ . To obtain the matric potential,  $h$ , the osmotic potential is typically subtracted from the total potential using the ionic concentration of the sample [Dane and Topp, 2002]. However, linear regression was fitted to obtain an equation to correct for the osmotic effects (see Appendix B for details).

The water in a biochar/soil mixture at a matric potential greater than  $pF > 3.85$  can be estimated by using the water content of the soil and biochar measured separately at the reference matric potential, and the mass fraction of biochar and soil in the mixture:

$$MC_i^m = \frac{[M^s \times MC_i^s] + [M^{bc} \times MC_i^{bc}]}{M^s + M^{bc}} \quad [3-3]$$

where  $MC_i^m$ ,  $MC_i^s$ , and  $MC_i^{bc}$  are moisture content ( $\text{g g}^{-1}$ ) of the biochar/soil mixture, soil, and biochar, respectively at matric potential  $i$ ; and  $M^{bc}$  and  $M^s$  are dry mass of biochar and soil, respectively, in the biochar/soil mixture. A dew-point potentiometer

can be used to measure the matric potential of soil and biochar samples prepared at different moisture contents, which are used in equation [3-3] to estimate the moisture content of biochar/soil mixtures. To obtain the volumetric water content associated with water retention ( $\theta_i^{ads}$ ), equation [3-3] is divided by water density ( $\rho_w$ ) and multiplied by the dry bulk density ( $M_t^m/V_t$ ) of the biochar/soil mixture, where  $M_t^m$  is the total dry mass (biochar/soil mixture) and  $V_t$  is the total sample volume. The change in water due to biochar amendment at  $pF > 3.85$  is then the difference between this volumetric water content and that for the native soil.

$$\Delta\theta_i^{ads} = \frac{MC_i^m M_t^m - MC_i^s M_t^s}{\rho_w V_t} \quad [3-4]$$

### 3.2.2 Intrapore water ( $pF < 3.85$ )

In addition to water adsorbed in biochar intrapores, additional water may fill the cavities of large biochar intrapores. The additional water retained in a biochar/soil mixture between  $pF < 3.85$  is estimated by mercury intrusion porosimetry (MIP) measurements of biochar, where care must be exercised to exclude interpore volume. With these measurements (described below) and the known mass of biochar in a biochar/soil mixture, the additional intrapore water retained at matric potential  $i$  due to biochar amendment is determined from:

$$\Delta\theta_i^{intra} = \frac{M^{bc}}{V_t} \left( \sum_{j=pF^*}^i V_j^{intra} \right) \quad [3-5]$$

where  $V_j^{intra}$  is the specific intrapore volume ( $\text{mL g}^{-1}$ ) determined by MIP at the  $j$ th matric potential increment, and  $pF^* = 3.85$  is the lower limit of detection water measured by a dew-point potentiometer. In order to determine intrapore volume at

particular matric potential from MIP data, estimates of contact angles of mercury and water in biochar intrapores were needed. These calculations are discussed below.

### 3.2.3 Interpore water

SWC models often use empirically fitted parameters to describe soil water retention [Brooks and Corey, 1964; Campbell, 1974; Mualem, 1976; van Genuchten, 1980]. However, number of models have been proposed to predict SWC using a limited number of soil measurements. For example, Gupta and Larson [1979] used multiple linear regression analysis of soil textural properties, organic matter, and/or dry bulk density to predict SWC [Gupta and Larson, 1979]. Alternatively, beginning with Arya and Paris [1981], models have been proposed relating particle size distribution (PSD) to water retention at particular matric potentials [Arya *et al.*, 1999; Arya and Heitman, 2015]. There are other models in this category, including the recent two-step model proposed by Jensen *et al.* [2015] that predicts SWC from saturation to oven-dryness ( $pF = 0 - 6.9$ ) using a limited number of measured textural data, organic matter content, and dry bulk density [Jensen *et al.*, 2015].

The SWC models are mostly based on empirical [Gupta and Larson, 1979; Schaap and Bouten, 1996] and physio-empirical methods [Arya and Paris, 1981; Haverkamp and Parlange, 1986]. Empirical approaches typically use statistical regressions to estimate soil water retention from soil properties. Regression models are easy to develop with sufficient data [Gupta and Larson, 1979]. Using soil texture and bulk density obtained from soil surveys conducted by USDA and UNSODA hydraulic property database [Nemes and Rawls, 2006], empirically based SWC models can also be developed [Hwang and Choi, 2006]. However, the accuracy and the reliability are limited in empirically based models because they depend on the number of data used to

adequately predict SWC properties, making these models inapplicable for biochar/soil mixtures since large data sets are not available for these mixtures. A physically based scaling method integrates spatial variations to assess soil hydraulic properties, which may overcome some limitations in empirical models since physio-empirical models are based on particle shape and the cumulative particle size distribution. Arya and Paris's [1981] work uses properties of spherical particles to estimate SWC, which was further advanced by Haverkamp and Parlange [1986] and other researchers [Mohammadi and Vanclouster, 2011; Jensen *et al.*, 2015]. Although the Arya model assumes spherical particles, it only requires information on particle sizes, masses, and dry bulk density, and thus can be used for biochar/soil mixtures where sufficient particle size and density information is available [Arya *et al.*, 1999; Arya and Heitman, 2015].

To predict the influence of biochar amendment on water retained in interpores,  $\Delta\theta_i^{inter}$ , the Arya model [Arya *et al.*, 1999; Arya and Heitman, 2015] was adopted for biochar/soil mixtures. Because of the significant intrapore volume in biochar and because the Arya model quantifies effects on interpores, the envelope density determined from MIP data [Webb, 2001; Brewer *et al.*, 2014] was used for biochar particle density to estimate the interpores. To determine the average particle density for each size fraction  $i$  of a PSD in the Arya model, a volume-weighted particle density was computed:

$$\rho_{s,i}^m = \frac{V_i^{bc}\rho_s^{bc} + V_i^s\rho_s^s}{V_i^{bc} + V_i^s} \quad [3-6]$$

where  $\rho_{s,i}^m$  is the volume-weighted particle density of the mixture for size fraction  $i$ ,  $\rho_s^{bc}$  is the envelope density of biochar,  $\rho_s^s$  is the soil particle density, and  $V_i^{bc}$  and  $V_i^s$  are the volume of biochar and soil particles, respectively, in size fraction  $i$ . Volume weighting

was used instead of mass weighting in the Arya model, since the pore radii are correlated to the number and size of spherical particles in a given size fraction in the Arya model, not the mass of particles. The volume of biochar and soil in size fraction  $i$  are:

$$V_i^{bc} = \frac{M_i^{bc}}{\rho_s^{bc}} \text{ and } V_i^s = \frac{M_i^s}{\rho_s^s} \quad [3-7]$$

where  $M_i^{bc}$  and  $M_i^s$  are the mass of biochar and soil, respectively, in each size fraction.

The particle density of the biochar mixture for size fraction  $i$  can be expressed as:

$$\rho_{s,i}^m = \frac{M_i^{bc} + M_i^s}{\frac{M_i^{bc}}{\rho_s^{bc}} + \frac{M_i^s}{\rho_s^s}} \quad [3-8]$$

The Arya model also requires the sample void ratio ( $\epsilon$ ) that is computed from:

$$\epsilon = \frac{\bar{\rho}_s - \rho_b}{\rho_b} \quad [3-9]$$

where  $\rho_b$  is the dry bulk density and  $\bar{\rho}_s$  is the average particle density of the entire sample:

$$\bar{\rho}_s = \frac{M^{bc} + M^s}{\frac{M^{bc}}{\rho_s^{bc}} + \frac{M^s}{\rho_s^s}} \quad [3-10]$$

where  $M^{bc}$  and  $M^s$  are the total dry mass of biochar and soil, respectively, in the biochar/soil mixture.

With these definitions, the fraction of the total particle volume of the mixture ( $V_i^m$ ) ( $\text{cm}^3/\text{cm}^3$ ) associated with size fraction  $i$  is:

$$V_i^m = \left( \frac{M_i^{bc}}{\rho_s^{bc}} + \frac{M_i^s}{\rho_s^s} \right) \frac{\bar{\rho}_s}{M^m} \quad [3-11]$$

where  $M^m = M^s + M^{bc}$  is the total mixture mass. This modified Arya model assumes that pore volume created by each particle size class is proportional to the volume of particles in that size class. With this assumption, the volumetric water content retained in pores associated with particle size fraction  $i$  of the mixture,  $\theta_i^m$ , is obtained from successive summations of water-filled pore volumes for that particle class and smaller:

$$\theta_i^m = \phi^m S_w^m \sum_{j=1}^i V_j^m \quad [3-12]$$

where  $\phi^m$  is the total interparticle porosity of the mixture (not total porosity) expressed as:

$$\phi^m = \frac{\epsilon}{1 + \epsilon} \quad [3-13]$$

and  $S_w^m$  is the degree of saturation of the interpores at  $pF \approx 1$ , which may be less than 1 with air entrapment. Subscript  $j$  is the index for particle size fraction and begins with the smallest particle class. Equation [3-12] is applied to each particle size fraction  $i$  to determine the volumetric water content associated with water-filled pores created by particles in that size class and smaller.

To obtain the matric potential associated with water retained in pores associated with particle size class  $i$ , the number of particles in each size class  $i$  ( $n_i$ ) is determined assuming spherical particles in each size class:

$$n_i = \frac{3M_i^m}{4\pi\rho_{s,i}^m R_i^3} \quad [3-14]$$

where  $M_i^m = M_i^{bc} + M_i^s$  is the total mass of particles in size class  $i$ , and  $R_i$  is the mean particle radius of size class  $i$ . The pore radius for each size class  $i$  ( $r_i$ ) is then estimated using a relationship that combines the attributes of natural-packed soil

structure with those of a counterpart hypothetical structure consisting of spherical particles [Arya and Heitman, 2015].

$$r_i = \sqrt{\frac{0.0717 \phi^m M_i^m}{n_i^{4/3} R_i \rho_b}} \quad [3-15]$$

The matric potential associated with water retained for particle size class  $i$ ,  $\theta_i^m$ , is then determined from  $h_i = \frac{2\sigma \cos\theta^o}{\rho g r_i}$ , where  $\rho$  is density of water and  $g$  is the gravitational constant.

This modified Arya model is used to estimate the change in water retention due to change in interpores with biochar amendment. The model is applied first to native soil and then to the biochar/soil mixture, using the same particle size classes for each medium. The estimated change in interpore space associated with biochar amendment at each matric potential  $i$  is determined from:

$$\Delta\theta_i^{inter} = \theta_i^m - \theta_i^s \quad [3-16]$$

where  $\Delta\theta_i^{inter}$  is the change in water retention due to change in interpores from the biochar addition,  $\theta_i^m$  is the Arya model-predicted volumetric water content retained in the biochar/soil mixture, and  $\theta_i^s$  is the Arya model-predicted volumetric water content retained in the reference soil.

It is important to note that in the Arya model capillary water in interpores is predicted assuming that samples have a fixed dry bulk density. Because samples in the dew-point potentiometer were loose and packed much less densely than samples for other water retention measurements, dew-point potentiometer data do not capture all capillary water in interpores. A looser packing results in larger interpores and less

retention of capillary water. Therefore, in applying the Arya model to predict water retention for  $pF < 3.85$  the entire particle size distribution that includes data from sieve analysis and the hydrometer measurements was used. In this way capillary interpore water not measured or predicted from WP4C data but that occurred in other water retention samples for  $pF > 3.85$  was accounted for.

### 3.2.4 Models for water retention in biochar-amended media

To evaluate the different mechanisms that alter water retention with biochar addition, four models are used:

Model 1: reference, native soil data without biochar addition.

$$\theta_i^m = \theta_i^s \quad [3-17]$$

Model 2: Model 1 and the effect of intrapore adsorbed and capillary water  $pF > 3.85$

$$\theta_i^m = \theta_i^s + \Delta\theta_i^{ads} \quad [3-18]$$

Model 3: Model 2 and the effect of intrapore water at  $pF < 3.85$

$$\theta_i^m = \theta_i^s + \Delta\theta_i^{ads} + \Delta\theta_i^{intra} \quad [3-19]$$

Model 4: Model 3 and changes in water stored in interpores

$$\theta_i^m = \theta_i^s + \Delta\theta_i^{ads} + \Delta\theta_i^{intra} + \Delta\theta_i^{inter} \quad [3-20]$$

Experiments described below were used to test the hypothesis that Model 4 is sufficient to describe changes in water retention when biochar is amended to soils.

### 3.3 Materials and Methods

#### 3.3.1 Biochars

Two biochars were selected: poultry litter biochar (PLBC) produced from poultry litter using a slow pyrolysis system at 300°C [Song and Guo, 2012], and Soil Reef™ biochar (SRBC) produced by heating Southern Yellow Pine in a continuous pyrolysis system at 550°C for 10 min (The Biochar Company in Berwyn, PA, USA). Additional information regarding the production and elemental composition of these biochars is found elsewhere [Teixido *et al.*, 2011; Song and Guo, 2012].

PLBC and SRBC were selected to provide particles with significantly different internal pore volume. PLBC [Song and Guo, 2012] has SSA of 2.68 m<sup>2</sup> g<sup>-1</sup>, while SRBC has SSA at 338 m<sup>2</sup> g<sup>-1</sup> [Teixido *et al.*, 2011] and thus much larger internal pore volume.

Water retention may be influenced by the transient biochar hydrophobicity [Yi *et al.*, 2015]. To reduce transient changes in contact angle, the biochars were rinsed in water to remove water soluble compounds and oven dried, steps that in prior work were shown to remove hydrophobicity [Yi *et al.*, 2015]. Each biochar was separately rinsed in deionized water three to four times at 1:50 ratio (biochar to DI water) at 50 rpm until the electrical conductivity of the rinsate was < 100 μS cm<sup>-1</sup>. The rinsed biochars were oven-dried at 105°C for 12 to 15 h and cooled to room temperature. The PLBC and SRBC were then checked for water repellency using the water drop penetration time test, and the contact angles were measured to verify that water rinsing was effective [Letey *et al.*, 2000; Yi *et al.*, 2015]. Both water drop penetration time test (< 0 sec) and the contact angle measurements (< 0.3°) showed that biochars were water wetting, and contact angles of 0.0° were assumed in all analyses.

The biochar samples were then separately sieved between #30 (0.595 mm opening) and #35 (0.5 mm opening) mesh, resulting in particles with a geometric mean diameter of 0.545 mm. The post-treated biochars are referred to as PLBC and SRBC, while samples that were sieved but not rinsed with water and oven-dried are referred to as fresh PLBC or fresh SRBC.

Following similar post-treatment procedures, a well-characterized sand (30/40 Accusand, Unimin Co., Le Sueur, MN, USA) was rinsed in deionized water until the water turned clear, oven-dried at 105°C for 24 h, and then sieved to a geometric mean diameter of 0.545 mm. Only rinsed, oven-dried, and sieved sand was used in this study.

A sandy loam agricultural soil (74% sand, 13% silt, 13% clay) was also used to understand the effect of biochar amendment on water retention. This soil was collected from the top 30 cm at the Delaware State University Outreach and Research Center (Smyrna, DE USA), dried at 105°C for 24 h, and then crushed using a mortar and rubber-tipped pestle to remove all aggregates.

The PLBC and SRBC were mixed separately with sand at 2% and 7% (w/w). The mixed biochar-sand samples were designated as 2%PLBC-Sand, 7%PLBC-Sand, 2%SRBC-Sand, and 7%SRBC-Sand. Because sand and biochar particles were sieved to the same size fraction, the biochar/sand mixtures were intended to have minimal change in interpores from biochar amendment. Thus, the biochar/sand mixtures primarily tested the effect of biochar on sorbed and capillary water in intrapores.

The sandy loam (SL) was also mixed with biochars at 2% and 7% (w/w) and samples are identified as 2%PLBC-SL, 7%PLBC-SL, 2%SRBC-SL, and 7%SRBC-SL, respectively, depending on the mass fraction of PLBC or SRBC. These PLBC and SRBC samples mixed with SL represent samples where both intrapore and interpore

spaces were modified with biochar amendment. The particle size distribution curves of biochar/sandy loam mixtures plotted based on volume and by mass are found in Appendix B.

### **3.3.2 Biochar particle density, surface area, and intrapore volume**

The particle density of sand and SL were measured using the pycnometer method [Dane and Topp, 2002]. Six to eight independent samples were tested for each material type. Duplicate samples of PLBC and SRBC were analyzed by Micrometrics Analytical Services (Norcross, GA, USA) to characterize biochar intrapores using MIP. The pore volume distribution, envelope density ( $\rho_s^{bc}$ ), and skeletal density ( $\rho_{sk}^{bc}$ ) were obtained from MIP data [ASTM Standard D4404-10, 2010]. This method was chosen since mercury is a non-wetting liquid that can penetrate pores, cracks, and crevices of porous materials up to  $\approx pF = 6.6$ , entering pores as small as  $\approx 0.003 \mu\text{m}$  in diameter [Webb, 2001].

SEM images (Hitachi S4700 Scanning Electron Microscope at 3.0 kV, Hitachi, Japan) of biochar particles were obtained to determine the largest pore diameter that allowed estimation of the mercury entry pressure for MIP data. The entry pressures required to penetrate the largest intrapore of each biochar were identified by measuring the largest pore diameters of SEM images using Image J software (National Institute of Health, Bethesda, MD, USA) [Impoco *et al.*, 2006; Hardie *et al.*, 2014] and using equation [3-1].

Brunauer, Emmett, and Teller (BET) specific surface area (SSA) measurements were carried out with an ASAP 2020 Micromeritics Physisorption Analyzer (Norcross, GA, USA) using  $N_2$ -adsorption at 77.3°K for PLBC and SRBC before and after post-treatment [Brunauer *et al.*, 1938; ASTM Standard D6556-14, 2012]. BET- $N_2$  adsorption

is a common technique utilized to obtain SSA of particles with a pore size distribution range 0.002 to 0.05  $\mu\text{m}$  [Brewer *et al.*, 2014].

### 3.3.3 Particle-size distribution

PSD were obtained for sand, SL, PLBC, and SRBC using standard methods [ASTM Standard C136-06, 2003] and plotted as both volume and mass distribution. The PSD for the biochar-mixtures were computed based upon the mass of material falling on each sieve. Using the density of sand, SL, and envelop density of biochar, the particle volume contributions from each biochar were calculated and plotted as volume distributions. The PSD were plotted using volume distribution to illustrate particle volume changes due to biochar amendment.

### 3.3.4 Intrapore adsorbed and capillary water ( $pF > 3.85$ )

The WP4C dew-point potentiometer (Decagon Pullman, WA, USA) was used to obtain data to estimate  $\theta_i^{ads}$  for  $3.85 < pF < 6.5$  (Equation [3-4]). Gubiani et al [2013] showed that the WP4, which is less precise than the WP4C, had decreasing accuracy for  $pF < 3.85$  [Gubiani *et al.*, 2013]. The WP4C manual [Decagon Devices, 2013] showed that the instrument limitation is up to  $pF = 6.48$ . Other studies have used  $pF = 4$  as the matric potential that separates the dry and the wet region of the SWRC [Campbell and Shiozawa, 1992; Jensen *et al.*, 2015]. The procedure from the instrument manufacturer was followed to obtain the adsorption and desorption isotherms for  $3.85 < pF < 6.5$  for all samples and sample mixtures: PLBC, SRBC, sand, 2%PLBC-Sand, 7%PLBC-Sand, 2%SRBC-Sand, 7%SRBC-Sand, SL, 2%PLBC-SL, 7%PLBC-SL, 2%SRBC-SL, and 7%SRBC-SL.

The measurement procedure is illustrated with PLBC. About 2 – 11 g of 100% rinsed and oven-dried PLBC was placed loosely inside a stainless steel cup, with approximately 10-13 samples prepared for analysis. To obtain the water adsorption isotherm for  $3.85 < pF < 6.5$ , deionized water was added to each cup starting with 10  $\mu\text{L}$  and incrementally increased to approximately 1000  $\mu\text{L}$ . The wet samples were covered with a plastic cap and set to equilibrate over-night before measurements in the WP4C. The dry bulk density in the WP4C ranged 1.29 – 1.65  $\text{g mL}^{-1}$  for PLBC/Sand, 1.27 – 1.72  $\text{g mL}^{-1}$  for SRBC/Sand, 1.05 – 1.36  $\text{g mL}^{-1}$  for PLBC/Sand, and 0.61 – 1.28  $\text{g mL}^{-1}$  for SRBC/SL.

Desorption isotherms for PLBC were collected by initially saturating the loosely packed samples with deionized water in the metal cups until a water film formed above the sample, followed by equilibration over-night. Samples were then dried incrementally in the oven, placed on the lab bench to cool between heating steps, and then measured using the WP4C. Some samples were also placed on the lab bench for further drying at ambient conditions and measured sequentially in WP4C. The adsorption and desorption isotherms for all samples were collected following the method describe above for PLBC. The number of data collected per individual sample and number of samples for each soil mixture are listed in Appendix B, Table B1.

WP4C measurements determine the total water potential,  $\psi$ , associated with a sample gravimetric moisture content,  $MC$ . For PLBC only, data indicated that osmotic effects were important: at high  $MC$  when a horizontal water layer formed on top of PLBC particles, the  $\psi$  was not  $\approx 0$ . For PLBC data, the measured total potential was corrected for osmotic effects following a procedure consistent with the manufacturers' guidelines [*Decagon Devices*, 2013]. At high  $MC$ , the total water potential became

linear for the PLBC as the water started to fill the cavities of biochar. The data was linearly regressed to quantify the potential required to correct for the osmotic potential. This correction is described in Figure B1, Appendix B.

### **3.3.5 Interpore capillary water ( $pF < 3.85$ )**

The sand and biochar-sand mixtures (sand, 2% PLBC-Sand, 7% PLBC-Sand, 2% SRBC-Sand, and 7% SRBC-Sand) were tightly packed dry by pouring well-mixed dry biochar or biochar/sand mixtures into a two-layer nest of screens and then into metal cores 7.7 cm inside diameter  $\times$  3.6 cm height. To pack the SL and biochar/SL mixtures, ~1 cm thick layers of sample mixtures were dry packed in metal cores 5.4 cm inside diameter  $\times$  3.0 cm height. Using a small rod, each layer was pressed down gently to avoid fracturing the biochar particles. Scratch marks were made on top of each soil layer to connect all the individual layers. This was repeated until the samples were packed tightly to the rim of the aluminum cores. The excess particles were brushed off and weighed. All samples were prepared in duplicate.

The sample cores were placed in a plastic bin then slowly saturated from below with deaired, deionized water in 1 – 3 cm increments hourly until the water level reached slightly below the height of sample cores. The plastic bin was covered overnight to saturate the samples. To reduce any interferences with the water retention measurements, calcium sulfate that is often used to reduce water evaporation was not used in this study. The results were not affected because coarse materials were used where the equilibration rate is faster than most soils.

SWC for  $pF < 3.85$  were measured by draining the saturated sample cores. The water-saturated sand and biochar-sand mixtures were placed on a tension table [Topp and Zebchuk, 1979; Dane and Topp, 2002] and matric potentials of -3, -7, -17, -22, -27,

-37 and -57 cm H<sub>2</sub>O were applied until equilibrium was reached with each step, defined as a mass change < 1% over 8 – 12 h period. Following tension table measurements, samples were transferred to a pressure plate extractor (15 bar Ceramic Plate Extractor, Cat. #1500, Soil Moisture Equipment Corp., Santa Barbara, CA, USA) and matric potentials of -129, -256, -383, -510, -764, -1400, -3500 and -6330 cm H<sub>2</sub>O were applied sequentially to the samples. Samples were weighed through time at each pressure step until equilibrium was reached, which was defined as mass change < 1% over 3 - 4 days.

Due to the different equilibration time between sand and SL, SWC for SL mixtures were measured separately [Topp and Zebchuk, 1979]. Saturated SL samples were placed on the tension table at -6.5 and at -21.5 cm H<sub>2</sub>O. Samples were weighed through time at each pressure step until equilibrium was reached, which was defined as mass change < 1% over 2 - 4 days. The samples were then transferred to the pressure plate extractor and matric potentials of -70.3, -246, -492, -1000, -1500, -2100, and -5200 cm H<sub>2</sub>O applied sequentially to the samples. Sample mass change < 1% over 6 days ( $h = -70.3$  cm H<sub>2</sub>O) to 31 days ( $h = -5200$  cm H<sub>2</sub>O) were defined as equilibrium conditions. At the completion of SWC measurements, samples were oven-dried and weighed.

### **3.4 Results & Discussion**

#### **3.4.1 Particle density**

MIP measurements were used to determine biochar envelope and skeletal densities. No biochar particle breakage was observed as mercury invaded pores at pressure steps ranging from  $pF = 0$  to  $pF = 6.5$ . The envelope densities for PLBC and SRBC are reported in Table 3-1:  $\rho_s^{bc} = 0.96$  g mL<sup>-1</sup> and 0.57 g mL<sup>-1</sup> for PLBC and

SRBC, respectively. Because the envelope density is 1.7 times larger for PLBC than SRBC, amending a soil with the same biochar mass will result in 70% more SRBC than PLBC particles. This may cause much different modifications to the interpore volume. The skeletal densities for PLBC and SRBC are  $\rho_{sk}^{bc} = 1.72 \text{ g mL}^{-1}$  and  $1.39 \text{ g mL}^{-1}$  for PLBC and SRBC, respectively. SRBC's smaller envelope and skeletal densities indicate that it has a larger total intrapore volume, which is discussed further below. From pycnometer measurements for sand and SL, the skeletal density (assumed equal to envelope density) was  $2.66 \pm 0.001 \text{ g mL}^{-1}$  and  $2.42 \pm 0.02 \text{ g mL}^{-1}$  for sand and SL, respectively.

### **3.4.2 Biochar specific surface area**

The SSA of biochars are reported in Table 3-1 and were affected by rinsing in deionized water. Rinsing increased SSA from  $0.8 \text{ m}^2 \text{ g}^{-1}$  to  $1.53 \text{ m}^2 \text{ g}^{-1}$  and from  $41 \text{ m}^2 \text{ g}^{-1}$  to  $350 \text{ m}^2 \text{ g}^{-1}$  for PLBC and SRBC, respectively. With vigorous rinsing, biochar may fracture and open inaccessible pores to create higher SSA and larger intrapores [Spokas *et al.*, 2014]. Because higher SSA indicates more sorption sites, SRBC is expected to adsorb significantly more water than PLBC.

### **3.4.3 Biochar intrapore volume**

Typical SEM images of PLBC and SRBC biochars are shown in Appendix B, Figure B2. From the analysis of these and other images, the largest pores are  $\approx 33 \text{ }\mu\text{m}$  in diameter for both biochars. While invasion pressures were measured for mercury, they were converted to  $pF$  for water entry into air-filled biochar, assuming a contact angle of  $0^\circ$  and  $130^\circ$  [Giesche, 2006] for air-water and air-mercury systems, respectively. The Young-Laplace equation was also used to estimate the pore diameter at each invasion

pressure step. Cumulative invaded volumes are plotted against  $pF$  (air-water system) in Figure 3-1a, and invaded pore volumes associated with equivalent pore diameters (cylindrical pores assumed) are plotted in Figure 3-1b. The plotted pore diameter range 33  $\mu\text{m}$  to 0.1  $\mu\text{m}$  represents the pressure range  $1.9 < pF < 4.4$ . Most of the intrapore volume occurs between  $1.9 < pF < 4.4$  for PLBC and  $1.9 < pF < 3.5$  for SRBC. The intrapore filling was linear for PLBC and sigmoidal for SRBC, indicating that SRBC intrapore volume is not distributed uniformly across pore sizes (Figure 3-2b). The total intrapore volume is 0.23  $\text{mL g}^{-1}$  for PLBC and 0.83  $\text{mL g}^{-1}$  for SRBC, which is consistent with the higher SSA measured for SRBC.

#### **3.4.4 Particle size distribution**

While the addition of SRBC or PLBC to sand will not change the PSD since sand and biochar particles are sieved to the same size, biochar amendment to SL will alter particle and pore size distributions. The PSDs of SL and biochar-amended SL are shown in Figure 3-2. They are plotted by mass in Figure 3-2a for PLBC/SL mixtures and Figure 3-2b for SRBC/SL mixtures, and by volume in Figure 3-2c for PLBC/SL mixtures and Figure 3-2d for SRBC/SL mixtures using the envelope density. The PSD was measured for SL and computed for biochar/SL mixtures, using measured PSD for SL and known biochar particle sizes and masses and the envelope density of biochars. For PLBC and SRBC, biochar addition has a minimal effect on PSD for 2% (w/w) by mass as shown in Figure 3-2a and Figure 3-2b. However, biochar amendment shifts the PSD mean particle diameter for mass-based PSD from  $D_{50} \approx 0.25$  to  $D_{50} \approx 0.42$  for 7% (w/w). Using the envelope density of biochar to plot the PSD as a function of % finer by volume, a larger shift in particle diameter is observed, especially between SRBC (Figure 3-2d) versus PLBC (Figure 3- 2c) for the same amendment of biochar. SRBC

contributes about 10% more particles by volume than PLBC at 7% (w/w) amendment. At the same particle diameter, % finer by volume is lowered with biochar amendment: the addition of biochar results in a reduction of small particles in biochar/SL mixtures. If PSD is determined based on mass of particles, though, there is no observable difference between PSD's with PLBC and SRBC amendment.

### **3.4.5 Porosity**

Using the measured dry bulk densities of biochar/sand and biochar/SL mixtures in the water retention cells, biochar envelope and skeletal densities (Table 3-1), and the particle densities of sand and SL, interpore and intrapore porosities of the water retention cell samples were computed and are reported in Table 3-2. Adding biochar to sand, sieved to the same particle diameter, had a negligible influence on interpore volume. For biochar amendment to SL, though, interpore volumes were altered. At 2% biochar addition, interpore porosities changed slightly, decreasing by 1.0% for PLBC and increasing by 3.3% for SRBC. At 7% biochar addition, more significant changes occurred: interpore porosity decreased by 5.6% and 6.3% for PLBC and SRBC, respectively. The decrease in interpore porosity with biochar amendment was expected, since relatively large biochar particles ( $0.545 \text{ mm} < D < 0.595 \text{ mm}$ ) were amended to SL, displacing silt and clay size material.

While biochar amendment at 7% (w/w) decreased interpores in SL, total porosities were increased for all biochar amendments in both sand and SL. On a relative basis, total porosities increased most for biochar-amended sand: increasing by 13.5 and 27.0% for 7% (w/w) PLBC and SRBC, respectively. Similarly, 7% (w/w) biochar amendment to SL resulted in a 6.1 and 16.2% increase in total porosity for PLBC and SRBC, respectively. These results illustrate two factors that affected total sample

porosity: (1) PLBC had smaller intrapore volume than SRBC, so equal masses added to sand where there was minimal change in interpore porosity resulted in smaller increases in total porosity for PLBC than SRBC amendment; and (2) although both PLBC and SRBC resulted in reductions in interpore porosity at 7% (w/w) in SL, the contribution of intrapore porosity offset these reductions causing a net increase in total sample porosity for both biochars. As will be shown below, the interplay between intrapore and interpore volumes both affect water retention in biochar-amended media.

### 3.4.6 Water retention $pF > 3.85$

The adsorption and desorption isotherms of rinsed biochar are shown in Figure 3-3. Hysteresis in sorption was not observed for these biochars, while it has occurred for others [Arthur *et al.*, 2015]. The non-hysteretic behavior may be the result of biochar aging in the lab, where biochars were rinsed, oven-dried, and sieved opening up pores not present in raw biochar. Figure 3-3 shows very different curvature of sorption isotherms: the PLBC sorption isotherm is concave up whereas the SRBC isotherm is concave down. SRBC retains more water than PLBC over the range of  $5.6 < pF < 6.5$ , while for  $4.4 < pF < 5.6$  PLBC adsorbs more. However, when PLBC data are corrected for osmotic effects such that matric potential rather than total potential is plotted, water retention for SRBC is larger than that for PLBC for most matric potentials, consistent with the larger SSA measured for SRBC.

Similar sorption isotherms were measured for sand and SL, and for these media amended with 2% and 7% PLBC. Water sorption data for PLBC-Sand are shown in Figure 3-4a, where measured water potential is plotted against volumetric water content ( $\theta^{ads} = (MC M_t^m)/(V_t \rho_w)$ ) of the packed sample in the tension table and the pressure plate extractor. While adsorption onto sand was negligible, amendment with PLBC

increased water adsorption dramatically. To estimate  $MC$  and  $\theta^{ads}$  of these biochar-amended sands,  $MC$  for PLBC and sand measured alone were used in equations [3-3] and [3-4] to generate the model predictions in Figure 3-4a. The model performed reasonably well for 2% PLBC-Sand, but over-predicted sorbed water for 7% PLBC-Sand at low  $pF$ . Osmotic pressures were small and assumed negligible in model-predictions for the PLBC-sand mixtures. The scatter in data is more significant for water sorption onto PLBC-sand mixtures than measurements of PLBC or sand alone, which may be due to limitations in achieving a representative sample with the 7-8 cm<sup>3</sup> sample volume of the dew point potentiometer.

Water sorption isotherms for 2% and 7% PLBC-SL mixtures are shown in Figures 3-4b and 3-4c. Because water sorption onto SL was significant, a regression line fitting these data is shown for reference. Model predictions for adsorbed water onto PLBC-SL mixtures using equations [3-3] and [3-4] are also shown, where osmotic pressures were assumed negligible. Overall, model predictions are in reasonable agreement with data, although the model underpredicted adsorption in 2% PLBC-SL for  $5.5 < pF < 6.5$ .

Water sorption isotherms for SRBC amended to sand and SL are shown in Figure 3-5. Because SRBC adsorbs more water than PLBC, SRBC-sand mixtures showed greater sorption than PLBC-sand mixtures. Model predictions (equations [3-3] and [3-4]) slightly overestimated adsorbed water for SRBC-sand mixtures. When amended to SL, SRBC increased water sorption over SL alone, although the data suggest a slight decrease in adsorption for 2% SRBC-SL near  $pF = 6$ . While there is considerable scatter in the data, overall model predictions captured the effect of SRBC amendment on water sorption.

The data from Figures 3-3 to 3-5 were used in equations [3-3] and [3-4] for the adsorption regions of the SWC ( $\theta^{ads}$ ) reported below for biochar/soil mixtures.

### 3.4.7 Soil water characteristic

#### 3.4.7.1 PLBC in sand

The SWC's for sand and PLBC-Sand are shown in Figure 3-6a to Figure 3-6c: the solid black line is fitted to sand data while individual data points for PLBC-sand experiments are shown. PLBC amendment at both 2% and 7% increased volumetric water content at all  $pF$ , with the largest effect near sample saturation. PLBC increased water retention by adsorbing more water and retaining additional capillary water in biochar intrapores. Predicted SWC from Model 1 (equation [3-17]) that describes only the native soil is shown in Figure 3-6a, while Model 2 (equation [3-18]) that includes the increase in water retention from adsorbed and capillary water at  $pF > 3.85$  is shown in Figure 3-6b. Predictions for water sorption were based on WP4C measurements of sand and biochar alone, using equations [3-3] and [3-4]. By accounting for adsorbed water, Model 2 described data well for  $2.5 < pF < 6.5$ , with model error increasing significantly for  $pF < 2$ . Model 3 (equation [3-19]) includes the increase in water retention from adsorbed water and capillary water ( $pF > 3.85$ ) and the additional capillary water in large biochar intrapores ( $pF < 3.85$ ) and is shown in Figure 3-6c. Overall, Model 3 improved predictions significantly with RMSE decreasing by  $\approx 50\%$  for both 2% and 7% PLBC amendment (Table 3-3). However, the inclusion of capillary water in biochar for  $pF < 3.85$  resulted in over-prediction of water retention for  $1.8 < pF < 3.85$  (Figure 3-6c) for the 7% PLBC. Biochar shape may have influenced the reduction in water retention of the samples in this region at 7% amendment. Although

PLBC particles are of somewhat different shape than sand, because both PLBC and sand were sieved to the same size for these packings changes in interpore volume were minor. Thus, accounting for only the effects of biochar intrapores on water retention (hygroscopic + capillary retention) was sufficient to predict the influence of PLBC amendment on water retention.

### **3.4.7.2 SRBC in sand**

The SWC's for sand and SRBC-Sand are shown in Figure 3-7a through Figure 3-7c: the solid black line is fitted to sand data while individual data points for SRBC-sand experiments are shown. While PLBC increased total porosity (and volumetric water content at saturation) to 0.395 at 7% amendment, SRBC increased total porosity to 0.442 at this same application rate (Table 3-2). This is because the intrapore volume in SRBC is almost 4 times larger than that for PLBC (Table 3-1).

When Model 2 was applied to account for only the increase in water retention from adsorbed and capillary water at  $pF > 3.85$  from SRBC amendment, model predictions are only improved for  $3.85 < pF < 6.5$  (Figure 3-7b). Water retention was significantly under-predicted for  $pF < 3.85$ . When Model 3 was applied that accounts for the increase in water retention from adsorbed water and capillary water ( $pF > 3.85$ ) and the additional capillary water in large biochar intrapores ( $pF < 3.85$ ), model predictions captured most of the increase in water retention at both 2% and 7% amendment (Figure 3-7c). RMSEs were  $\approx 30\%$  smaller for Model 2 than Model 1, and  $\approx 50\%$  smaller for Model 3 than Model 1 (Table 3-3).

The one region where Model 3 did not describe water retention well was for 7% SRBC-sand at  $2.5 < pF < 3.85$ . Here, Model 3 predicted less water retention than measured. The discrepancy between Model 3 and data may be due to inadequate time

for sample equilibration: more time may have been required to drain capillary water retained in SRBC intrapores.

### **3.4.7.3 PLBC in sandy loam**

The SWC's for SL and PLBC-SL are shown in Figure 3-8a through 3-8d. Application of 2% PLBC to SL decreased water retention for  $0.5 < pF < 3.5$ . While application of 7% PLBC increased water retention in SL for  $0.5 < pF < 3.5$ , the effect was much less significant than observed in PLBC-sand samples (Figure 3-6). The reason for the dramatic smaller impact of PLBC amendment on water retention is that large PLBC particles amended to SL replaced smaller particles, reducing interpore volume. While PLBC amendment increased total porosity from 0.396 (SL) to 0.405 (2% PLBC) and 0.420 (7% PLBC), interpore porosity decreased from 0.396 (SL) to 0.392 (2% PLBC) and 0.377 (7% PLBC). Figure 3-2c also shows that the finer particles were reduced with higher application of PLBC, suggesting smaller water retention for small interpore radii. Thus, the beneficial effects of biochar intrapores were mitigated in PLBC-SL mixtures, since biochar amendment decreased interpore porosity. If PLBC amendments were made with smaller particles, the reduction in interpore porosity might have been reduced or eliminated, as Model 4 predicts. These results illustrate the interplay between biochar particle size and native soil PSD.

Models 2, 3, and 4 were used to predict the effect of PLBC amendment on water retention in sandy loam and results are shown in Figures 3-8b-d and RMSEs for model fits reported in Table 3-3. While including the influence of water adsorption and capillary water retention in PLBC intrapores (Models 2 and 3) improved for 7% PLBC-SL, these models resulted in poorer predictions for 2% PLBC-SL compared to Model 1. When Model 4 was employed that includes PLBC's influence on both intrapores

(adsorbed and capillary water) and interpores (Arya model), model fits were significantly improved with RMSEs decreasing from Model 1 by 66% and 61% for 2% and 7% PLBC, respectively.

It is important to note that total sample porosities at  $pF = 0.0$  for PLBC-SL samples were larger than measured volumetric water contents at  $pF = 1$  for both 2% and 7% amendments (Figure 3-8a). This indicates air entrapment. Model 4 accounts for air entrapment by fixing the maximum volumetric water content to that measured at  $pF \approx 1$ . If instead air entrapment was assumed negligible, Model 4 would perform more poorly and significantly over-predict water retention at small  $pF$ .

#### **3.4.7.4 SRBC in sandy loam**

The SWC's for SL and SRBC-SL are shown in Figure 3-9a through 3-9d. Similar to PLBC, the influence of SRBC amendment on water retention in SL was much less than in sand (Figure 3-7a-c). However, while 2% PLBC amendment resulted in less water retention in SL over a wide  $pF$  range ( $0.5 < pF < 3.5$ ), 2% SRBC amendment decreased water retention only for  $2.5 < pF < 3.5$ . Overall, water retention was improved more significantly with SRBC than PLBC amendment because of greater intrapore volume of SRBC (Table 3-1) and smaller air entrapment at  $pF \approx 1$ .

Models 2, 3, and 4 were used to predict the effect of SRBC amendment on water retention and results are shown in Figures 9b-d, and RMSEs for model fits are reported in Table 3-3. Similar to PLBC-SL mixtures, while including the influence of water adsorption and capillary water retention in SRBC intrapores, Models 2 and 3 improved model fits for 7% SRBC-SL, these models resulted in no improvement in prediction of 2% SRBC-SL data. When Model 4 was employed that included SRBC's influence on both intrapores (adsorbed and capillary water) and interpores (Arya model), model fits

were significantly improved with RMSEs decreasing from Model 1 by 47% and 67% for 2% and 7% SRBC, respectively.

It is important to note that improvement in the Model 4 prediction is due to two effects: accounting for changes in interpore volume and air entrapment at  $pF \approx 1$ . Similar to PLBC-SL samples, the sieved SRBC lowered the amount of fine particles in sandy loam (Figure 3-2d) and decreased the interpore volume. To reduce or eliminate the reduction in interpore volume, finer biochar particles could be added to sandy loam. Changes in interpore volumes were estimated in the Arya model using the PSD and dry bulk density. Air entrapment can be determined directly from water retention measurements, but is difficult to predict a priori.

#### **3.4.7.5 Available water capacity**

Available water capacity can be defined as water retained between  $pF = 1.8$  (field capacity) to 4.2 (wilting point), and was determined for the samples in this study using measurements and the model predictions: Model 3 for sand/biochar mixtures, and Model 4 for SL/biochar mixtures. The predicted versus measured plot is of averages of the samples and presented in Figure 3-10. The available water capacity increased in sand/biochar, where higher water capacity (0.06 to 0.1) was found in mixtures with higher biochar content. However, in SL/biochar mixtures, available water capacity decreased with PLBC amendment (-0.005 to -0.026). The available water capacity was lower in PLBC/SL than SRBC/SL mixtures since the water stored in intrapores is higher in SRBC than PLBC. Biochars can increase the available water capacity in coarse materials [Abel *et al.*, 2013; Kerre *et al.*, 2017], and Sun *et al.* [2014] suggests that biochars increase soil macropores to enhance water retention [Sun and Lu, 2014]. However, when organic matter was present  $> 9.1\%$  in loamy sand, available water

capacity was reduced with biochar amendment [Abel *et al.*, 2013]. In soils with high available water capacity, such as soils with high contents of clays or organic matter, biochar can further reduce available water capacity [Tryon, 1948; Abel *et al.*, 2013].

Models 3 and 4 were able to predict the direction and magnitude of the observed change in available water capacity reasonably well, as shown in Figure 3-10. For all but the 2% PLBC/SL mixture, biochar amendment resulted in an increase in available water content. The results in Figure 3-10 suggest that changes in available water capacity because of biochar amendment to an existing soil can be predicted reasonably well if the following information is available: water retained by pure biochar and soil for  $pF > 3.85$ , PSD of both soil and biochar, MIP measurements of biochar to quantify intrapore volume and biochar density, and estimates of dry bulk density and air entrapment in the biochar/soil mixture.

### **3.5 Conclusions**

In this work a conceptual model for the effect of biochar amendment on water retention in soil was proposed that includes three processes: changes in water retention due to adsorption in biochar intrapores, changes due to capillary water filling intrapores, and changes due to modification of interpores. This conceptual model was then tested on two types of biochar added to sand or sandy loam at two different mass fractions. Four different model predictions to water retention data were tested: Model 1 is water retention in the reference soil, Model 2 adds to the first model changes in retained water from adsorbed and capillary water for  $pF < 3.85$ , Model 3 adds the additional capillary water retained in biochar intrapores, and Model 4 adds changes in water retention due to alteration of interpores.

The impact of biochar amendment on adsorbed and capillary water for  $pF < 3.85$  was tested with mixtures of biochar/sand and biochar/sandy loam. A simple mixing model that incorporates the mass fractions of soil and biochar and the independently-measured retention properties of each material worked well.

Mixtures of biochar and sand where there were minimal change in interpore porosity permitted testing the impact of additional water retained in biochar intrapores on water retention. Model 3 described these data well, demonstrating that mercury intrusion porosimetry and dew point potentiometer measurements of biochar were sufficient to predict biochar impact on water retention from intrapores.

When biochar was amended to sandy loam, changes in both intrapores and interpores were important. Amending sandy loam with 2% (w/w) PLBC resulted in a reduction in water retention for  $0.5 < pF < 3.5$ . While PLBC increased water storage in biochar intrapores, it resulted in a decrease in interpore porosity and water retention in interpores in sandy loam, which exceeded the increase from intrapores. At 7% PLBC amendment and for both 2% and 7% SRBC amendment, though, biochar amendment increased water retention. Model 4 that accounted for both changes to intrapores and interpores described these data well, although the model required air entrapment data.

In addition to advancing our conceptual understanding of how biochar alters water retention in soil, this work provides the first example of using independent measurements of biochar and soil properties to predict water retention in biochar-amended media. For biochar, mercury intrusion porosimetry measurements, dew point potentiometer data, and the particle size distribution were needed. For soil, dew point potentiometer data, particle density, particle size distribution, and water retention data were required. In addition, the dry bulk density of the biochar/soil mixture was needed

and some estimate of the degree of air entrapment. These data are not expensive to collect and can be readily obtained. Alternatively, only biochar measurements may be made and models used to estimate the required soil properties. With such an approach, estimates of the benefit of biochar amendment on water retention for different biochar/soil mixtures can be made independent of direct measurement.

One limitation of this work is that the experiments and models neglect soil aggregation, which biochar has been shown to impact in some settings. Aggregate formation is a naturally-occurring process influenced by soil chemistry and microbial activity, both of which are affected by biochar. In settings where soil aggregation is significant, the models developed in this work will not apply. Future work is necessary to develop models for understanding and predicting the influence of biochar amendment on soil aggregation and subsequent effects on water retention.

Table 3-1: Biochar specific surface area, intrapore volume, intrapore air-entry pressure, and biochar densities

Sample type <sup>a</sup>	Envelope density	Skeletal density	Specific surface area	Intrapore volume	Intrapore air-entry pressure	Pore diameter at air entry pressure
	g mL <sup>-1</sup>	g mL <sup>-1</sup>	m <sup>2</sup> g <sup>-1</sup>	mL g <sup>-1</sup>	$pF = \log  -h $ cm-H <sub>2</sub> O	μm
Fresh PLBC	n.a. <sup>b</sup>	n.a.	0.8 ± 0.2	n.a.	n.a.	n.a.
PLBC	0.96 ± 0.01 <sup>c</sup>	1.72 ± 0.04	1.53 ± 0.15	0.23 ± 0.01	1.9 ± 0.1	33 ± 1
Fresh SRBC	n.a.	n.a.	41 ± 19	n.a.	n.a.	n.a.
SRBC	0.57 ± 0.01	1.39 ± 0.03	350 ± 30	0.83 ± 0.01	1.9 ± 0.1	33 ± 1

<sup>a</sup> PLBC = poultry litter biochar, SRBC = Soil Reef biochar

<sup>b</sup> not available

<sup>c</sup> standard error

Table 3-2: Porosities and dry bulk density of samples with different biochar mass fractions

Sample type	Interpore porosity	Total porosity	Bulk density g cm <sup>-3</sup>
Sand		0.348 ± 0.001	1.74 ± 0.01
2% PLBC-Sand <sup>a</sup>	0.349 ± 0.001 <sup>e</sup>	0.365 ± 0.001	1.67 ± 0.01
7% PLBC-Sand	0.346 ± 0.001	0.395 ± 0.001	1.55 ± 0.01
2% SRBC-Sand <sup>b</sup>	0.350 ± 0.001	0.383 ± 0.001	1.61 ± 0.01
7% SRBC-Sand	0.342 ± 0.001	0.442 ± 0.001	1.40 ± 0.01
Sandy Loam		0.396 ± 0.001	1.46 ± 0.01
2% PLBC-SL <sup>c</sup>	0.392 ± 0.001	0.405 ± 0.001	1.43 ± 0.01
7% PLBC-SL	0.377 ± 0.004	0.420 ± 0.004	1.36 ± 0.01
2% SRBC-SL <sup>d</sup>	0.409 ± 0.002	0.437 ± 0.002	1.34 ± 0.01
7% SRBC-SL	0.371 ± 0.001	0.460 ± 0.001	1.24 ± 0.01

<sup>a</sup>PLBC-Sand = poultry litter biochar in 30/40 Accusand at 2% and 7% by weight

<sup>b</sup>SRBC-Sand = Soil Reef™ biochar in 30/40 Accusand at 2% and 7% by weight

<sup>c</sup>PLBC-SL = poultry litter biochar in sandy loam (SL) at 2% and 7% by weight

<sup>d</sup>SRBC-SL = Soil Reef™ biochar in sandy loam at 2% and 7% by weight

<sup>e</sup> ± indicates standard error

Table 3-3: Root-mean-square errors of biochar water retention models

Sample type	Sand			Sandy Loam			
	Model 1 <sup>c</sup>	Model 2 <sup>d</sup>	Model 3 <sup>e</sup>	Model 1	Model 2	Model 3	Model 4 <sup>f</sup>
2% PLBC <sup>a</sup>	0.015	0.009	0.008	0.012	0.015	0.016	0.007
7% PLBC	0.031	0.015	0.017	0.011	0.014	0.020	0.008
2% SRBC <sup>b</sup>	0.016	0.011	0.008	0.012	0.013	0.014	0.008
7% SRBC	0.059	0.042	0.023	0.020	0.016	0.021	0.011

<sup>a</sup> PLBC = poultry litter biochar at 2% and 7% by weight

<sup>b</sup> SRBC = Soil Reef™ biochar at 2% and 7% by weight

<sup>c</sup> Model 1: reference soil only

<sup>d</sup> Model 2: reference soil + biochar intrapore water pF > 3.85

<sup>e</sup> Model 3: reference soil + biochar intrapore water pF > 3.85 + biochar intrapore water pF < 3.85

<sup>f</sup> Model 4: reference soil + sorption + biochar intrapore water pF > 3.85 + biochar intrapore water pF < 3.85 + change in inter pore volume

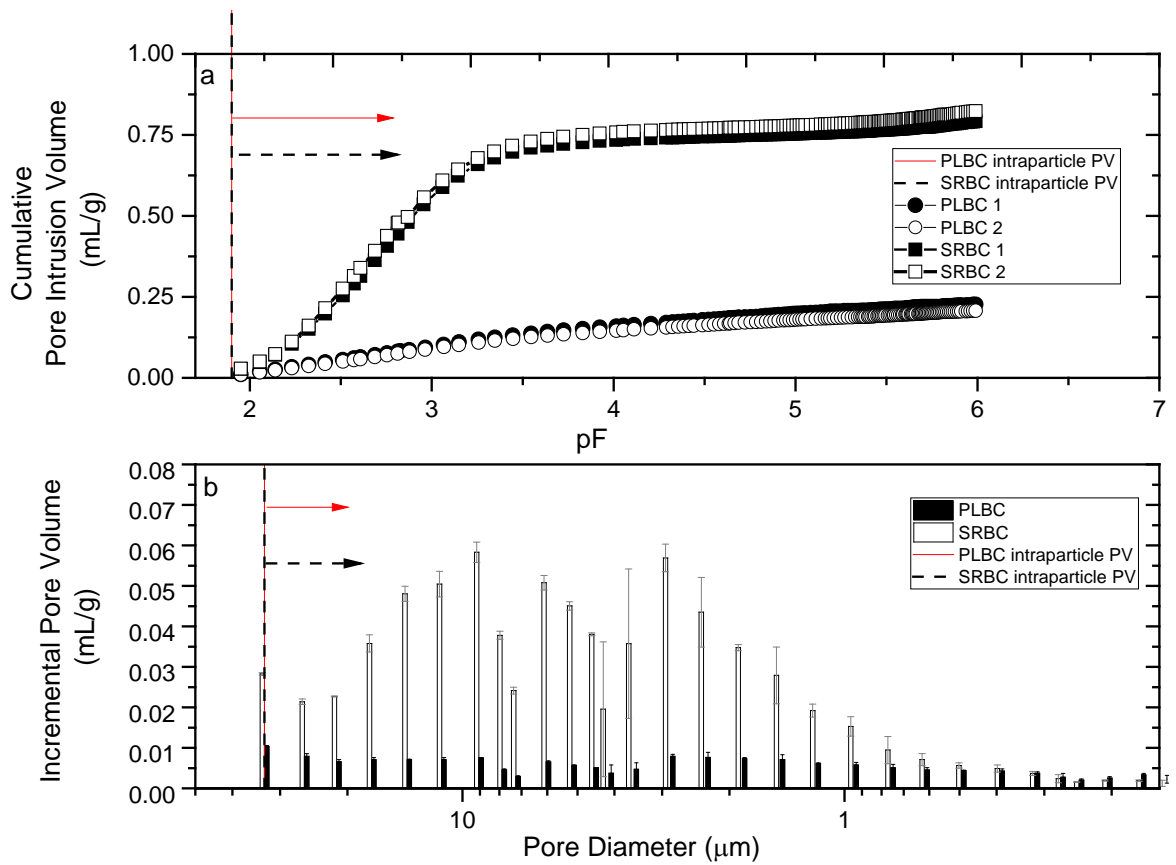


Figure 3-1: Intrapore volumes from mercury intrusion porosimetry: (a) cumulative intrapore volumes from duplicate measurements of poultry litter biochar (PLBC) (●/○) or Soil Reef™ biochar (SRBC) (■/□), where  $pF$  for mercury-air system are converted to  $pF$  for air-water system; and (b) pore volume distribution of PLBC and SRBC.

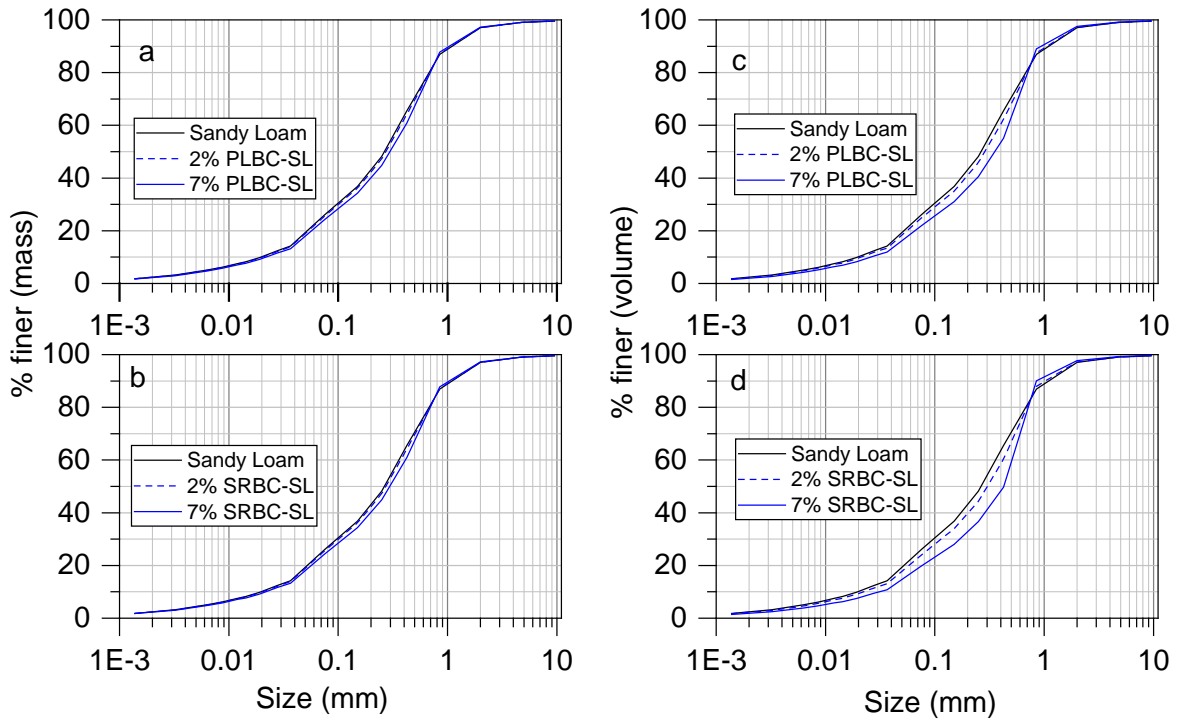


Figure 3-2. Particle size distribution by mass (a, b) and volume (c, d) of PLBC in sandy loam (SL) and SRBC in sandy loam at 2% and 7% by weight, respectively.

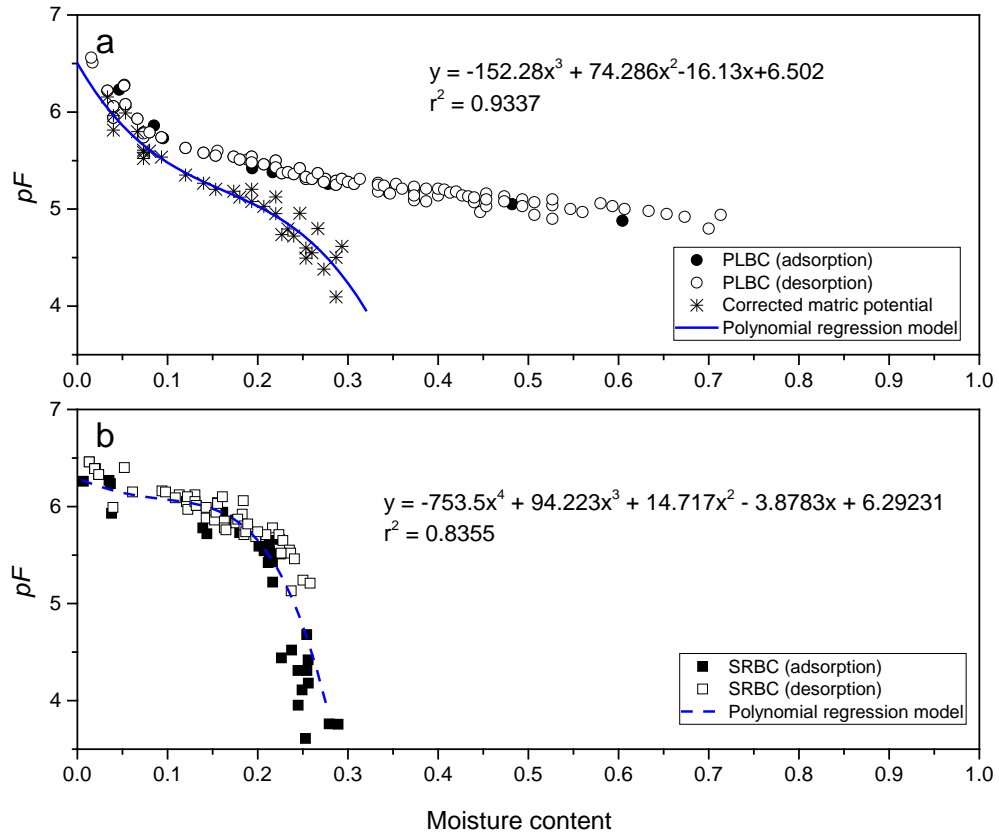


Figure 3-3. Water sorption data for biochar: (a) total and matric potential measurements for PLBC, and (b) total potential measurements for SRBC where osmotic effects were negligible.

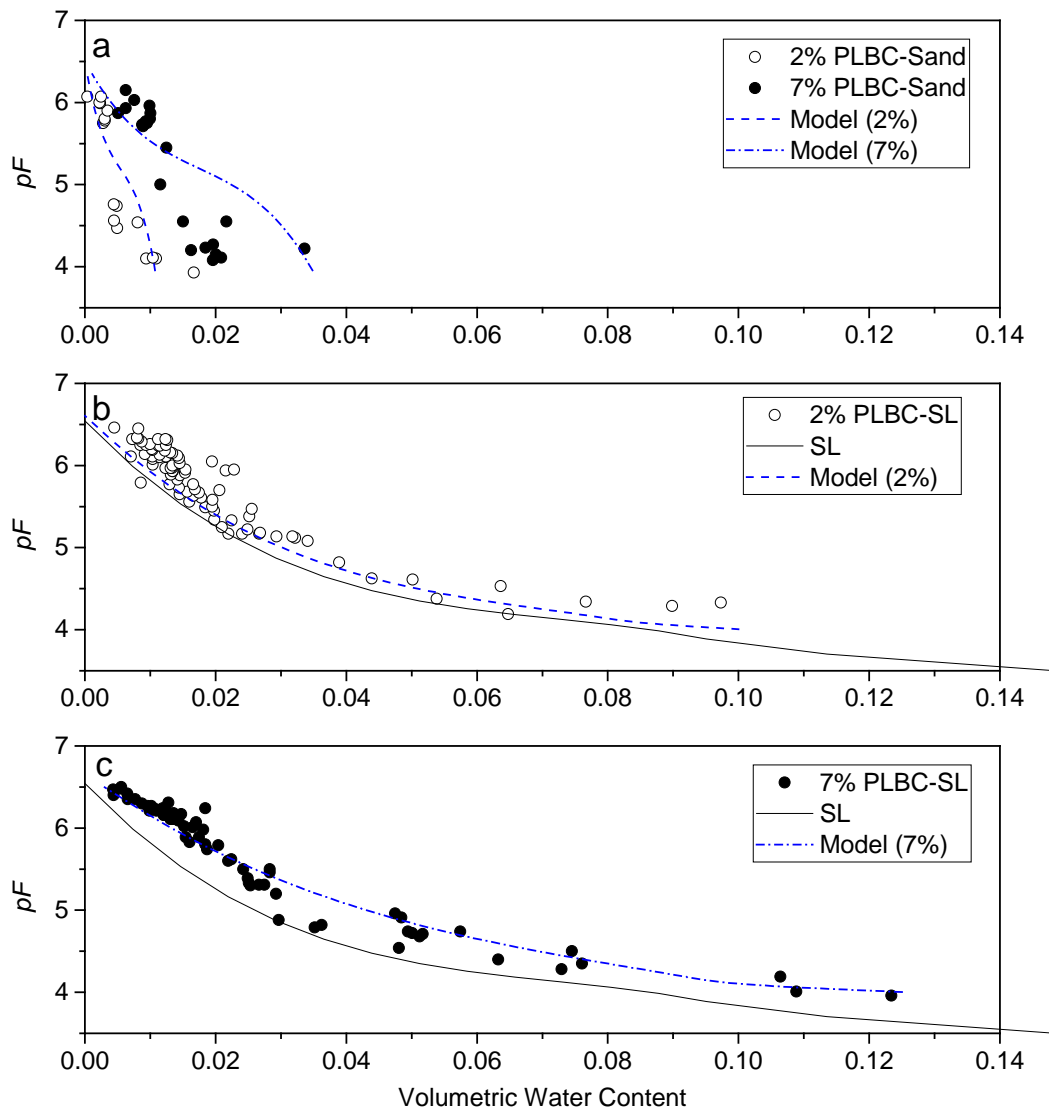


Figure 3-4. Water sorption data for PLBC/sediment mixtures and model predictions: (a) 2 and 7% (w/w) PLBC in sand, (b) 2% PLBC in sandy loam (SL), and (c) 7% (w/w) PLBC in SL. Solid lines in (b) and (c) are best-fits to SL data.

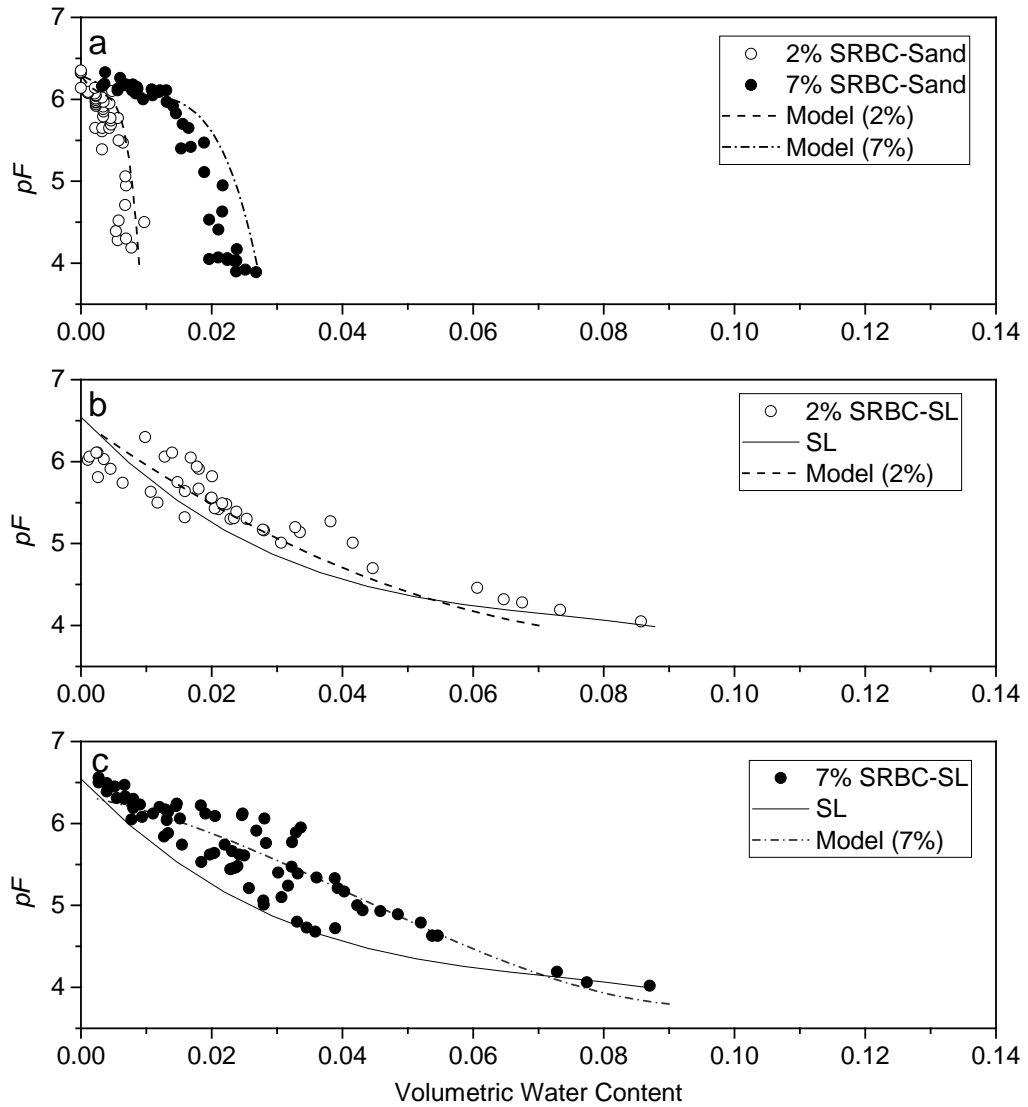


Figure 3-5. Water sorption data for SRBC/sediment mixtures and model predictions: (a) 2 and 7% (w/w) SRBC mixtures in sand, (b) 2% SRBC in sandy loam (SL), and (c) 7% (w/w) SRBC in SL. Solid lines in (b) and (c) are best-fits to SL data.

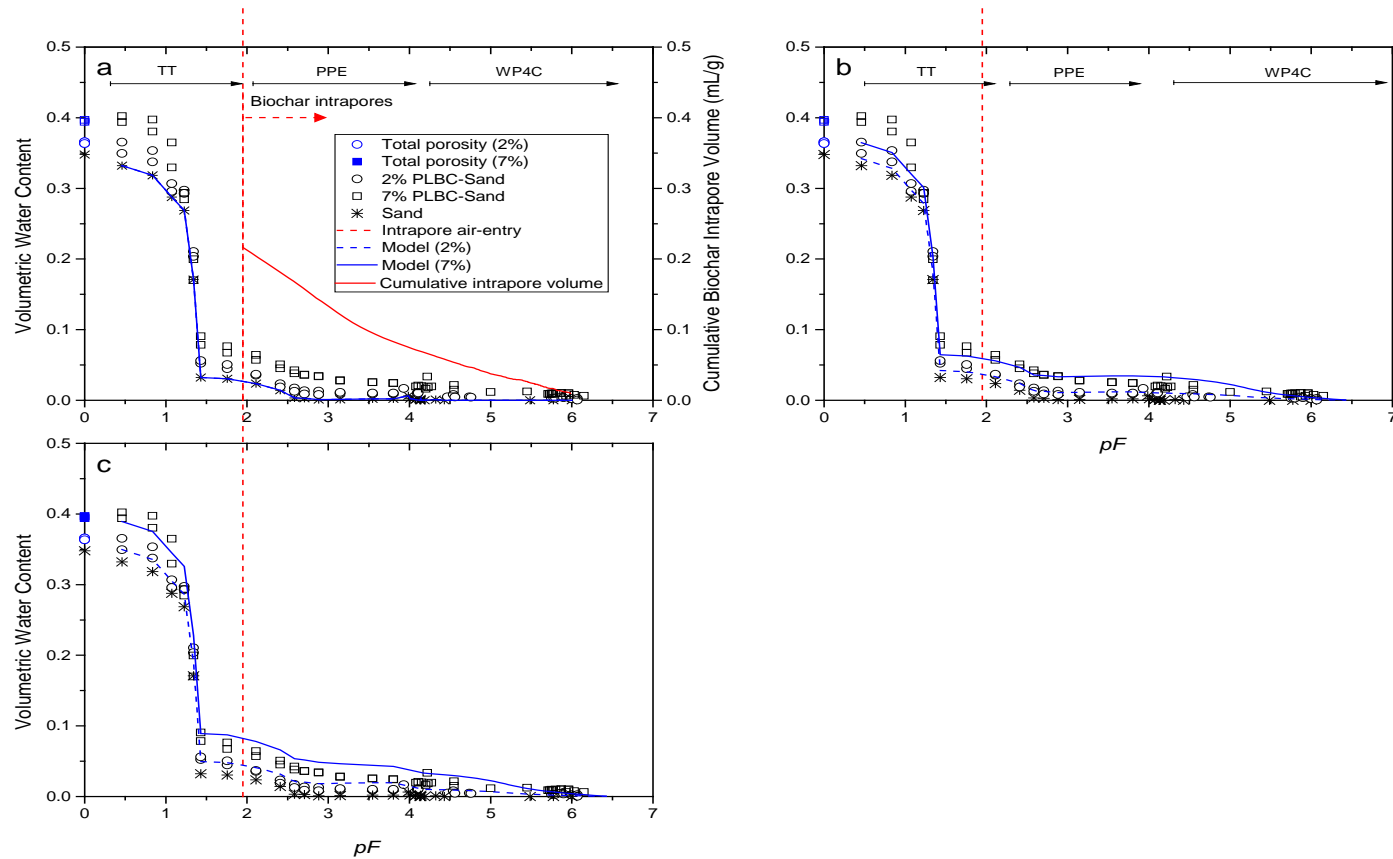


Figure 3-6. Soil water retention data and model predictions for mixtures of PLBC and sand. Data collected from tension table (TT), pressure plate extractor (PPE), or dew point tensiometer (WP4C). (a) Model 1, reference soil; (b) Model 2, reference soil + intrapores  $pF > 3.85$ ; and (c) Model 3, reference soil + all intrapores.

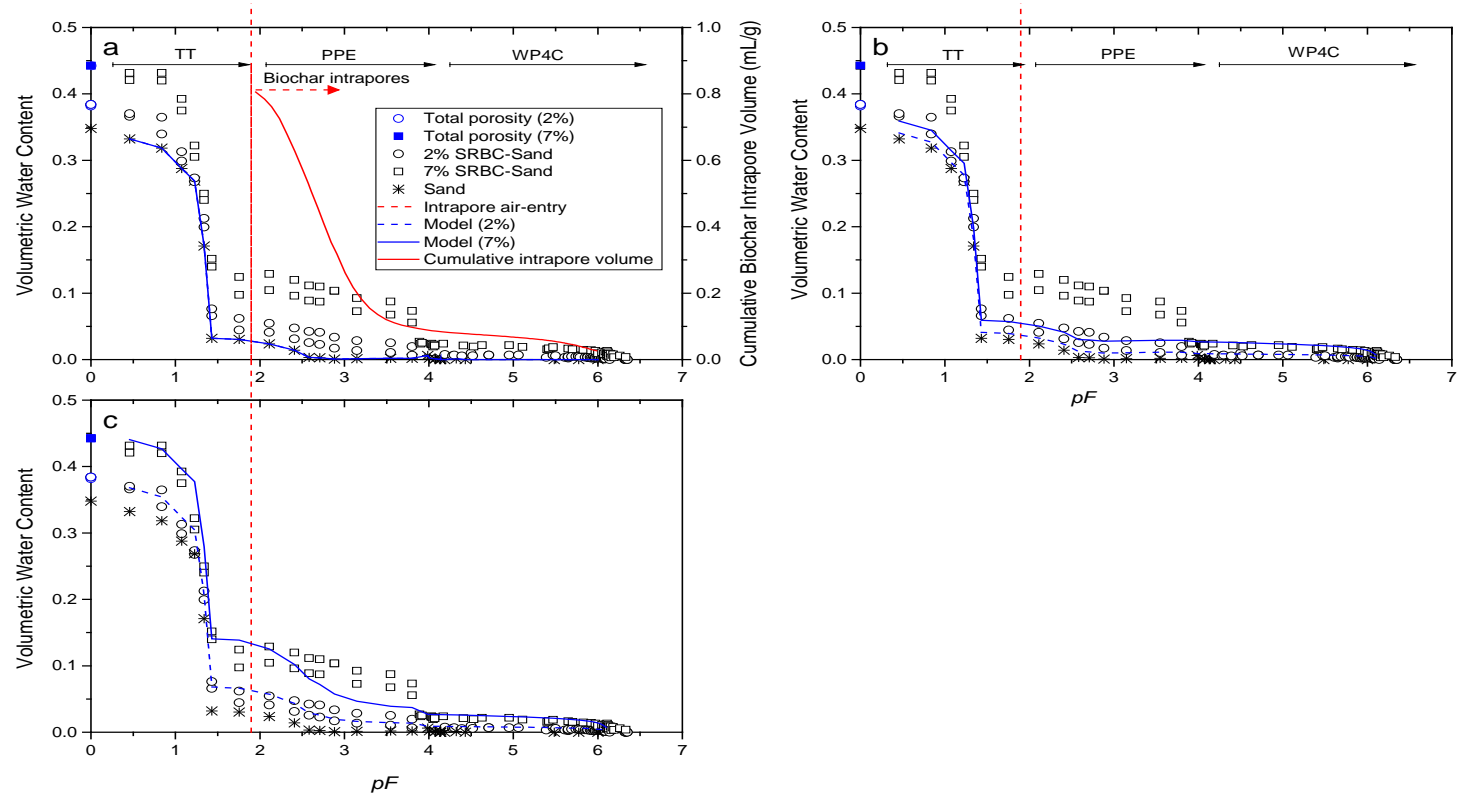


Figure 3-7. Soil water retention data and model predictions for mixtures of SRBC and sand. (a) Model 1, reference soil; (b) Model 2, reference soil + intrapores  $pF > 3.85$ ; and (c) Model 3, reference soil + all intrapores.

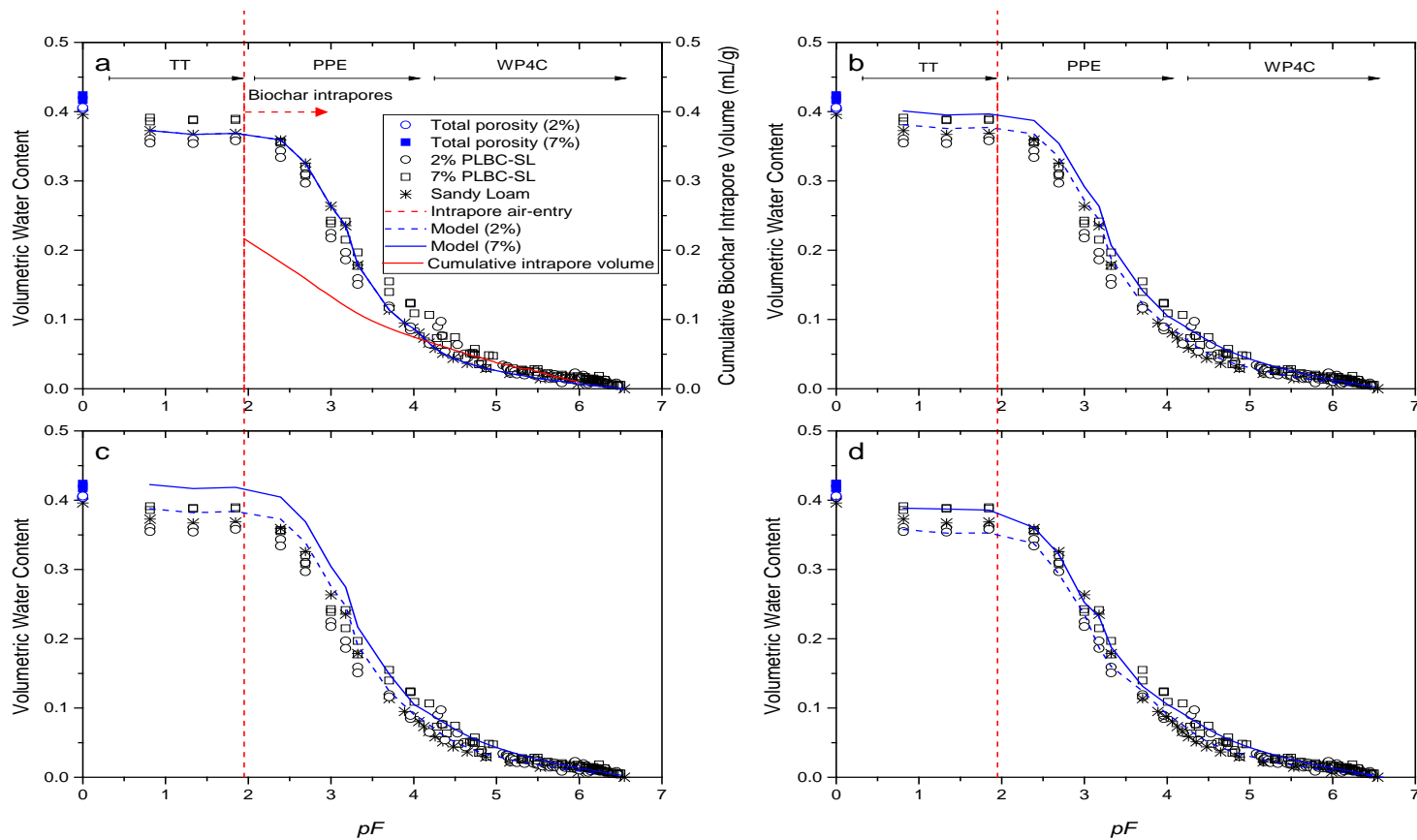


Figure 3-8. Soil water retention data and model predictions for mixtures of PLBC and SL. (a) Model 1, reference soil; (b) Model 2, reference soil + intrapores  $pF > 3.85$ ; and (c) Model 3, reference soil + all intrapores; and (d) Model 4, reference soil + all intrapores + changes in interpores

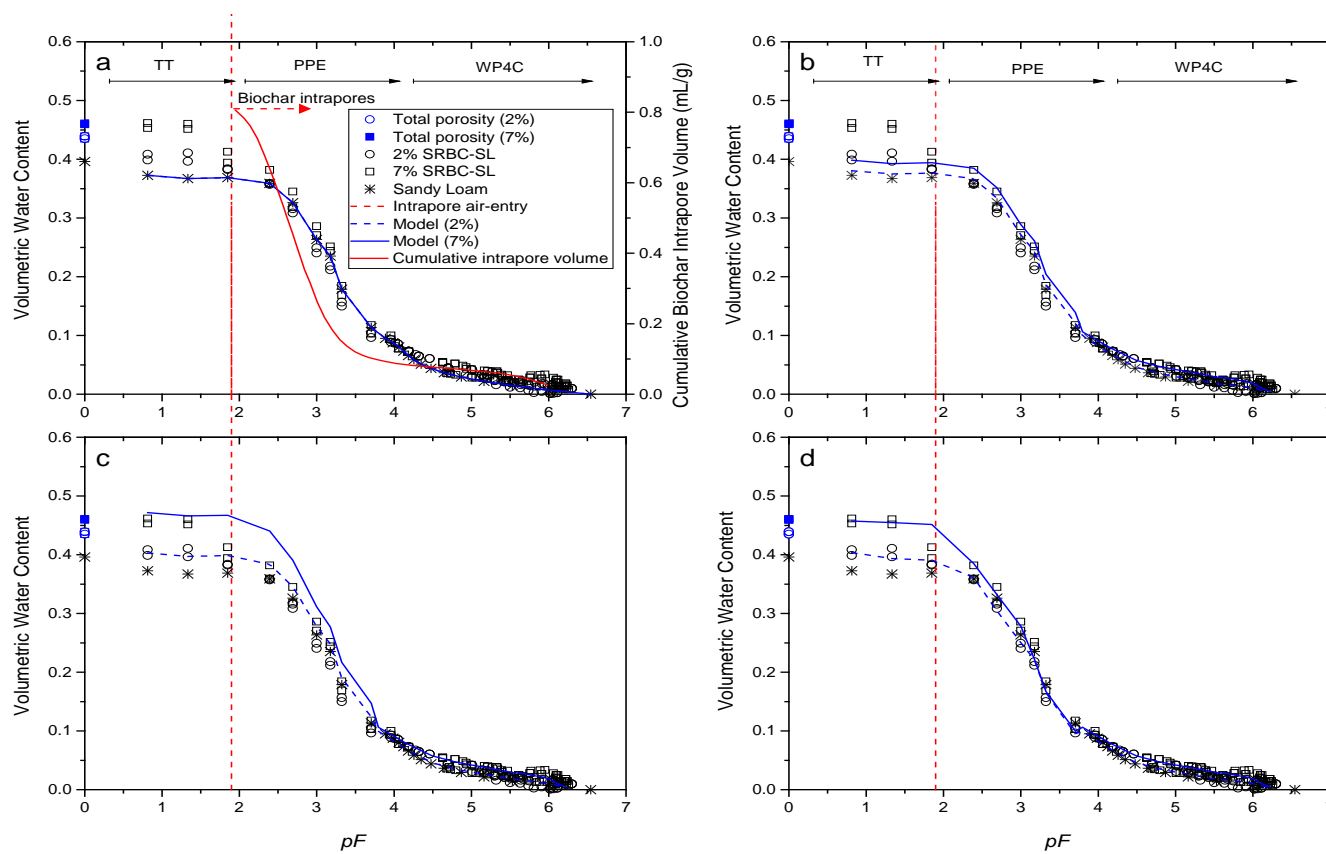


Figure 3-9. Soil water retention data and model predictions for mixtures of SRBC and SL. (a) Model 1, reference soil; (b) Model 2, reference soil + intrapores  $pF > 3.85$ ; and (c) Model 3, reference soil + all intrapores; and (d) Model 4, reference soil + all intrapores + changes in interpores.

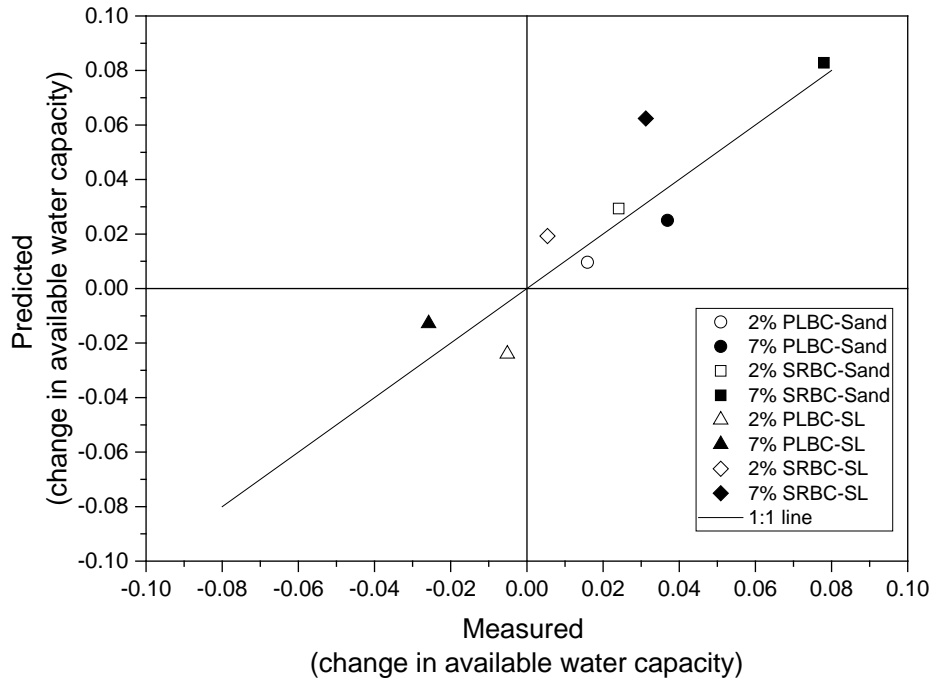


Figure 3-10. Average measured and model-predicted changes in available water capacity with biochar addition.

## Chapter 4

### THE EFFECTS OF BIOCHAR ON GAS TRANSPORT IN VARIABLY SATURATED SAND AND SANDY LOAM SOIL

#### 4.1 Background

Anthropogenic greenhouse gases have been increasing in the atmosphere with the agriculture sector being a significant contributor, emitting 69% of the total  $N_2O$  emissions [USEPA, 2013]. A suggested strategy to reduce greenhouse gases from agriculture production is to apply biochars. Recently,  $N_2O$  emissions were reduced by 57, 57 and 74% from silt loam soil when amended with woodchip biochar of 20, 40, and 60% (w/w), respectively [Spokas K.A. *et al.*, 2009]. Biochar-amended soils have reduced greenhouse gas emissions in some soils but the level of reduction may vary [Yanai *et al.*, 2007; Sohi *et al.*, 2010; Spokas *et al.*, 2012a; Luz Cayuela *et al.*, 2013].

Understanding the processes affecting gas migration through soils is important when predicting the emission of greenhouse gases. Biochar amendment to soil can alter soil-gas transport properties, which could play a significant role in  $N_2O$  flux. The two gas transport parameters, relative gas diffusivity ( $D_p/D_o$ ) and gas permeability ( $k_a$ ), are traditionally used to characterize soil gas transport, and they depend on the air-filled porosity ( $\epsilon$ ). Relative gas diffusivity is the ratio between the gas diffusion coefficient in soil ( $D_p$ ) and the gas diffusion coefficient in free air ( $D_o$ ). The gas permeability,  $k_a$  ( $\mu\text{m}^2$ ), is similar to water permeability where the flow of gas is governed by the pore structure of materials. It is another gas transport parameter where the air pressure gradients drive the gas movement through air-filled pores, often used in conjunction with  $D_p/D_o$  to characterize soil structure [Kawamoto *et al.*, 2006b; Arthur *et al.*, 2012;

*Sun et al.*, 2013]. Pore size and pore connectivity significantly affect gas transport: gas permeability is most significantly affected by the diameter of the pores, whereas the relative gas diffusivity is governed by the pore connectivity [*Jury et al.*, 1991].

To understand the effect of biochar on gas transport parameters, Sun et al. [2013] measured gas transport in biochar-amended sandy loam where ~20 tons ha<sup>-1</sup> of Birchwood biochar produced at 500°C was harrowed into the top 0 – 20 cm of sandy loam (Typic Hapludalf). Ryegrass was grown on the plot for seven months before intact cores (3.5 cm x 6.1 cm, length x diameter) were collected for  $D_p/D_o$ , gas permeability, and soil-water retention measurements [*Sun et al.*, 2013]. For samples at the same air-filled porosity ( $\varepsilon$ ), biochar did not alter  $D_p/D_o$  or  $k_a$ : over the range  $0.05 < \varepsilon < 0.5$ , when  $\varepsilon$  was the independent variable  $D_p/D_o$  and  $k_a$  were the same for biochar-amended and biochar-free samples. On the other hand, biochar amendment increased total porosity and water retention of the sandy loam by 11% and 3%, respectively [*Sun et al.*, 2013]. Sun et al. [2013] suggested that the 20 ton ha<sup>-1</sup> application rate was too small to show an improvement in gas transport, and higher gas transport parameters ( $D_p/D_o$ , and  $k_a$ ) were expected with larger biochar application rates. When Sun et al [2013] plotted  $D_p/D_o$  and  $k_a$  as a function of matric potential (in  $pF$ ) between  $2.0 < pF < 3.0$  instead of as a function of  $\varepsilon$ , there were increases in  $\varepsilon$  (28 – 34%),  $D_p/D_o$  (53 – 161%), and  $k_a$  (69 – 223%) with biochar-amendment. It was suggested that biochars changed the pore characteristics of amended soils resulting in increased  $\varepsilon$  at particular  $pF$  that led to increases in  $D_p/D_o$  and  $k_a$  [*Sun et al.*, 2013].

As an extension to the Sun et al. [2013] study, gas permeability was measured by Kumari et al. [2014] in intact cores (8 cm x 10 cm, length x diameter) collected from

the same site [Kumari *et al.*, 2014]. Higher gas permeability was measured for sandy loam than biochar-amended sandy loam for samples with nearly identical volumetric water contents (0.25 – 0.28). Kumari *et al.* [2014] suggested that small pockets of high water content in biochar-amended sandy loam may have reduced  $k_a$  [Kumari *et al.*, 2014].

Recently, compacted biochar-amended clay was evaluated as an alternative landfill final cover [Wong *et al.*, 2016]. The purpose of having a final cover is to reduce landfill gas generation and to minimize stormwater infiltration that leads to the production of leachate. Compacted clay is commonly used, but biomass compost and wastewater sludge have been used as an alternative to produce biologically active landfill covers by increasing both the water content and air-filled porosity to enhance microbial populations responsible for reducing landfill gas emissions. The major disadvantage of using compost or sludge is that they are easily degradable, reducing the lifespan of the landfill final cover. Biochars are known to be more recalcitrant from degradation than compost [Lehmann and Joseph, 2009]. Thus, Wong *et al.* [2016] investigated the effect of peanut shell biochar amended clay on gas permeability to test its feasibility as an alternative component in landfill final covers [Wong *et al.*, 2016]. The peanut shell biochars were produced by slow pyrolysis at 500°C and sieved to 425 µm then amended to kaolin clay at 5, 10, and 15% (w/w) [Wong *et al.*, 2016]. Wong *et al.* [2016] suggest that biochars decreased  $k_a$  with increasing biochar application rates when the gas permeability was measured at 35% gravimetric water content. Further examination of scanning electron microscope (SEM) images suggested that while the sieved biochars were larger than clay particles, clay clogged biochar intrapores (pores

on biochar surfaces) and interpores (pores between particles), reducing the gas permeability especially in samples with higher compaction [Wong *et al.*, 2016].

Very few studies have examined the impact of biochar amendment on gas transport properties of soil. For soils, relative gas diffusion and gas permeability are usually described as functions of air-filled porosity. In the single study that examined biochar-amended soil in this fashion, data from biochar-free and biochar-amended soils collapsed when plotted against air-filled porosity. This implies that air-filled porosity is the single parameter that can be used to describe biochar's impact on gas transport properties. However, I hypothesize that air-filled porosity alone is not sufficient to describe the influence of biochar-amendment on relative gas diffusion and gas permeability. Air-filled pores may be interpores or intrapores when biochar is present, and the division of air-filled porosity between these two pore classes should affect gas transport. Secondly, I hypothesize that in many soils biochar particles, which are typically more angular and elongated than soil grains, will increase tortuosity and thus reduce gas transport, and thus result in different gas transport parameters for biochar-free and biochar-amended soil at the same air-filled porosity. These two hypothesis will be tested by amending a uniform sand and a sandy loam with two biochars: poultry litter biochar (PLBC) and Soil Reef™ biochar (SRBC).

The PLBC particles are more rounded and less angular than SRBC, and thus are expected to affect tortuosity less. SRBC has 113% more intrapore space than PLBC. Experiments using these sediments and biochar particles are described next.

## 4.2 Materials and Methods

### 4.2.1 Sample preparation

Two biochars were employed: poultry litter biochar (PLBC) produced from poultry litter obtained from Purdue AgriRecycle (Seaford, DE, USA), and Soil Reef™ biochar (SRBC) (The Biochar Company in Berwyn, PA, USA). These two biochars were chosen for comparison since the feedstock source, production, and physical characteristics differed. The poultry litter biochars were produced from a slow pyrolysis system at 300°C [Song and Guo, 2012], and SRBC was produced from Southern Yellow Pine by a continuous system heated to 550°C for 10 min. The elemental contents for these biochars are reported elsewhere [Teixido *et al.*, 2011; Song and Guo, 2012].

Biochars were rinsed separately in deionized water until they were classified as wettable after carrying out the Water Drop Penetration Time tests on rinsed/oven-dried biochars [Yi *et al.*, 2015]. The biochars were subsequently sieved between #30 (0.595 mm opening) and #35 (0.5 mm opening) sieves. The biochar particles with a geometric mean diameter of 0.545 mm collected on #35 sieve were used.

Each biochar was mixed at 7% (w/w) with uniform sand (30/40 Accusand, Unimin Co., Le Sueur, MN, USA). The sand was pretreated first by rinsing in deionized water until the water turned clear, oven-dried at 105°C for 24 hr, then sieved between #30 and #35 sieves before mixing with the biochars. Samples of 7% PLBC mixed with sand is referred to as 7% PLBC-Sand, and 7% SRBC mixed with sand as 7% SRBC-Sand.

An agricultural soil collected from the top 30 cm of soil in Smyrna, Delaware (USA) was dried at 105<sup>0</sup>C for 24 h and then crushed using a mortar and a rubber-tipped pestle to break apart aggregates. The particle size distribution was determined using sieve analysis [*ASTM Standard C136-06*, 2003], and the soil was characterized as sandy loam (SL). Biochars were then mixed at 7% (w/w) with SL and identified as 7%PLBC-SL for poultry litter biochar and 7%SRBC-SL for Soil Reef biochar.

All sample mixtures were packed into individual aluminum cores 4.2 cm height and 8 cm inner diameter. The empty core volume was checked individually by filling with water and weighing the weight of water on a tared scale. The volumes of the aluminum cores were all ~ 210 cm<sup>3</sup>.

The sand and biochar-sand mixtures were packed dry using a two-tiered screen system to ensure uniform packing inside the metal cores by using momentum to minimize preferential settling [*Arya and Paris*, 1981]. Because the density of sand and biochar were different, segregation of sand and biochar particles may occur during packing; therefore, the samples were packed using a funnel at the end of the screen system and the free-fall height was reduced to minimize sand-biochar segregation. The samples were tapped and compacted to evenly distribute the particles until the cores were packed to the rim. Excess particles that collected around the outside perimeter of each sample core were carefully brushed off and weighed, and these masses used to correct the actual sample masses packed into the cores. The samples were individually weighed to obtain the dry bulk densities.

Particle segregation increases with increasing particle size range, and sandy loam is expected to segregate more easily during packing than uniform sand because it

has a wider particle size distribution [Tang and Puri, 2004]. Therefore, a published procedure for repacking soil was employed to prepare the SL and biochar-SL sample cores [Poulsen *et al.*, 2008]. In this procedure ~1 cm thick layer of the oven-dried samples was placed at the bottom of each metal core. Then, this layer was gently compacted using a glass rod to gently press the sample while avoiding breakage of biochar particles. The top surface of the 1-cm tall section was scratched with a thin metal spatula, and the next 1 cm thick layer added. This procedure was repeated until each sample core was packed to the rim. The samples were individually weighed to obtain the dry bulk densities.

All sample cores were slowly saturated in de-aired deionized water. Samples were placed in a large plastic container, and water was added to this container in 1-cm increments hourly until the water level was near the top of the sample cores (~2 mm). The samples were then set overnight in water to reach full saturation. Samples were then drained incrementally using the tension table and the pressure plate extractor to achieve desired water contents. At each desired volumetric water content, samples were weighed and gas transport measurements conducted, as described below. The samples were then placed back on the water extractors (tension table or pressure plate extractor) to further remove water in the samples, and gas transport measurements repeated at selected volumetric water contents. When samples were near residual water content, the samples were discarded. The cores were repacked with fresh materials and the experiments were repeated. Eight repacked samples were made for sand, three repacked samples for 7%PLBC-Sand, and three repacked samples for 7%SRBC-Sand. Two repacked samples were made for each sample type for SL and biochar-SL samples.

#### 4.2.2 Air-filled porosity

Intrapore volume was measured on both rinsed/sieved biochars using mercury intrusion porosimetry (MIP) (Micrometrics Analytical Services, Norcross, GA, USA). The skeletal density of biochar, which is the absolute density of biochar, was also determined using MIP. The detailed MIP results for PLBC and SRBC are described in Chapter 3. From the MIP data, water that drained from intrapores at each pressure step was estimated (Figure 4-1).

The average particle skeletal density for each sample was calculated from

$$\bar{\rho}_s = \frac{1}{\frac{\%bc}{\rho_{bc}} + \frac{\%s}{\rho_s}} \quad [4-1]$$

where  $\%bc$  is percent weight of biochar (7%),  $\%s$  is percent weight of sand or sandy loam (93%),  $\rho_{bc}$  is the skeletal density of biochar obtained from the MIP test, and  $\rho_s$  is the particle density of sand or sandy loam. The particle densities of the reference materials were obtained from the pycnometer test and were  $2.66 \text{ g cm}^{-3}$  for sand and  $2.42 \text{ g cm}^{-3}$  for sandy loam.

The air-filled porosity of each sample was found by determining the volume of air in the sample,  $V_a$ , at a given sample water content

$$V_a = V_T - \frac{M_s}{\rho_s} - \frac{M_w}{\rho_w} \quad [4-2]$$

where  $V_T$  is the total volume (volume of the aluminum core),  $M_s$  is the dry mass of solids in the sample,  $M_w$  is the mass of water in the sample, and  $\rho_w$  is the density of water.

The total porosity ( $\Phi$ ) at the total air filled volume ( $V_a$ ) was determined by

$$\Phi = \frac{V_a}{V_T} = \Phi^{intra} + \Phi^{inter} \quad [4-3]$$

where the total porosity is the sum of the total intrapore porosity ( $\Phi^{intra}$ ) and the total interpore porosity ( $\Phi^{inter}$ ).

The total air-filled porosity at each pressure step  $i$  ( $\varepsilon_i$ ) is the sum of the air inside the intrapores ( $\varepsilon_i^{intra}$ ) with air filled inside the interpores ( $\varepsilon_i^{inter}$ ), expressed as

$$\varepsilon_i = \varepsilon_i^{intra} + \varepsilon_i^{inter} = V_T - \frac{M_s}{\bar{\rho}_s} - \frac{M_{w,i}}{\rho_w} \quad [4-4]$$

where the  $\varepsilon_i^{intra}$  is estimated from the MIP results using the volumetric water content inside biochar at each pressure step  $i$  ( $\Delta\theta_i^{intra}$ ) from equations [3-5] in Chapter 3. This was accomplished by using the cubic spline function to interpolate the data at the same matric potential to find  $\varepsilon_i^{intra}$ . Using equation [4-4], the air-filled porosity at each pressure step  $i$  can be obtained by using the mass of water at each step  $i$  ( $M_{w,i}$ ). The  $\varepsilon_i$  and  $\varepsilon_i^{intra}$  are measured and  $\varepsilon_i^{inter}$  is calculated from the difference between  $\varepsilon_i$  and  $\varepsilon_i^{intra}$ .

The actual measurements of the intrapore and interpore drainage for the biochar mixtures were determined using the water retention curves from Chapter 3 to obtain the equivalent pressure using porosity as the independent variable. Because pressure controls the draining of water from soil pores, it will then control the  $\varepsilon$ . Therefore, these plots were included in this chapter.

Thus, the % water filled in intrapores (%  $\theta_i^{intra}$ ) from each pressure step  $i$  can be obtained from

$$\% \theta_i^{intra} = \frac{\bar{V}_{w,i}^{intra}}{\bar{V}_t^{intra}} \times 100\% \quad [4-5]$$

where  $\bar{V}_{w,i}^{intra}$  is the incremental water volume inside biochar at pressure step  $i$ , and  $\bar{V}_t^{intra}$  is the total intrapore volume of biochar estimated from MIP data (details in Chapter 3, Figure 3-2). The % air-filled porosity inside the intrapores (%  $\varepsilon_i^{intra}$ ) can be obtained from  $\frac{\bar{V}_{a,i}^{intra}}{\bar{V}_t^{intra}} \times 100\%$  where  $\bar{V}_{a,i}^{intra}$  is the volume of air inside the intrapores at each pressure step  $i$  found using  $\bar{V}_{a,i}^{intra} = \bar{V}_t^{intra} - \bar{V}_{w,i}^{intra}$ .

Similarly, the % air-filled porosity of the interpores at pressure step  $i$  (%  $\varepsilon_i^{inter}$ ) was also calculated by the volume of air inside the interopore space at each pressure step  $i$  ( $\bar{V}_{air,i}^{inter}$ ) divided by the total interopore volume ( $\bar{V}_t^{inter}$ ), where  $\bar{V}_{air,i}^{inter} = V_a - \bar{V}_{air,i}^{intra}$ , and  $V_a$  is the total air filled pore volume from equation [4-2].

$$\% \varepsilon_i^{inter} = \frac{\bar{V}_{air,i}^{inter}}{\bar{V}_t^{inter}} \times 100\% \quad [4-6]$$

### 4.2.3 Gas diffusion

Relative gas diffusivity of all samples was measured using the Currie method [Currie, 1960a; Currie, 1960b]. Each repacked sample core was placed on top of the sliding plate diffusion apparatus and sealed tightly with rubber O-rings and Dow Corning® High Vacuum Grease to prevent leaks [Dane and Topp, 2002; Mostafid *et al.*, 2012]. The diagram and the specifications of the diffusion apparatus are shown in

Figures C1 and C2 in Appendix C. Once a soil sample was secure and the sliding plate closed, 3 mL of Grade 5 (99.99 % pure) helium tracer gas was injected into the bottom of the diffusion chamber. A small fan inside the diffusion chamber mixed helium and resident air, and 1 mL sample was extracted from the bottom diffusion chamber to measure the initial helium concentration ( $C_o$ ) using a gas chromatograph equipped with a thermal conductive detector (GC-TCD) (Model 8610C, SRI Instruments, Inc., Torrance, CA, USA). About 3 – 5 samples were measured to quantify  $C_o$  for each experiment.

After  $C_o$  was determined, the metal plate separating the bottom chamber from the soil-sample chamber was slid open allowing helium to diffuse through the soil sample. Gas samples from the bottom chamber were then collected and measured to obtain the helium concentrations through time: 1 mL of gas from the bottom diffusion chamber was injected into the gas chromatograph every 2 – 3 min. The time was recorded for every measurement until the helium was nondetectable.

The Currie method was used to obtain  $D_p$  by applying Fick's first law of diffusion to the diffusion apparatus [Dane and Topp, 2002]. The Curry method assumes that the soil is uniform with respect to the diffusion coefficient and the air-filled porosity is constant over space and time. In an open system, the relative helium concentration in the bottom chamber,  $C_r$ , reduces to

$$C_r = \frac{2C_h \exp\left(-\frac{D_p \alpha_1^2 t}{\varepsilon}\right)}{L(\alpha_1^2 + C_h^2) + C_h} \quad [4-7]$$

where the helium-air content at the upper boundary of the soil sample chamber ( $C_h$ ) is calculated using  $C_h = \varepsilon/a\varepsilon_c$ , where  $\varepsilon$  is the air-filled porosity of the sample,  $a$  is the

length of the diffusion chamber, and  $\varepsilon_c$  is the air content inside the diffusion chamber which is 1.0.  $L$  is the depth of the soil,  $t$  is time, and  $\alpha_l$  is the positive root of  $(\alpha L) \tan(\alpha L) = C_h L$ . Thus, the plot of  $\ln(C_r)$  as a function of time becomes linear with slope  $-D_p \alpha_1^2 / \varepsilon$  for sufficiently large  $t$  [Dane and Topp, 2002].

The diffusion coefficient ( $D_p$ ) in  $\text{cm}^2 \text{sec}^{-1}$  is normalized by  $D_o$  ( $\text{cm}^2 \text{sec}^{-1}$ ), which is the binary diffusion coefficient of helium in air [Fuller et al., 1966]:

$$D_o = \frac{0.001 T^{1.75} \sqrt{\frac{M_a + M_{He}}{M_a M_{He}}}}{P(V_a^{1/3} + V_{He}^{1/3})^2} \quad [4-8]$$

where  $T$  is temperature ( $\text{K}^\circ$ ),  $M_a$  is molecular weight of air ( $28.97 \text{ g mol}^{-1}$ ),  $M_{He}$  is the molecular weight of helium ( $4 \text{ g mol}^{-1}$ ),  $V_a$  is molar volume of air ( $20 \text{ cm}^3 \text{ mol}^{-1}$ ),  $V_{He}$  is molar volume of helium ( $2.88 \text{ cm}^3 \text{ mol}^{-1}$ ), and  $P$  is pressure in atm [Fuller et al., 1966]. The method was tested by determining the diffusion coefficient of helium in pure, dry sand which was then compared to a published reference value for this sand. The  $D_p/D_o$  of 20/30 Accusand ranged between 0.12 to 0.21 for air-filled porosity between 0.35 to 0.36, values consistent with those from previous studies for this medium [AbuElShar and Abriola, 1997].

#### 4.2.4 Gas diffusion models

Several classic models that describe relative gas diffusivity of sieved and repacked soils as a function of air-filled porosity were used to analyze the laboratory data. One of the oldest models is the Buckingham model [1904] expressed as

$$\frac{D_p}{D_o} = \Phi^2 \quad [4-9]$$

The Buckingham model is used for describing diffusivity of granular materials using total air-filled porosity ( $\Phi$ ) as a single parameter [*Buckingham, 1904*].

The Penman-Call (PC) model [1957] includes a constant inactive pore space term ( $\varepsilon_{in}$ ) where the inactive pore space is typically  $\varepsilon_{in} = 0.1$  with air-filled porosity ( $\varepsilon$ ).

$$\begin{aligned} \frac{D_p}{D_o} &= 0.66 (\varepsilon - \varepsilon_{in}) \quad ; \text{ if } \varepsilon_{in} \leq \varepsilon \\ \frac{D_p}{D_o} &= 0 \quad \quad \quad ; \text{ if } \varepsilon_{in} > \varepsilon \end{aligned} \quad [4-10]$$

This model has a tendency to overestimate diffusion when relative gas diffusivities are small, and it is often used for estimating gas diffusion of soils with high organic matter content.

The Millington-Quirk (MQ) model [1961] is the most commonly used model to predict relative gas diffusivity of granular materials or repacked soils

$$\frac{D_p}{D_o} = \frac{\varepsilon^{10/3}}{\Phi^2} \quad [4-11]$$

The theory behind the MQ model was developed by assuming that particles are spherical, and therefore the solid and pore systems are symmetrical.

The Penman-Millington-Quirk (PMQ) model derived by Moldrup [1997] and best describes the relative gas diffusivity in sieved, repacked soils and is independent of soil type [*Moldrup et al., 1997*]. It is expressed as

$$\frac{D_p}{D_o} = 0.66 \Phi \left(\frac{\varepsilon}{\Phi}\right)^{(12-m)/3} \quad [4-12]$$

where  $m$  is a fitting constant that represents tortuosity. For soils with high tortuosity  $m = 3$ , while for soils with medium tortuosity  $m = 6$ . For pure sands and different loamy soils that are sieved/repacked,  $m = 6$  best described gas diffusivity [Moldrup *et al.*, 1997; Moldrup *et al.*, 2000].

The variable inactive pore space (VIPS) model has also been used to describe gas diffusion in repacked soils

$$\frac{D_p}{D_o} = \left(\varepsilon - \left[\frac{\Phi - \varepsilon}{\Phi - \varepsilon_{th}}\right] \varepsilon_{th}\right)^V \quad [4-13]$$

where  $\varepsilon_{th}$  is the threshold air-filled porosity below which gas-filled pores are disconnected and gas diffusion ceases. Typically,  $\varepsilon_{th} = 0.1$  is assumed even though it can range from 0 to 0.2. A fitting parameter  $V$  is also used in the model, where  $V = 1.58$  worked well for repacked soils [Moldrup *et al.*, 2005a].

Archie's law correlates relative gas diffusivity with air-filled porosity and is similar to the Buckingham equation, but uses a fitting parameter [Archie, 1942; Grathwohl, 1998].

$$\frac{D_p}{D_o} = \varepsilon^{m^*} \quad [4-14]$$

where  $m^*$  is the cementation factor and is fitted using the measured data. The  $m^*$  value depends on the pore geometry of the porous media. Buckingham assumed  $m^* = 2$  [Buckingham, 1904]. Peng *et al.* (2012) reported several  $m^*$  values and concluded that  $m^*$  is related to the mean pore diameter ( $d_{50}$ ) [Peng *et al.*, 2012]

$$m^* = -0.59 \ln d_{50} + 1.63 \quad [4-15]$$

These six models for gas diffusion in soil are used below when analyzing gas diffusion data from biochar-amended soil.

#### **4.2.5 Air permeability**

After the diffusion measurement, air permeability was measured for each sample. The packed soil columns were individually placed on top of an apparatus flowing with air from the bottom chamber with adjustable flow rates ranging from 0 – 20 L min<sup>-1</sup> using a flow meter (Cole-Parmer Flow Meter, Vernon Hills, IL) to measure  $k_a$  of biochar-amended soils directly after measuring the diffusion coefficients. A number of the soil samples during the experiment started forming cracks during the tests and these data are not presented. A visual inspection also showed some samples were drying out excessively during the experiment. The air from the installed air-line in the laboratory was used. It is unclear if the air used for the analysis were saturated with water vapor. The samples were weighed before and after the experiment to check for moisture loss. The data with a change in weight after the experiment are not presented here.

The diagram of the air permeability apparatus is shown in Figure C3, Appendix C. The outlet was attached to a pressure gauge (Testo 506, Lenzkirch, Germany) to measure the pressure difference at each flow rate across the soil sample. The Darcy-Forchheimer equation that describes the energy losses through both viscous and inertial effects was applied to obtain  $k_a$ .

$$\frac{dP_a}{dL} = \frac{\mu_a}{k_a} q_a + C_f \rho_a q_a^2 \quad [4-16]$$

where  $P$  in  $dP_a/dL$  is the air pressure gradient across the sample length ( $L$ ),  $\mu_a$  is the kinematic viscosity of air,  $k_a$  is the gas permeability,  $q_a$  is the Darcy velocity for gas,  $C_f$  is the fitted coefficient from the  $q_a - dP_a$  data that depends on air filled porosity, and  $\rho_a$  is the air density. Equation [4-16] was used to determine  $C_f$  and  $k_a$  using Excel function of SOLVER by fitting the nonlinear regression. This expression accounts for turbulent flow in the sample through the second  $q_a$  term with  $C_f$  [Poulsen and Blendstrup, 2008].

#### 4.2.6 Statistical analysis of gas diffusion

Bias was measured to evaluate overestimation or underestimation of data with the models and was computed from

$$bias = \frac{1}{N} \sum_{i=1}^N d_i^2 \quad [4-17]$$

where  $d_i$  is the difference between the predicted and the measured value of relative gas diffusivity ( $D_p/D_o$ ) at a given air-filled porosity (or at a given soil-water matric potential) and  $N$  is the number of measurements in the data set. The root mean square error (RMSE) was also used to evaluate the model performance.

$$RMSE = \sqrt{\frac{1}{N} \sum_{i=1}^N d_i^2} \quad [4-18]$$

## 4.3 Results & Discussion

### 4.3.1 Air-filled porosity

The averaged total porosities ( $\Phi$ ), total intraparticle porosity ( $\Phi^{intra}$ ), the ratio between intraparticle air-filled porosity and interporosity ( $\Phi^{intra}/\Phi^{inter}$ ), and the bulk densities for gas transport samples are tabulated in Table 4-1. In general, total porosity increased with biochar addition in both sand and sandy loam mixtures, and the bulk density decreased with biochar addition. Table 4-1 shows that the  $\Phi^{intra}$  was 0.024 (sand) and 0.023 (SL) for PLBC, and 0.076 (sand) to 0.077 (SL) for SRBC. The increase in the intraparticle porosity is variable depending on the biochar type [Brewer *et al.*, 2014]. The ratio of  $\Phi^{intra}/\Phi^{inter}$ , which likely represents the immobile fraction of porosity, also depended on the biochar type as shown in Table 4-1. Because SRBC had a higher intraparticle volume than PLBC (PLBC = 0.23 ml g<sup>-1</sup>, SRBC = 0.83 ml g<sup>-1</sup>), the porosity was higher in SRBC mixtures than PLBC: 5% more in sand and 16% more in SL. The ratio of  $\Phi^{intra}/\Phi^{inter}$  was also lower in PLBC mixtures (~0.06) than SRBC mixtures (0.18 - 0.22). Adding biochar increased  $\Phi^{inter}$  in sand by 9% with PLBC and 13% with SRBC, decreased  $\Phi^{inter}$  by 2% with PLBC in SL, and increased  $\Phi^{inter}$  by 4% with SRBC in SL. As will be shown below, SRBC particles although sieved to the size as PLBC are more elongated and thus resulted in more interparticle volume when packed with the uniform sand.

There was a large difference in interporosity in biochar/sand mixtures in Chapter 3 versus Chapter 4. There was a difference up to 13% in interporosity, while there was a difference of 2% in Chapter 3. The packing methods were the same, but the column size

may have affected the packing of the columns. The metal cores used in this chapter had taller columns (4.2 cm height  $\times$  8 cm inner diameter) than metal cores in Chapter 3 that measured 3.6 cm height  $\times$  7.7 cm. This may have caused a larger interporosity in the samples used in this chapter.

In sand, PLBC lowered the bulk density by 10% and SRBC lowered the bulk density by 26%. Adding biochar to sandy loam also lowered the bulk density by 9% in PLBC-SL and 16% in SRBC-SL. The bulk densities were lowered because of larger intrapore volume and smaller skeletal density of SRBC versus PLBC: the skeletal density was 1.72 g ml<sup>-1</sup> and 1.39 g ml<sup>-1</sup> for PLBC and SRBC, respectively (Chapter 3).

It should be noted that skeletal densities from the same feedstock material can vary with pyrolysis temperature. Brewer et al. [2014] showed that wood biochar pyrolyzed at  $\sim$ 300°C had an intraposity of 0.55, whereas at 700°C the intraposity was  $\sim$ 0.7 [Brewer et al., 2014]. The total porosities and bulk densities from samples used to measure water retention data are also shown in Table 4-1.

### **4.3.2 Biochar intrapores**

The intrapore drainage curves for 7%PLBC-Sand and 7%SRBC-Sand as a function of  $\varepsilon_i$  at 7% (w/w) are shown in Figure 4-1a. The bulk densities of these samples were different than the bulk densities of samples used to measure gas transport (Table 4-1). These plots were calculated from the water retention curves from Chapter 3, to obtain  $\varepsilon_i$  at their equivalent matric pressure. For the water retention measurements in sand, the  $\Phi$  were lower with higher bulk densities. Therefore, in Figure 4-1a, the measured water retention data did not exceed the  $\Phi = 0.4$ . In biochar sandy loam

mixtures, the total porosity was slightly higher in the water retention measurements with lower bulk densities. Therefore, the interpolation was not performed for  $\Phi > 0.4$  from limited data at higher porosities.

Young-Laplace equation of capillarity shows that pores release water at pressures inversely proportional to the pore size (Chapter 3, equation [3-1]). The pore size distribution is believed to yield the most general form of water retention model; therefore, the soil-water retention curves from Chapter 3 were used to interpolate the corresponding matric potential. The purpose of interpolating the data was to find the corresponding matric potential for the gas transport/air-filled porosity, assuming that at the same matric potential, the air-filled pore space dimensions (pore radius,  $r_p$ ) will be comparable between the samples with the same biochar amendment. The details of water retention measurements and results are found in Chapter 3, Section 3.4.5.

The volumetric water contents of biochar intrapores from the water retention curves in Chapter 3 were also plotted on the secondary axis of Figure 4-1. Figure 4-1a shows that water held inside intrapores for both biochars did not drain when  $\varepsilon$  increased from 0 to 0.33, since water from larger interpores drained first. The data suggest that the interpores drained similarly between the two samples at the same matric potential, because the biochars-sand mixtures were sieved to the same size and thus had similar interpores. The biochar volumetric water content was higher in 7%SRBC-Sand than 7%PLBC-Sand at full saturation, since SRBC larger intrapore volume that held more water [Marsiello *et al.*, 2015]. Beyond the total air-filled porosity of  $\varepsilon > 0.33$  (matric potential of  $pF = 1.9$ ) (Figure 4-1b), water drained from the intrapores. The air-entry pressure was  $pF = 1.9$  for both biochars (Figure 4-1b, and Chapter 3).

Figure 4-1c and Figure 4-1d show intrapore drainage for 7%PLBC-SL and 7% SRBC-SL when particle size distribution of reference soil is different than that of biochar. Volumetric water content of intrapores are also plotted on the secondary axes in these figures. The percentage of water filling intrapores decreases with increasing  $\varepsilon$ , similar to results for biochar-sand mixtures. The 7%PLBC-SL released water from intrapores at  $\varepsilon \sim 0.03$  and at  $\varepsilon \sim 0.06$  for 7% SRBC-SL, even though the air-entry pressure for both biochars were  $pF = 1.9$ .

For both sand and SL mixtures, SRBC had higher intrapore volumetric water content, but had lower percentage of water filled inside the intrapores at the same air-filled porosity than PLBC: SRBC drained more readily, since a larger percentage of the intrapore volume was associated with larger intrapores. However, the total air-filled porosity from the intrapores was higher for SRBC for both sand and SL. Larger pores promote gas transport, whereas smaller pore sizes reduce gas transport in comparison. Because gas diffusion only occurs through connected air-filled pores [Moldrup *et al.*, 2000], intrapores may not participate significantly in gas transport, even if they are air-filled. Some intrapores in biochar may be dead end pores. Soil pores that are not involved in gas transport is often referred to as ineffective pore space [Moldrup *et al.*, 2000; Fujikawa and Miyazaki, 2005]. Thus, biochars with higher intrapore volume may not improve gas transport in soils despite increasing soil porosity.

### **4.3.3 Gas diffusion**

Figure 4-2a shows the relative gas diffusivity as a function of  $\varepsilon$  for biochar-amended sand samples. The summary of the total porosity, intraporosity, and bulk

density for these samples are listed in Table 4-1. The red lines indicate the percentage of air-filled porosity contribution from interpores for each biochar, calculated using equation [4-6]. The diffusivity increased with increasing air-filled porosity proportionately for the samples in Figure 4-2a after interpores started draining around  $\varepsilon = 0.14$ . The interpores in biochar-sand mixtures accounted for 100% of the air-filled porosity until  $\varepsilon \sim 0.33$  ( $pF = 1.9$ ), when water started draining from intrapores.

Because biochars were sieved to the same particle size as sand, it was presumed that both PLBC and SRBC would have similar diffusivity in sand until the water in intrapores started draining. The air-filled porosity included both interpores and intrapores beyond  $\varepsilon > 0.33$ . However, the 7%SRBC-sand mixture had a lower  $D_p/D_o$  for  $0.2 < \varepsilon < 0.3$  compared to sand and 7%PLBC-Sand. The relative gas diffusivity decreased with both 7% biochar amendments at  $\varepsilon < 0.3$  (Figure 4-2a).

Figure 4-2b shows relative gas diffusion in sand as a function of air-filled interporosity ( $\varepsilon^{inter}$ ), which was postulated to be a better measure of connected gas-filled pores than the total air-filled porosity. Even when plotting data against  $\varepsilon^{inter}$  the lowest relative gas diffusivity was observed on 7%SRBC-Sand similar to Figure 4-2a. At both  $\varepsilon$  and  $\varepsilon^{inter} < 0.33$ , the  $D_p/D_o$  of 7%SRBC-Sand was 18% lower than 7%PLBC-Sand. Even though biochars and sands were sieved to the same particle size, data suggests that the connectivity of interpores were lower and the tortuosity higher for 7%SRBC-Sand when water in intrapores were completely filled with water. Once the biochar intrapores began to drain ( $\varepsilon^{inter} > 0.33$ ), there were no observable differences in  $D_p/D_o$  in Figure 4-2b.

Figure 4-2c shows the  $D_p/D_o$  of biochar in SL as a function of total air-filled porosity. Water inside the intrapores started draining at  $\varepsilon = 0.04$  and  $\varepsilon = 0.06$  for PLBC and SRBC, respectively. Both inter/intrapores started releasing water at a relatively low air-filled porosity ( $\varepsilon > 0.1$ ) compared to sand ( $\varepsilon > 0.3$ ). The diffusivities were similar for all media at  $\varepsilon > 0.2$ , even though both biochar amendments increased interpores and intrapores in the samples. Both biochar amendments had only a small effect on relative gas diffusivity for the entire  $\varepsilon$  range (Figure 4-2c).

Figure 4-2d shows the relative diffusivity of SL and biochar-SL mixtures as a function of  $\varepsilon^{inter}$ . PLBC and SRBC had higher diffusivity than SL after removing the effect of intrapore porosity. When the intrapores started draining along with the interpores, the tortuosity was lowered and relative gas diffusivity was higher in both biochar-SL mixtures. As the water drained between the particles simultaneously with water trapped inside the intrapores, higher interconnected pore spaces were likely available for gases to migrate through the biochar-SL mixtures.

The two major parameters that control the migration of gases in porous media are  $\varepsilon$  and the degree of connectivity, as typically expressed by tortuosity [Moldrup *et al.*, 2001]. Gas diffusion decreased in sand with the addition of biochar when plotted against total air-filled porosity. When the gas diffusion was assessed against the air-filled interporosity, it showed that tortuosity was reduced with biochar, both in sand and SL. The data suggest that the intrapores contribute to gas diffusion much less than an equivalent volume of interpores, likely because intrapores have reduced pore continuity. When intraporosity was removed as shown in Figure 4-2b and Figure 4-2d, the tortuosity of the biochar mixtures decreased and  $D_p/D_o$  increased. Hence, larger total

porosity of biochar-amended media does not always provide higher gas diffusion through soils.

Data further suggest that the shapes of PLBC and SRBC biochars altered the interpores. Despite 7%SRBC-Sand having higher total porosity (0.5) than 7%PLBC-Sand (0.43) and sand (0.37) (Table 4-1), the relative gas diffusivity was the lowest for 7%SRBC-Sand even before intrapores water started draining. Porosity tends to increase when elongated shaped particles are added to spherical particles [Deng and Dave, 2013], indicating that biochar shape may have altered the interpores despite sieving the sand and biochar particles to the same diameter. However, when the volume of inactive pores exceeds the volume of active pores that influence tortuosity, diffusivity can decrease even at a higher air-filled porosity [Fujikawa and Miyazaki, 2005]. It is likely that this process was occurring in biochar amended mixtures, which was more evident in sand than in SL.

#### **4.3.4 Gas diffusion models**

Figure 4-3 and Figure 4-4 show predictions or fits of the gas diffusion models for the experimental systems. The Buckingham, PC, and MQ models are predictive models with no fitting parameters, whereas the PMQ and the VIPS models were fitted to data (equations [4-9] to [4-13]). The value of inactive pore space constant (PC) or the threshold air-filled porosity (VIPS) when gas diffusion ceases was assumed to be  $\varepsilon_{in} = 0.1$  and  $\varepsilon_{th} = 0.1$ ; model accuracy improved when using  $\varepsilon_{in} = 0.1$  for 18 repacked soils tested with the PC model [Moldrup *et al.*, 2005a]. Biochar may increase the threshold air-filled porosity by increasing the variation of pore spaces for air entrapment and air

connectivity in the media. Nevertheless,  $\varepsilon_{in} = 0.1$  and  $\varepsilon_{th} = 0.1$  was assumed when evaluating the PC and VIPS models.

In Figure 4-3 the models were applied using the total porosity for  $\Phi$  and traditional total air-filled porosity for  $\varepsilon$  in the models. Table 4-2 lists the RMSE of these model results shown in Figure 4-3. Figure 4-3 shows the simultaneous effects of both interpore and intrapore porosity on tortuosity and inactive pore space. In Figure 4.4 the models were applied using interporosity for  $\Phi$  and air-filled interporosity for  $\varepsilon$  in the models. Evaluating the data this way shows the influence of interpores on tortuosity and inactive pore spaces by removing the intraporosity in the models. This will distinguish if either interpore or intrapores are responsible for the changes in the gas connectivity. It will also show if air-filled intrapore volume is an important parameter affecting the models. Table 4-3 lists the RMSE of the models when air-filled interporosity was used.

The Buckingham model predicted the data relatively well in 7%PLBC-Sand (RMSE = 0.049 in Figure 4-3, RMSE = 0.063 in Figure 4-4), but overestimated 7%SRBC-Sand (RMSE = 0.065 in Figure 4-3, RMSE = 0.062 in Figure 4-4). The Buckingham model performed particularly well in sand at low air-filled porosities but underestimated diffusion at high air-filled porosities. It predicted the data better in SL mixtures with RMSE ~ 0.02 in Figure 4-3 compared to sand (RMSE = 0.046). The RMSE for 7%PLBC-SL and 7%SRBC-SL were higher at 0.03 and 0.047 when air-filled interporosity was used as shown in Figure 4-4. The Buckingham model has limitations for repacked soils with high clay content [Moldrup *et al.*, 2005b], thus using this model for predicting relative gas diffusivity is not advised for all soil textures.

The PC model was the worst performing model for all samples, with RMSE ranging from 0.026 to 0.09 for all mixtures in sand and SL mixtures. The PC model is best applied on samples with high organic content, and it overestimated relative gas diffusivity for all samples in this study. The PC model includes a constant inactive pore space for the entire range of data that may have caused the overprediction.

The performance of predictive models in Figure 4-3 and Figure 4-4 shows that the MQ model performed the best for models without any fitting parameters for sand (Figure 4-3) (RMSE = 0.016, Table 4-2), since this model is best applied on pore systems with spherical particles. However, the MQ model overpredicted diffusion in 7%SRBC-Sand (RMSE = 0.089 in Figure 4-3, RMSE = 0.062 in Figure 4-4), and underpredicted it in SL (RMSE = 0.04), 7%PLBC-SL (RMSE = 0.026 in Figure 4-3, RMSE = 0.027 in Figure 4-4), and 7%SRBC-SL (RMSE = 0.019 in Figure 4-3, RMSE = 0.034 in Figure 4-4).

The fitted PMQ and VIPS models yielded the best performance among all models tested, as shown in Figure 4-3 and Figure 4-4. The PMQ model fitted a tortuosity parameter ( $m$ ). The tortuosity parameter range is  $1 < m < 6$ , where  $m = 6$  represents lower tortuosity,  $m = 3$  for medium tortuosity, and  $m = 1$  for high tortuosity [Moldrup *et al.*, 1997]. The PMQ model results with  $\Phi$  = total porosity and  $\varepsilon$  = total air-filled porosity showed that sand had the lowest tortuosity  $m = 3$  (RMSE = 0.015), followed by 7%PLBC-Sand with  $m = 1.8$  (RMSE = 0.045), then 7%SRBC-Sand with  $m = 1$  (RMSE = 0.042). Thus, addition of biochar increased sample tortuosity. The PMQ model in Figure 4-4 and Table 4-3 had  $m = 1.9$  (RMSE = 0.04) and 1.0 (RMSE 0.053) in 7%PLBC-Sand and 7%SRBC-Sand, respectively, when  $\Phi$  = interpore porosity and  $\varepsilon$

= air-filled interporosity. Thus, even when only interpores are considered, biochar amendment increased tortuosity when amended to the uniform sand.

The PMQ model showed that tortuosity was the lowest in 7%PLBC-SL ( $m = 5.4$ , RMSE = 0.008), followed by 7%SRBC-SL ( $m = 3.6$ , RMSE = 0.015) when  $\Phi =$  total porosity and  $\varepsilon =$  air-filled porosity. The highest tortuosity ( $m = 2.3$ , RMSE 0.027) was on SL as estimated by the PMQ model. When the intrapores were removed to evaluate the effects of interpores alone as shown in Figure 4-4 and Table 4-3, the tortuosity remained low for 7%PLBC-SL ( $m = 6.1$ , RMSE = 0.008), but 7%SRBC-SL had the lowest tortuosity ( $m = 6.4$ , RMSE = 0.011). This shows that intrapores affect tortuosity, and SRBC with a higher interporosity had lower  $D_p/D$ , as shown in Figure 4-2a and 4-2b.

The VIPS model performed well overall for all samples tested. The VIPS model fitted the parameter  $V$  that represents variable inactive pore space, which was developed based on the concept that inactive pore space decreases linearly with increasing air-filled porosity [Troeh *et al.*, 1982; Moldrup *et al.*, 2005a]. The VIPS model (Figure 4-3 and Table 4-2) shows that the variable inactive pore space was highest in 7%SRBC-Sand ( $V = 2.08$ , RMSE = 0.056), followed by 7%PLBC-Sand ( $V = 1.69$ , RMSE = 0.041) and sand ( $V = 1.57$ , RMSE = 0.024), with  $\Phi =$  total porosity and  $\varepsilon =$  air-filled porosity. The models supported the assumption that increased total porosity with biochar addition may not enhance gas diffusion, but reduce the relative gas diffusivity by increasing both tortuosity and inactive pore spaces – at least when biochar is amended to sand.

In SL mixtures, the highest tortuosity was estimated for SL ( $m = 2.3$ , RMSE = 0.027), then 7%SRBC-SL ( $m = 3.6$ , RMSE = 0.015). The 7%PLBC-SL had the lowest tortuosity with  $m = 5.4$  (RMSE = 0.008). This was consistent with the relative gas diffusivity measurements from Figure 4-2a and Figure 4-2b. The VIPS model also performed well for the SL mixtures using  $\Phi$  = interporosity and  $\varepsilon$  = air-filled porosity contribution from interpores (Figure 4-4 and Table 4-3). The VIPS model  $V = 1.43$  for 7%PLBC-SL and  $V = 1.36$  for 7%SRBC-SL show that the variable inactive pore space was the highest in SL.

Archie's law was fitted to the biochar sandy loam data and results are plotted in Figure 4-5 and tabulated in Tables 4-2 and 4-3. Direct measurements of the pore size distribution of the biochar mixtures were not available so  $m^*$  values were fitted using the Archie's law since  $m^*$  signifies the pore geometry of soils [Archie, 1942; Grathwohl, 1998]. Sand mixtures were ignored since it was clear that pore sizes change with biochar addition. The effects of biochar on natural soil and its correlation between total air-filled porosity and air-filled interporosity were examined in Figure 4-5 since clays may compete with biochars and alter pore structures.

When total air-filled porosity was used in the model, Archie's law fit the data well with RMSE = 0.006 for 7%PLBC-SL when  $m^* = 1.72$  (Figure 4-5b). The RMSE = 0.103 was 7%SRBC-SL when  $m^* = 1.81$  (Figure 4-5d). Increasing pore size diameter (lower value of  $m^*$ ) increases  $D_p/D_o$ , and repacked samples have smaller  $m^*$  values ranging from 1.65 to 2.56 [Peng *et al.*, 2012]. Using equation [4-15], the volumetric mean pore diameter ( $d_{50}$ ) was calculated as 0.86  $\mu\text{m}$  for 7%PLBC-SL and 0.74  $\mu\text{m}$  for 7%SRBC-SL for a given  $\varepsilon$ . For sandy loam (Figure 4-5a), the  $d_{50}$  was 0.58  $\mu\text{m}$ . The  $m^*$

value closely relates pore structure to gas diffusion, and when it was evaluated against the total air-filled porosity, the pore diameter increased with biochar in SL. However, the  $d_{50}$  for PLBC was higher than SRBC.

When the Archie's law was fitted against the measurements as a function of interporosity in Figure 4-5c and Figure 4-5d,  $m^*$  values for biochar mixtures were also lower than SL: 7%PLBC-SL had 1.65 and 7%SRBC-SL had 1.52 values of  $m^*$ . However, when the intrapores were removed to evaluate the effects of interpores on gas diffusion, the  $d_{50}$  for 7%SRBC-SL was 1.2  $\mu\text{m}$  and 0.97  $\mu\text{m}$  for 7%PLBC-SL. This suggests that SRBC with higher intrapores than PLBC have the ability to lower air-filled pores and possibly lower gas diffusivity as shown in Figure 4-2a and 4-2b.

The volume-based particle size distribution curve in Chapter 3, Figure 3-1 shows how biochar changes the particle size distribution in sandy loam. The particle size and composition of SL used in this study consisted of 74% sand ( $> 0.075$  mm), 13% silt (0.005-0.05 mm) and 13% clay ( $< 0.005$  mm). Adding sieved biochar (~geometric mean diameter of 0.545 mm) with a high intrapore volume like SRBC will shift the pore size distribution by increasing the content of large particles, especially at 7% (w/w) of biochar. This may also affect interporosity of soils. Even though SL is a coarse textured soil, SRBC-SL mixtures increased the content of large particles and decreased tortuosity, particularly in dry soils. The air-filled porosity contributing from the changes in intra/interporosity from biochar addition increased  $D_p/D_o$  when the biochar particle size was larger than the soil particles. This was demonstrated when Archie's model was applied to gas diffusion measurements as a function of both total air filled porosity and interporosity.

### 4.3.5 Gas permeability

To examine the properties of gas moving through the connected pores,  $\log(k_a)$  was plotted as a function of  $\log(\epsilon)$  in Figure 4-6a for total porosity and Figure 4-6b for inter-pore porosity for PLBC or SRBC mixed with sand. The data were plotted as  $\log(\epsilon)$  versus  $\log(k_a)$  to show the different structural phases and their impact on air permeability [Poulsen *et al.*, 2008]. In sand,  $k_a$  ( $\mu\text{m}^2$ ) was measured from  $-0.87 \leq \log(\epsilon) \leq -0.42$ , where  $\log(k_a)$  ranged from 1.5 to 2.3 (Figure 4-6a). The measurements for biochar-sand mixtures were made when inter-pores were draining ( $pF < 1.9$ ), mostly in wet to moderately wet conditions in sand mixtures. Air-filled porosities were  $-1 \leq \log(\epsilon) \leq -0.43$  for 7% PLBC-Sand, with  $1.6 \leq \log(k_a) \leq 2.3$ . The 7% SRBC-Sand had  $1.55 \leq \log(k_a) \leq 2.3$  for porosities  $-0.7 \leq \log(\epsilon) \leq -0.35$ .

Figures 4-6a and Figure 4-6b show that the log-transformed  $k_a$  did not improve with PLBC or SRBC amendment to sand with it was evaluated against  $\epsilon$  and  $\epsilon^{intra}$ . Air permeability is influenced by soil water content and  $k_a$  increases with higher  $\epsilon$ , as expected. Although adding biochar created higher  $\Phi$  (Table 4-1), measurements did not reflect an increased air permeability with biochar amendment, since water between the intrapores did not drain significantly for the air-permeability measurements collected.

The biochars and sands were sieved to be uniform ( $\sim 0.5$  mm) and repacked. Air permeability increased for all samples in Figure 4-6a and 4-6b, but from lack of data it was difficult to determine the influence of biochar on  $k_a$  when PLBC or SRBC were added to uniform sand at 7%. What was more evident was that between  $\log(\epsilon)$  range of  $-0.75$  to  $-0.5$ , slightly lower  $k_a$  was measured in 7% SRBC-Sand than sand, which is consistent with Figure 4-2. The SRBC particle shape (see Figure C-4, Appendix C) may

have influenced the connectivity and tortuosity to lower air permeability. The shape of PLBC was less angular than SRBC, potentially resulting in smaller changes to interpores when amended to the uniform sand.

Figure 4-6c and Figure 4-6d show  $k_a$  increased from  $-1.1 < \varepsilon < 0.75$  for 7%PLBC-SL and 7%SRBC-SL, but  $k_a$  decreased near  $\log(\varepsilon) < -0.6$  for both  $\varepsilon$  and  $\varepsilon^{inter}$ , respectively. The measurements of  $k_a$  were all made after the intrapores started draining of water. Figure 4-6d shows biochar-SL mixtures as a function of log-transformed air-filled interpore porosity and also show that at  $\log(\varepsilon^{inter}) < -0.65$  both 7%PLBC-SL and 7%SRBC-SL reduce  $\log(k_a)$ . There was a significant reduction of air permeability in 7%PLBC-SL than SRBC samples between  $-0.6 < \varepsilon < 0.5$  (Figure 4-6c). The  $k_a$  for 7%PLBC-SL decreased by about a factor of 10 compared to 7%SRBC-SL with increasing  $\varepsilon$ . The 7%PLBC-SL and 7%SRBC-SL mixtures trended lower than SL overall, which is indicative of air permeability changing as water-filled pores drained. The results showed that gas permeability performed similarly between  $\varepsilon$  and  $\varepsilon^{inter}$ , showing a negligible affect from intrapores, but suggested differences between the sample mixtures.

#### **4.4 Conclusions**

Biochars have the ability to alter interporosity and intraporosity of soils. Because gas transport through soils is governed by air-filled porosity ( $\varepsilon$ ), gas transport parameters were measured on materials with and without biochar to evaluate the effects of inter/intraporosity on gas transport. Biochars lowered gas diffusivity when amended to sand, but increased gas diffusivity in sandy loam. When the intrapores from biochars

were removed to evaluate the gas transport parameters against air-filled interporosity, the gas diffusion increased showing that intrapores can influence relative gas diffusion. The SRBC in sand lowered diffusivity more than the PLBC, possibly from SRBC holding more water than PLBC in the intrapores and from biochar particle shapes that increased tortuosity.

Classic gas diffusion models were used to predict and fit the  $D_p/D_o$  to verify the changes in tortuosity and pore connectivity. The results showed that biochars can influence gas transport by influencing tortuosity by altering inter/intrapores from biochar particle shape, water holding capacity, and the mean pore diameter ( $d_{50}$ ). The models showed that intraporosity should not be neglected, particularly in the dry regions of the curve when these pores drain and may affect gas transport. Biochars with high water retention may not always increase gas transport as it may alter air-filled porosity by reducing interparticle pore spaces. We further observed that the air-permeability decreased with biochar amendment to sandy loam, suggesting that bulk density, soil structure, water blockage, biochar shape, and pore geometry may all have affected the  $k_a$ . The pore characteristics of soils and air-filled porosity were important properties, and biochar distinctly can alter the soil pores structures to drive gas transport.

Biochars have high water retention capacity that can increase water blockage, which requires high matric potential to make inactive pores available by draining sufficient amounts of water trapped inside the intrapores. It is likely that water blockage decreased gas diffusion and air permeability that lowered gas migration (e.g. greenhouse gas emissions) by entrapping the gases between the soil-biochar particles.

Complex pore geometry is prevalent in heterogeneous mixtures, even more so with biochar, which then affects gas transfer processes by providing different flow paths, and/or by impeding the pathways. The geometric configurations of mixtures between soils, biochar, water, and air needs further assessment. The pore size distribution of biochar-sand and biochar-SL should be evaluated to get a better understanding of the pore morphology of biochar amended soils.

Table 4-1: Summary of air-filled porosities and dry bulk density of samples

Sample type	Gas transport				Water retention	
	Total porosity ( $\Phi$ )	Mean total intrapore porosity ( $\Phi^{intra}$ )	Ratio ( $\Phi^{intra}/\Phi^{inter}$ )	Bulk density ( $\rho_b$ , g/ml)	Total porosity	Bulk density ( $\rho_b$ , g/ml)
Sand	$0.368 \pm 0.014$ (8)	-		$1.68 \pm 0.04$ (8)	$0.348 \pm 0.001$ (2)	$1.74 \pm 0.01$ (2)
7%PLBC-Sand	$0.427 \pm 0.007$ (3)	$0.024 \pm 0.001$	0.060	$1.52 \pm 0.01$ (3)	$0.395 \pm 0.002$ (2)	$1.55 \pm 0.01$ (2)
7%SRBC-Sand	$0.500 \pm 0.035$ (3)	$0.076 \pm 0.004$	0.179	$1.29 \pm 0.09$ (3)	$0.442 \pm 0.001$ (2)	$1.40 \pm 0.01$ (2)
Sandy Loam (SL)	$0.418 \pm 0.008$ (2)	-		$1.55 \pm 0.01$ (2)	$0.396 \pm 0.001$ (2)	$1.46 \pm 0.01$ (2)
7%PLBC-SL	$0.411 \pm 0.005$ (2)	$0.023 \pm 0.001$	0.059	$1.42 \pm 0.01$ (2)	$0.420 \pm 0.005$ (2)	$1.36 \pm 0.01$ (2)
7%SRBC-SL	$0.433 \pm 0.011$ (2)	$0.077 \pm 0.001$	0.216	$1.32 \pm 0.01$ (2)	$0.460 \pm 0.001$ (2)	$1.24 \pm 0.01$ (2)

Sandy Loam (SL); 7% (w/w) poultry litter biochar (PLBC) mixed with sand (7% PLBC-Sand); 7% (w/w) Soil Reef biochar (SRBC) mixed with sand (7% SRBC-Sand); 7% (w/w) PLBC mixed with sandy loam (7% PLBC-SL), and 7% (w/w) SRBC mixed with sandy loam (7% SRBC-SL); values after  $\pm$  are standard error, and values in parenthesis are sample number.

Table 4.2: Root mean square error (RMSE) of gas diffusion models evaluated using total porosity and the fitted parameters

Sample type	Buckingham	Penman -Call	Millington -Quirk (1961)	Penman- Millington- Quirk		Variable inactive pore space		Archie	
	RMSE	RMSE	RMSE	RMSE	$m$	RMSE	$V$	RMSE	$m^*$
Sand	0.046	0.042	0.016	0.011	$1.0 \pm 0.3$	0.024	$1.57 \pm 0.02$		
7%PLBC-Sand	0.049	0.052	0.059	0.045	$1.8 \pm 0.4$	0.041	$1.69 \pm 0.02$		
7%SRBC-Sand	0.065	0.090	0.089	0.042	$1.0 \pm 0.6$	0.056	$2.08 \pm 0.05$		
Sandy Loam (SL)	0.020	0.041	0.040	0.027	$2.3 \pm 0.6$	0.012	$1.75 \pm 0.02$	0.098	$1.95 \pm 0.03$
7%PLBC-SL	0.025	0.026	0.026	0.008	$5.4 \pm 0.3$	0.014	$1.50 \pm 0.02$	0.006	$1.72 \pm 0.01$
7%SRBC-SL	0.019	0.032	0.019	0.015	$3.6 \pm 0.3$	0.016	$1.68 \pm 0.03$	0.103	$1.81 \pm 0.02$

Table 4-3: Root mean square error (RMSE) of gas diffusion models evaluated using inter pore porosity and the fitted parameters

Sample type	Buckingham	Penman- Call	Millington- Quirk (1961)	Penman- Millington- Quirk	Variable inactive pore space		Archie		
	RMSE	RMSE	RMSE	RMSE	$m$	RMSE	$V$	RMSE	$m^*$
7%PLBC-Sand	0.063	0.055	0.041	0.040	$1.9 \pm 0.1$	0.046	$1.59 \pm 0.03$		
7%SRBC-Sand	0.062	0.092	0.062	0.053	$1.0 \pm 1.2$	0.055	$1.99 \pm 0.05$		
7%PLBC-SL	0.030	0.023	0.027	0.008	$6.1 \pm 0.3$	0.009	$1.43 \pm 0.02$	0.013	$1.65 \pm 0.02$
7%SRBC-SL	0.047	0.019	0.034	0.011	$6.4 \pm 1.5$	0.040	$1.36 \pm 0.08$	0.064	$1.52 \pm 0.02$

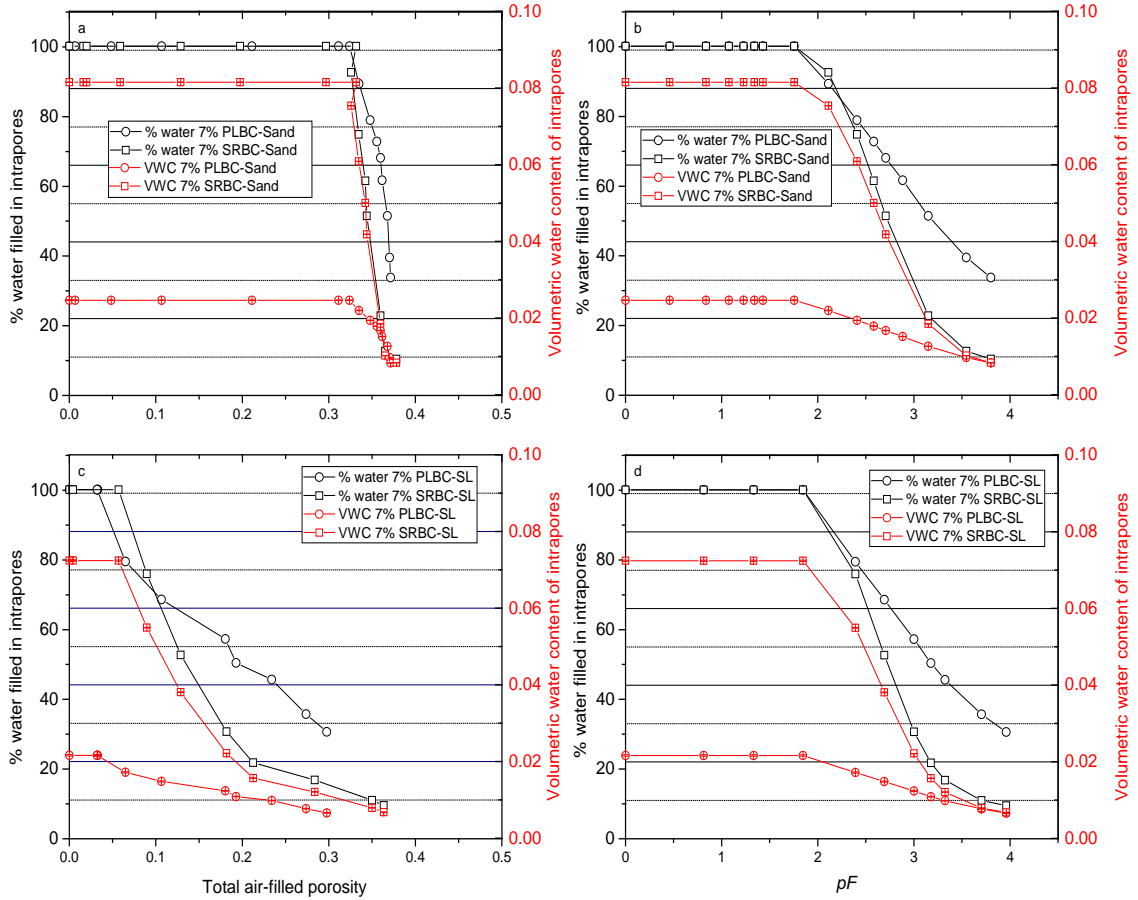


Figure 4-1: Mercury intrusion porosimetry and water retention data from Chapter 3 were used to plot % water filled in intrapores and the volumetric water content (VWC) of the intrapores (in red) as a function of total air-filled porosity in (a) for sand mixtures and (c) for sandy loam (SL) mixtures. The % water filled in intrapores and the VWC are plotted as a function of pressure ( $pF = -\log |h, \text{cm-H}_2\text{O}|$ ) in (b) for sand mixtures and in (d) for SL mixtures. Sand and sandy loam were not plotted since they were assumed to have negligible intrapores.

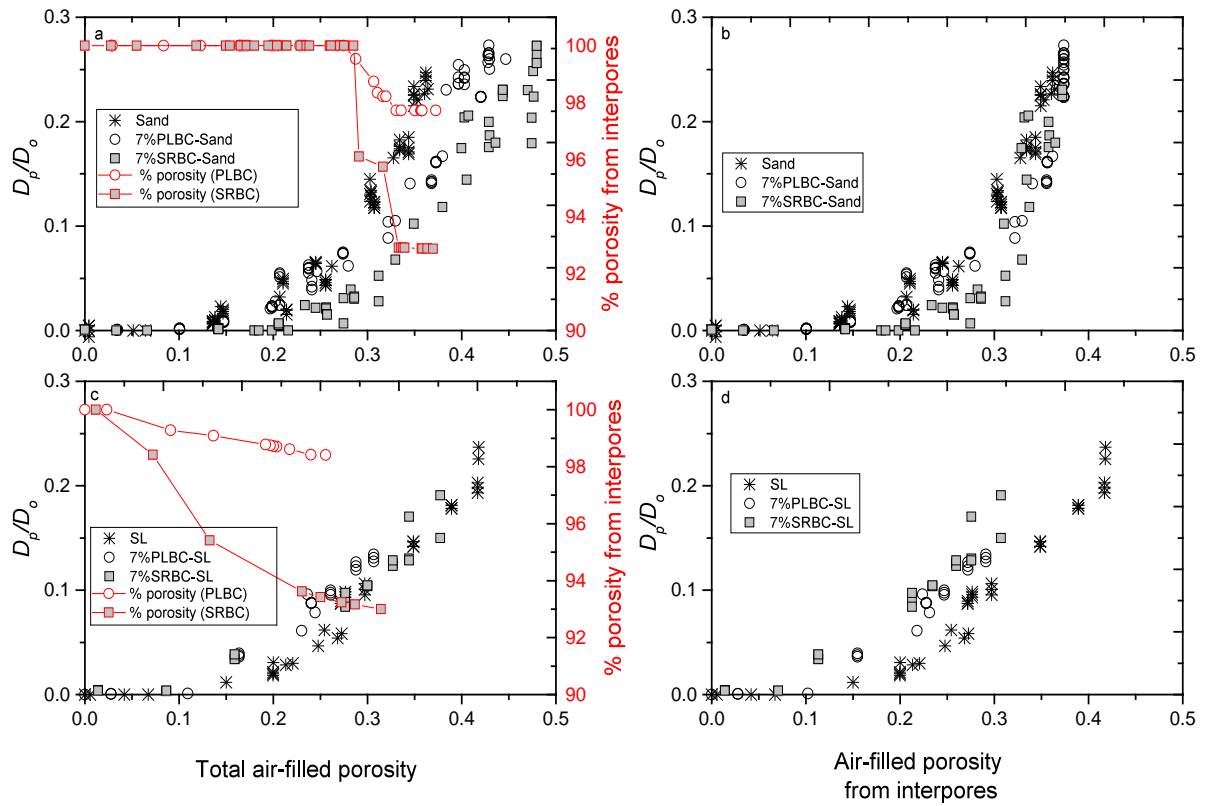


Figure 4-2: Relative gas diffusivity ( $D_p/D_o$ ) as a function of total air-filled porosity ( $\epsilon$ ) where (a) includes sand mixtures, and (c) is of mixtures in sandy loam (SL). The plots  $D_p/D_o$  as a function of air-filled porosity from interpores ( $\epsilon^{inter}$ ) are shown in (b) for sand mixtures and in (d) for SL mixtures. Plots (a) and (c) show the % porosity contribution from interpores of PLBC and SRBC mixtures in red.

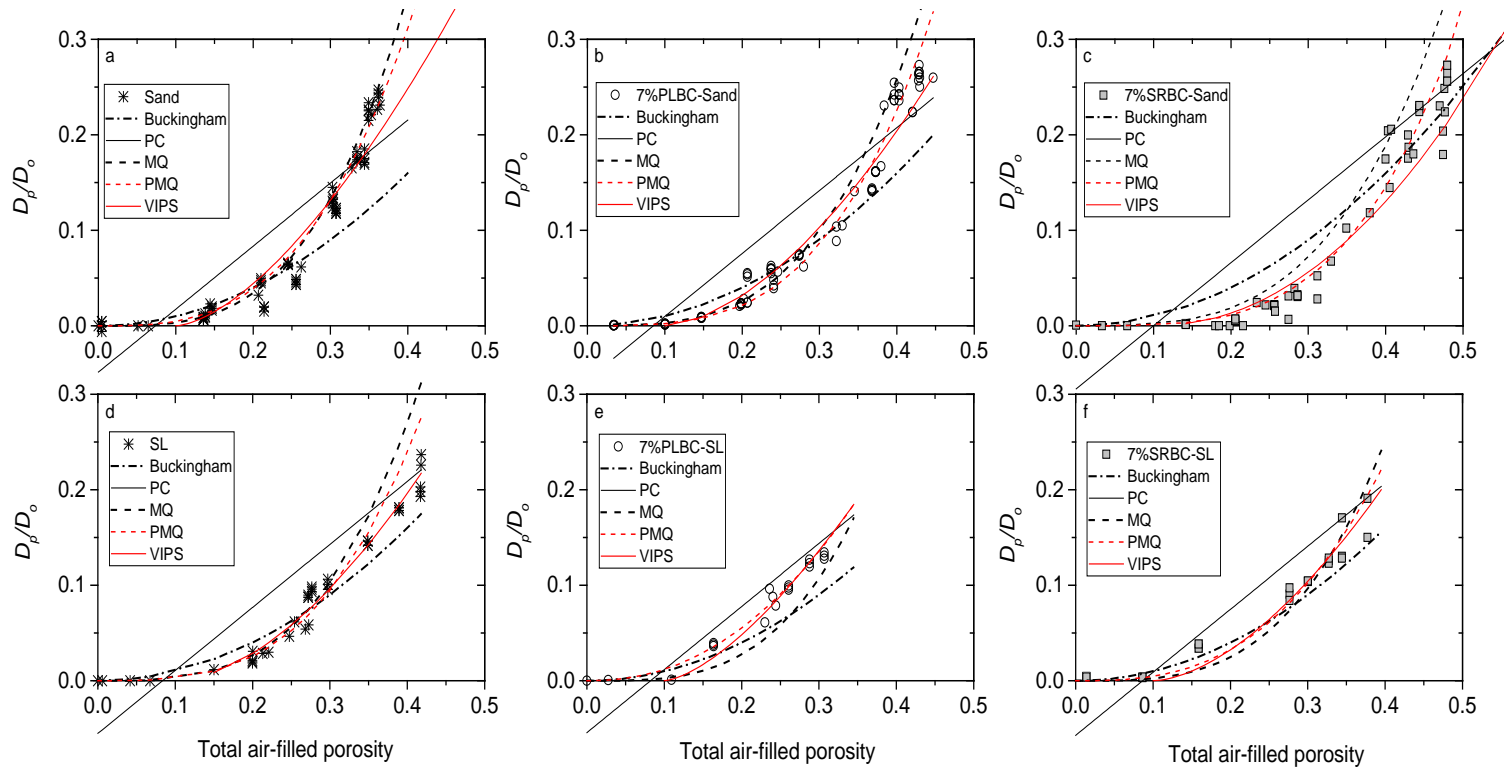


Figure 4-3: Relative gas diffusivity ( $D_p/D_o$ ) as a function of total air-filled porosity ( $\varepsilon$ ) where plots are of: (a) Sand, (b) 7% PLBC-Sand, (c) 7% SRBC-Sand, (d) sandy loam, (e) 7% PLBC-SL, and (f) 7% SRBC-SL. The lines are the comparison of the Buckingham model, Penman-Call (PC) model, Millington-Quirk (MQ) model, Penman-Millington-Quirk (PMQ) model, and the Variable Inactive Pore Space (VIPS) model.

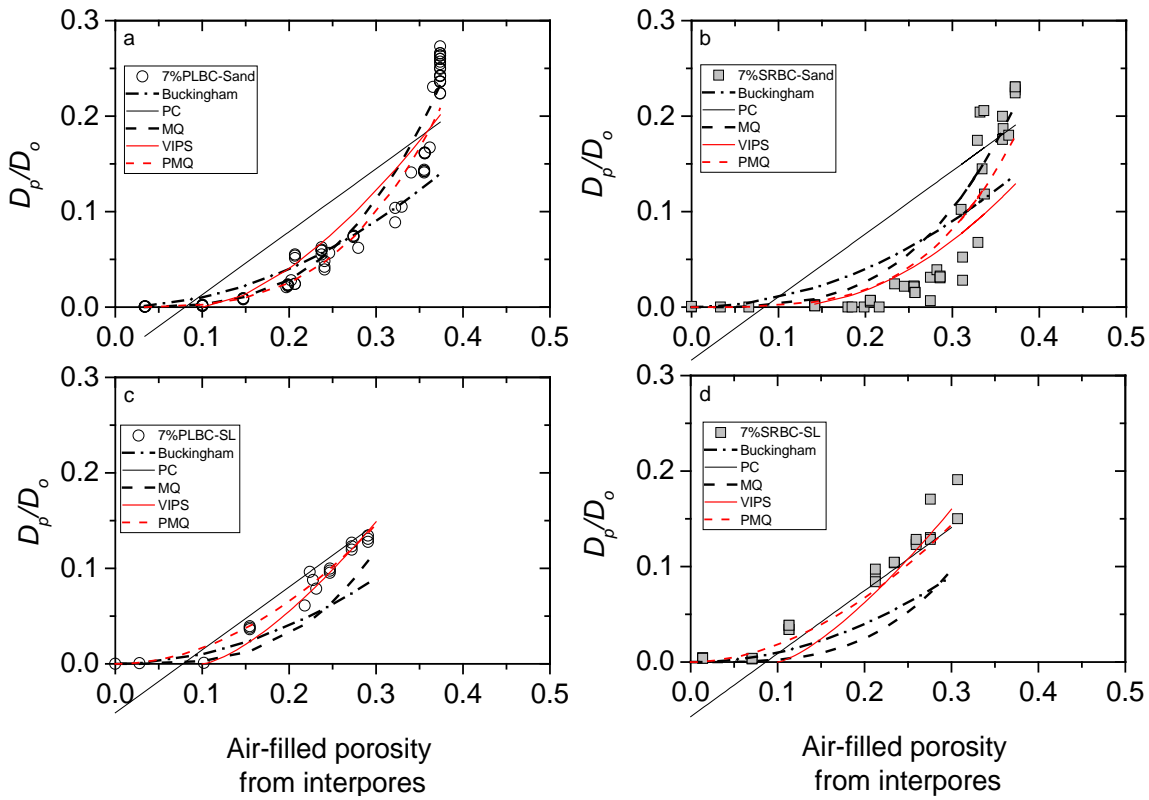


Figure 4-4: Relative gas diffusivity ( $D_p/D_o$ ) as a function of air-filled porosity from inter pores ( $\epsilon^{inter}$ ) where the plots are: (a) 7% PLBC-Sand, (b) 7% SRBC-Sand, (c) 7% PLBC-SL, and (d) 7% SRBC-SL. The lines are the comparison of the Buckingham model, Penman-Call (PC) model, Millington-Quirk (MQ) model, Penman-Millington-Quirk (PMQ) model, and the Variable Inactive Pore Space (VIPS) model.

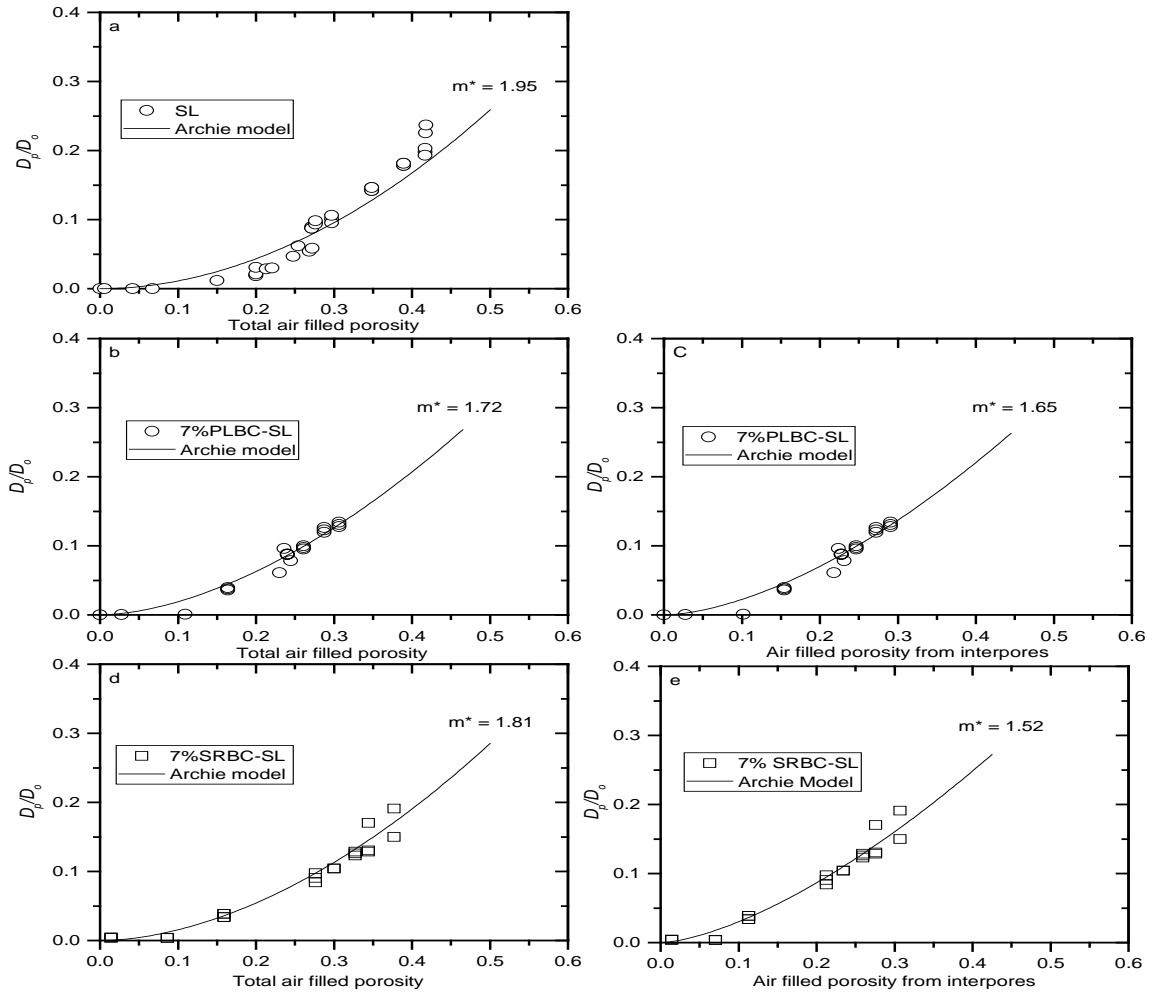


Figure 4-5: Fitted Archie's law model plots of relative gas diffusivity ( $D_p/D_o$ ) as a function of total air-filled porosity ( $\epsilon$ ) in (a) for sandy loam, (b) for 7% PLBC-SL, and (d) for 7% SRBC-SL. Plots of  $D_p/D_o$  as a function air-filled porosity from interpores ( $\epsilon^{inter}$ ) are in (c) for 7% PLBC-SL and (e) for 7% SRBC-SL. Sand mixtures were not plotted since the particle size distribution was not affected.

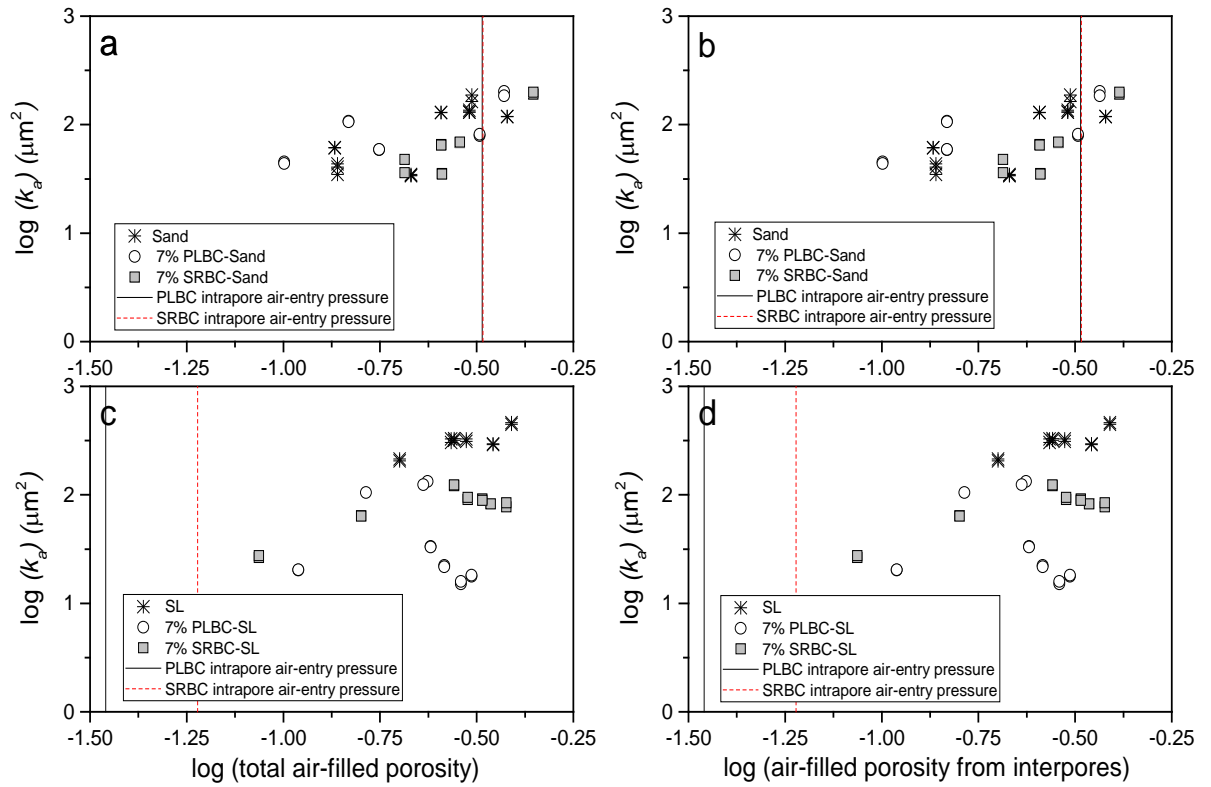


Figure 4-6: Plots of gas permeability ( $k_a$ ) as a function of total air-filled porosity ( $\varepsilon$ ) in (a) for sand mixtures, and (c) for sandy loam (SL) mixtures. The gas permeability plotted as a function of air-filled porosity from intrapores ( $\varepsilon^{inter}$ ) are in (b) for sand mixtures, and in (d) for sandy loam mixtures. Vertical lines indicate logarithmic intrapore air-entry pressure for PLBC (black line) and SRBC (red dotted line).

## Chapter 5

### FUTURE WORK

Understanding the mechanisms that govern the soil physical properties of biochar-amended soil is important to accurately describe water and gas transport processes. Biochar performance in soils can vary, as biochar surface properties, shape, and particle size are all affected by parent feedstock, pyrolysis temperature, and weathering. The internal porosity and surface roughness of biochar can be significant at high pyrolysis temperature, and such properties may result in long lasting changes in soil pore structure that impact soil-water relationships. This dissertation presented three studies conducted to better understand the changes in soil properties with biochar application: 1) biochar hydrophobicity, 2) soil-water retention, and 3) gas transport parameters. Future work is briefly discussed in this chapter to improve the presented work and to provide a better mechanistic understanding of the processes that govern changes in soil associated with biochar amendment.

#### 5.1 Biochar on soil-water repellency

Three potential mechanisms that cause biochar hydrophobicity were postulated and tested in Chapter 2. The pyrolysis temperature was shown to affect hydrophobicity of poultry litter biochar, as higher pyrolysis temperatures produced biochars of lower hydrophobicity [Kinney *et al.*, 2012]. The hydrophobic organic compounds likely coated the poultry litter biochar during cooling after pyrolysis, and pyrolysis temperature dictated the amount of carbon coating biochar surfaces. The hydrophobicity

of poultry litter biochars was transient and results showed the presence of organic compounds on biochar surfaces that were easily leached.

Currently, there is limited understanding of the effects of organic carbon leaching from poultry litter biochar on the surrounding environment. The expectation is that hydrophobic compounds may alter soil water retention characteristic curves and gas transport properties, making it difficult to develop predictive models. However, it is well documented that biochars have beneficial effects on soils. Poultry litter biochars can improve water holding capacity, increase cation exchange capacity, and increase extractable nutrients [Revell *et al.*, 2012]. It is also suggested that the organic coatings on biochars may promote microbial proliferation and increase plant growth.

The organic coatings were released in different concentrations over time from poultry litter biochar produced at 300°C. Poultry litter biochar produced at 600°C released smaller quantities of organic carbon than biochar produced at 300°C. Future study should explore the effects of poultry litter biochar leachate on soils. Organic solutes leached from poultry litter biochar may improve crop yield and alter greenhouse gas emissions by promoting microbial activity. It is unclear if the leachable organic carbons from poultry litter biochar are a nutrient source for the soil biomass, or if the changes in biochar surface pores, evidenced by an increase in poultry litter biochar surface area, might also promote microbial growth. Future work should address these questions.

## 5.2 Biochar impact on soil-water retention

A model was developed and tested to predict the effect of biochar amendment on soil water retention in Chapter 3. This was achieved by quantifying pores within biochar particles (intrapores) using mercury intrusion porosimetry. Water sorption data were collected using a dew-point potentiometer. Changes in interpores (pore spaces between particles) were also estimated using the Arya model [Arya *et al.*, 1999; Arya and Heitman, 2015]. Combining these three components produced a predictive model for soil water retention.

Using this predictive model, changes caused by biochar amendment on soil water retention were assessed. The results showed that poultry litter and pinewood biochar retained different quantities of water and the amount depended on the size of the interpores and intrapores. The model was developed using sieved biochars applied to a coarsely grained soil and a uniform sand. Because of this limitation, future work requires testing the model on biochar-soil media with different soil texture, especially in soils with higher clay content than the sandy loam studied here. Studies suggest that clay particles with smaller diameter than biochar intrapores may clog pores thus reducing biochar intrapore volume. This reduces the water storage volume of biochar-amended soil. If intrapores on biochar are partially clogged by clay particles, the model predictions of water retention may be inaccurate, since the intrapores measured by mercury intrusion porosimetry would not be available for water storage. Therefore, the interaction between biochar and variable textures soils needs to be quantified and tested to validate the utility of the model.

Biochar aging changes the surface structure of biochar, sometimes leading to particle breakage through weathering. It is unclear if aging significantly alters biochar

intrapore volume. The size and shape of biochar particles will change with weathering, which will result in dynamic changes in interpores of biochar-amended soil. Rates of these changes in interpores and intrapores should be better understood and quantified for model refinement.

### **5.3 Biochar impact on soil-gas transport**

Chapter 4 presents the effects of poultry litter and wood biochar on gas transport parameters: diffusivity and air permeability. The gas transport properties of biochar-amended sand and biochar amended sandy loam were investigated. The results showed that sieved biochars can alter interpores and intrapores that affect gas transport, and such changes were important. Adding biochar to sand altered air-filled porosity, and biochars with a high intrapore volume lowered gas diffusion the most.

Additional work needed is on the air permeability of biochar-amended soils. The air permeability data in this study were limited. With additional laboratory data, air permeability models might be applied to further evaluate the relationship between air-filled porosity and air permeability of biochar-amended soils.

Furthermore, laboratory measurements are needed where water contents and air permeability are measured complimentary to each other since air permeability is strongly affected by soil water content. Biochars have the ability to hold water like clays, but more data is needed to confirm if the biochar results in a reduction in air permeability for a given air-filled porosity.

## REFERENCES

- Abel, S., A. Peters, S. Trinks, H. Schonsky, M. Facklam, and G. Wessolek (2013), Impact of biochar and hydrochar addition on water retention and water repellency of sandy soil, *Geoderma*, 202, 183-191, doi: 10.1016/j.geoderma.2013.03.003.
- AbuElShar, W. and L. Abriola (1997), Experimental assessment of gas transport mechanisms in natural porous media: Parameter evaluation, *Water Resour. Res.*, 33(4), 505-516, doi: 10.1029/96WR03536.
- Ahmad, M., S. S. Lee, X. Dou, D. Mohan, J. Sung, J. E. Yang, and Y. S. Ok (2012), Effects of pyrolysis temperature on soybean stover- and peanut shell-derived biochar properties and TCE adsorption in water., *Bioresour. Technol.*, 118.
- Archie, G. (1942), The electrical resistivity log as an aid in determining some reservoir characteristics, *Transactions of the American Institute of Mining and Metallurgical Engineers*, 146, 54-61.
- Arthur, E., M. Tuller, P. Moldrup, and L. W. de Jonge (2015), Effects of biochar and manure amendments on water vapor sorption in a sandy loam soil, *Geoderma*, 243, 175-182, doi: 10.1016/j.geoderma.2015.01.001.
- Arthur, E., P. Moldrup, P. Schjonning, and L. W. de Jonge (2012), Linking Particle and Pore Size Distribution Parameters to Soil Gas Transport Properties, *Soil Sci. Soc. Am. J.*, 76(1), 18-27, doi: 10.2136/sssaj2011.0125.
- Arya, L. M. and J. F. Paris (1981), A physicoempirical model to predict the soil moisture characteristic from particle-size distribution and bulk density data, *Soil Sci. Soc. Am. J.*, 45(6), 1023-1030.
- Arya, L. M. and J. L. Heitman (2015), A Non-Empirical Method for Computing Pore Radii and Soil Water Characteristics from Particle-Size Distribution, *Soil Sci. Soc. Am. J.*, 79(6), 1537-1544, doi: 10.2136/sssaj2015.04.0145.

Arya, L., F. Leij, M. van Genuchten, and P. Shouse (1999), Scaling parameter to predict the soil water characteristic from particle-size distribution data, *Soil Sci. Soc. Am. J.*, 63(3), 510-519.

Arye, G., I. Nadav, and Y. Chen (2007), Short-term reestablishment of soil water repellency after wetting: Effect on capillary pressure-saturation relationship, *Soil Sci. Soc. Am. J.*, 71(3), 692-702, doi: 10.2136/sssaj2006.0239.

ASTM Standard C136-06 (2003), Standard test method for sieve analysis of fine and coarse aggregates, in Anonymous, ASTM International, West Conshohocken, PA.

ASTM Standard D4404-10 (2010), Standard test method for determination of pore volume and pore volume distribution of soil and rock by mercury intrusion porosimetry, *ASTM International, West Conshohocken, PA.*

ASTM Standard D6556-14 (2012), Standard test method for carbon black--Total and external surface area by nitrogen adsorption, *ASTM International, West Conshohocken, PA.*

Atanassova, I. and S. H. Doerr (2011), Changes in soil organic compound composition associated with heat-induced increases in soil water repellency, *Eur. J. Soil Sci.*, 62(4), 516-532, doi: 10.1111/j.1365-2389.2011.01350.x.

Atkinson, C. J., J. D. Fitzgerald, and N. A. Hips (2010), Potential mechanisms for achieving agricultural benefits from biochar application to temperate soils: a review, *Plant Soil*, 337(1-2), 1-18, doi: 10.1007/s11104-010-0464-5.

Bachmann, J., A. Ellies, and K. Hartge (2000), Development and application of a new sessile drop contact angle method to assess soil water repellency, *Journal of Hydrology*, 231, 66-75, doi: 10.1016/S0022-1694(00)00184-0.

Bachmann, J. and G. McHale (2009), Superhydrophobic surfaces: a model approach to predict contact angle and surface energy of soil particles, *Eur. J. Soil Sci.*, 60(3), 420-430, doi: 10.1111/j.1365-2389.2008.01118.x.

Bachmann, J., S. Woche, M. Goebel, M. Kirkham, and R. Horton (2003), Extended methodology for determining wetting properties of porous media, *Water Resources Research*, 39(12), 1353, SBH 11-1-SBH 11-14, doi: 10.1029/2003WR002143.

Bauters, T. W. J., T. S. Steenhuis, D. A. DiCarlo, J. L. Nieber, L. W. Dekker, C. J. Ritsema, J. Y. Parlange, and R. Haverkamp (2000a), Physics of water repellent soils, *Journal of Hydrology*, 231, 233-243, doi: 10.1016/S0022-1694(00)00197-9.

- Bauters, T., T. Steenhuis, D. DiCarlo, J. Nieber, L. Dekker, C. Ritsema, J. Parlange, and R. Haverkamp (2000b), Physics of water repellent soils, *J. Hydrol.*, 231, 233-243, doi: 10.1016/S0022-1694(00)00197-9.
- Bear, J., J. Bensabat, and A. Nir (1991), Heat and Mass-Transfer in Unsaturated Porous-Media at a Hot Boundary .1. One-Dimensional Analytical Model, *Transp. Porous Media*, 6(3), 281-298.
- Beatty, S. M. and J. E. Smith (2010), Fractional wettability and contact angle dynamics in burned water repellent soils, *J. Hydrol.*, 391(1-2), 99-110, doi: 10.1016/j.jhydrol.2010.07.007.
- Beck, D. A., G. R. Johnson, and G. A. Spolek (2011), Amending greenroof soil with biochar to affect runoff water quantity and quality, *Environ. Pollut.*, 159(8-9), 2111-2118, doi: 10.1016/j.envpol.2011.01.022.
- Beesley, L., E. Moreno-Jimenez, J. L. Gomez-Eyles, E. Harris, B. Robinson, and T. Sizmur (2011), A review of biochars' potential role in the remediation, revegetation and restoration of contaminated soils RID F-8022-2010, *Environ. Pollut.*, 159(12), 3269-3282, doi: 10.1016/j.envpol.2011.07.023.
- Boethling, Robert S, Mackay, Donald, Sheppard, Steve, (2001), BOOK REVIEWS - Handbook of Property Estimation Methods for Chemicals, Environmental and Health Sciences, *Journal of environmental quality.*, 30(3), 1099.
- Brewer, C. E., V. J. Chuang, C. A. Masiello, H. Gonnermann, X. Gao, B. Dugan, L. E. Driver, P. Panzacchi, K. Zygourakis, and C. A. Davies (2014), New approaches to measuring biochar density and porosity, *Biomass & Bioenergy*, 66, 176-185, doi: 10.1016/j.biombioe.2014.03.059.
- Briggs, C., J. M. Breiner, and R. C. Graham (2012), Physical and Chemical Properties of Pinus ponderosa Charcoal: Implications for Soil Modification, *Soil Sci.*, 177(4), 263-268, doi: 10.1097/SS.0b013e3182482784.
- Brooks, R. H. and A. T. Corey (1964), Hydraulic properties of porous media and their relation to drainage design, *Trans. ASAE*, 7(1), 26-0028.
- Brown, R., A. Kercher, T. Nguyen, D. Nagle, and W. Ball (2006), Production and characterization of synthetic wood chars for use as surrogates for natural sorbents, *Org. Geochem.*, 37(3), 321-333, doi: 10.1016/j.orggeochem.2005.10.008.
- Brunauer, S., P. Emmett, and E. Teller (1938), Adsorption of gases in multimolecular layers, *J. Am. Chem. Soc.*, 60, 309-319, doi: 10.1021/ja01269a023.

Bruun, E. (2011), Application of fast pyrolysis biochar to a loamy soil, PhD thesis, Technical University of Denmark.

Bryant, R., S. Doerr, and M. Helbig (2005), Effect of oxygen deprivation on soil hydrophobicity during heating, *Int. J. Wildland Fire*, 14(4), 449-455, doi: 10.1071/WF05035.

Buckingham, E. (1904), Contributions to our knowledge of the aeration of soils, *U. S. Department of Agriculture, Bureau of Soils Bulletin*, 25. U.S. Gov. Print. Office.

Campbell, G. S. (1974), A simple method for determining unsaturated conductivity from moisture retention data., *Soil Sci.*, 117(6), 311-314.

Campbell, G. and S. Shiozawa (1992), Prediction of hydraulic properties of soils using particle-size distribution and bulk density data, Proc. Int. Workshop on Indirect Methods for Estimating the Hydraulic Properties of Unsaturated Soils. University of California, Riverside.

Cao, X., L. Ma, Y. Liang, B. Gao, and W. Harris (2011), Simultaneous Immobilization of Lead and Atrazine in Contaminated Soils Using Dairy-Manure Biochar, *Environ. Sci. Technol.*, 45, 4884-4889.

Capriel, P., T. Beck, H. Borchert, J. Gronholz, and G. Zachmann (1995), Hydrophobicity of the Organic-Matter in Arable Soils, *Soil Biology & Biochemistry*, 27(11), 1453-1458, doi: 10.1016/0038-0717(95)00068-P.

Cassie, A. B. D. and S. Baxter (1944), Wettability of porous surfaces., *Transactions of the Faraday Society*, 40, 0546-0550, doi: 10.1039/tf9444000546.

Cetin, E., B. Moghtaderi, R. Gupta, and T. Wall (2004), Influence of pyrolysis conditions on the structure and gasification reactivity of biomass chars, *Fuel*, 83(16), 2139-2150, doi: 10.1016/j.fuel.2004.05.008.

Cheng, C. and J. Lehmann (2009), Ageing of black carbon along a temperature gradient, *Chemosphere*, 75(8), 1021-1027, doi: 10.1016/j.chemosphere.2009.01.045.

Cheng, C., J. Lehmann, and M. H. Engelhard (2008), Natural oxidation of black carbon in soils: Changes in molecular form and surface charge along a climosequence, *Geochim. Cosmochim. Acta*, 72(6), 1598-1610, doi: 10.1016/j.gca.2008.01.010.

Cheng, C., J. Lehmann, J. E. Thies, S. D. Burton, and M. H. Engelhard (2006), Oxidation of black carbon by biotic and abiotic processes, *Org. Geochem.*, 37(11), 1477-1488, doi: 10.1016/j.orggeochem.2006.06.022.

Clough, T. J., J. E. Bertram, J. L. Ray, L. M. Condrón, M. O'Callaghan, R. R. Sherlock, and N. S. Wells (2010), Unweathered Wood Biochar Impact on Nitrous Oxide Emissions from a Bovine-Urine-Amended Pasture Soil, *Soil Sci. Soc. Am. J.*, 74, 852-860.

Conklin, A. R. (2005), *Introduction to Soil Chemistry*, vol. 167, John Wiley & Sons, Inc., Hoboken, New Jersey.

Currie, J. A. (1960a), Gaseous Diffusion in Porous Media .1. a Non-Steady State Method, *British Journal of Applied Physics*, 11(8), 314-317, doi: 10.1088/0508-3443/11/8/302.

Currie, J. A. (1960b), Gaseous Diffusion in Porous Media .2. Dry Granular Materials, *British Journal of Applied Physics*, 11(8), 318-324, doi: 10.1088/0508-3443/11/8/303.

Dane, J. H. and G. C. Topp (2002), *Methods of Soil Analysis: Part 4, Physical Methods*, SSSA Book Series, vol. 5, Soil Science Society of America, Madison, WI.

de la Rosa, J. M., M. Paneque, A. Z. Miller, and H. Knicker (2014), Relating physical and chemical properties of four different biochars and their application rate to biomass production of *Lolium perenne* on a Calcic Cambisol during a pot experiment of 79 days, *Sci. Total Environ.*, 499, 175-184, doi: 10.1016/j.scitotenv.2014.08.025.

DeBano, L. F. (1981), Water repellent soils: A state-of-the-art, in , vol. 46 Anonymous , pp. 2-17, US Department of Agriculture, Forest Service, Pacific Southwest Forest and Range Experiment Station.

DeBano, L. (2000), The role of fire and soil heating on water repellency in wildland environments: a review, *Journal of Hydrology*, 231, 195-206, doi: 10.1016/S0022-1694(00)00194-3.

Decagon Devices, I. (2013), Tools and tips for measuring the full soil moisture release curve.

Dekker, L. and P. Jungerius (1990), Water repellency in the dunes with special reference to the Netherlands, *Catena Suppl.*, 18, 173-183.

Dekker, L. and C. Ritsema (2000), Wetting patterns and moisture variability in water repellent Dutch soils, *J. Hydrol.*, 231, 148-164, doi: 10.1016/S0022-1694(00)00191-8.

Deng, X. L. and R. N. Dave (2013), Dynamic simulation of particle packing influenced by size, aspect ratio and surface energy, *Granul. Matter*, 15(4), 401-415, doi: 10.1007/s10035-013-0413-0.

Diamantopoulos, E., W. Durner, A. Reszkowska, and J. Bachmann (2013), Effect of soil water repellency on soil hydraulic properties estimated under dynamic conditions, *J. Hydrol.*, 486, 175-186, doi: 10.1016/j.jhydrol.2013.01.020.

Diehl, D. (2013), Soil water repellency: Dynamics of heterogeneous surfaces, *Colloids and Surfaces A-Physicochemical and Engineering Aspects*, 432, 8-18, doi: 10.1016/j.colsurfa.2013.05.011.

Dlapa, P., M. B. Bodi, J. Mataix-Solera, A. Cerda, and S. H. Doerr (2013), FT-IR spectroscopy reveals that ash water repellency is highly dependent on ash chemical composition, *Catena*, 108, 35-43, doi: 10.1016/j.catena.2012.02.011.

Doerr, S. H. and A. D. Thomas (2003), Soil moisture: A controlling factor in water repellency?, in *Soil Water Repellency*, edited by C. J. Ritsema and L. W. Dekker, pp. 137-149, Elsevier, Amsterdam, the Netherlands.

Doerr, S. et al. (2005), Extraction of compounds associated with water repellency in sandy soils of different origin, *Aust. J. Soil Res.*, 43(3), 225-237, doi: 10.1071/SR04091.

Doerr, S., R. Shakesby, and R. Walsh (2000), Soil water repellency: its causes, characteristics and hydro-geomorphological significance, *Earth-Sci. Rev.*, 51(1-4), 33-65, doi: 10.1016/S0012-8252(00)00011-8.

Doerr, S. and A. Thomas (2000), The role of soil moisture in controlling water repellency: new evidence from forest soils in Portugal, *J. Hydrol.*, 231, 134-147, doi: 10.1016/S0022-1694(00)00190-6.

Dyrness, C. (1976), Effect of wildfire on soil wettability in the High Cascade of Oregon., *United States Department of Agriculture Forest Service Research Paper PNW-202*, 444.

Eden, M., P. Moldrup, P. Schjonning, K. M. Scow, and L. W. de Jonge (2012), Soil-Gas Phase Transport and Structure Parameters for a Soil Under Different Management Regimes and at Two Moisture Levels, *Soil Sci.*, 177(9), 527-534, doi: 10.1097/SS.0b013e318267ec85.

Ellerbrock, R. H., H. H. Gerke, J. Bachmann, and M. O. Goebel (2005), Composition of organic matter fractions for explaining wettability of three forest soils, *Soil Sci. Soc. Am. J.*, 69(1), 57-66.

Ellerbrock, R. H. and H. H. Gerke (2013), Characterization of Organic Matter Composition of Soil and Flow Path Surfaces Based on Physicochemical Principles-A Review, *Advances in Agronomy, Vol 121, 121*, 117-177, doi: 10.1016/B978-0-12-407685-3.00003-7.

Fellet, G., L. Marchiol, G. Delle Vedove, and A. Peressotti (2011), Application of biochar on mine tailings: Effects and perspectives for land reclamation, *Chemosphere*, 83, 1262-1267.

Fujikawa, T. and T. Miyazaki (2005), Effects of bulk density and soil type on the gas diffusion coefficient in repacked and undisturbed soils, *Soil Sci.*, 170(11), 892-901, doi: 10.1097/01.ss.0000196771.53574.79.

Fuller, E. N., P. D. Schettler, and J. C. and Giddings (1966), **A new method for prediction of binary gas-phase diffusion coefficients**, *Industrial & Engineering Chemistry*, 58, 18-27.

Giesche, H. (2006), Mercury porosimetry: A general (practical) overview, *Particle & Particle Systems Characterization*, 23(1), 9-19, doi: 10.1002/ppsc.200601009.

Granged, A. J. P., A. Jordan, L. M. Zavala, and G. Barcenas (2011), Fire-induced changes in soil water repellency increased fingered flow and runoff rates following the 2004 Huelva wildfire, *Hydrol. Process.*, 25(10), 1614-1629, doi: 10.1002/hyp.7923.

Grathwohl, P. (1998), *Diffusion in Natural Porous Media: Contaminant Transport, Sorption/Desorption and Dissolution Kinetics*, 224 pp., Kluwer Academic Publishers, Boston, MA.

Gubiani, P. I., J. M. Reichert, C. Campbell, D. J. Reinert, and N. S. Gelain (2013), Assessing Errors and Accuracy in Dew-Point Potentiometer and Pressure Plate Extractor Measurements, *Soil Sci. Soc. Am. J.*, 77(1), 19-24, doi: 10.2136/sssaj2012.0024.

Gupta, S. and W. Larson (1979), Estimating Soil-Water Retention Characteristics from Particle-Size Distribution, Organic-Matter Percent, and Bulk-Density, *Water Resour. Res.*, 15(6), 1633-1635, doi: 10.1029/WR015i006p01633.

Hardie, M., B. Clothier, S. Bound, G. Oliver, and D. Close (2014), Does biochar influence soil physical properties and soil water availability?, *Plant Soil*, 376(1-2), 347-361, doi: 10.1007/s11104-013-1980-x.

Haverkamp, R. and J. Parlange (1986), Predicting the Water-Retention Curve from Particle-Size Distribution .1. Sandy Soils without Organic-Matter, *Soil Sci.*, 142(6), 325-339, doi: 10.1097/00010694-198612000-00001.

Hodson, M., M. Lee, and I. Parsons (1997), Origins of the surface roughness of unweathered alkali feldspar grains, *Geochim. Cosmochim. Acta*, 61(18), 3885-3896, doi: 10.1016/S0016-7037(97)00197-X.

Hsieh, C., J. Chen, R. Kuo, T. Lin, and C. Wu (2005), Influence of surface roughness on water- and oil-repellent surfaces coated with nanoparticles, *Appl. Surf. Sci.*, 240(1-4), 318-326, doi: 10.1016/j.apsusc.2004.07.016.

Hubbert, K. and V. Oriol (2005), Temporal fluctuations in soil water repellency following wildfire in chaparral steplands, southern California, *Int. J. Wildland Fire*, 14(4), 439-447, doi: 10.1071/WF05036.

Huffman, E., L. MacDonald, and J. Stednick (2001), Strength and persistence of fire-induced soil hydrophobicity under ponderosa and lodgepole pine, Colorado Front Range, *Hydrol. Process.*, 15(15), 2877-2892, doi: 10.1002/hyp.379.

Hwang, S. and S. Choi (2006), Use of a lognormal distribution model for estimating soil water retention curves from particle-size distribution data, *J. Hydrol.*, 323(1-4), 325-334, doi: 10.1016/j.jhydrol.2005.09.005.

Impoco, G., S. Carrato, M. Caccamo, L. Tuminello, and G. Licitra (2006), Quantitative Analysis of Cheese Microstructure Using SEM Imagery, 22-26.

Israelachvili, J. N. (1991), *Intermolecular and Surface Forces*, Academic Press London.

Jeffery, S., F. G. A. Verheijen, M. van der Velde, and A. C. Bastos (2011), A quantitative review of the effects of biochar application to soils on crop productivity using meta-analysis, *Agric. , Ecosyst. Environ.*, 144(1), 175-187, doi: <http://dx.doi.org/10.1016/j.agee.2011.08.015>.

Jensen, D. K., M. Tuller, L. W. de Jonge, E. Arthur, and P. Moldrup (2015), A New Two-Stage Approach to predicting the soil water characteristic from saturation to oven-dryness, *J. Hydrol.*, 521, 498-507, doi: 10.1016/j.jhydrol.2014.12.018.

Joseph, S. D. et al. (2010), An investigation into the reactions of biochar in soil RID D-6805-2011, *Aust. J. Soil Res.*, 48(6-7), 501-515, doi: 10.1071/SR10009.

Jury, W. A., W. Gardner, and W. H. Gardner (1991), *Soil Physics*, J. Wiley, New York.

Kasozi, G. N., A. R. Zimmerman, P. Nkedi-Kizza, and B. Gao (2010), Catechol and Humic Acid Sorption onto a Range of Laboratory-Produced Black Carbons (Biochars), *Environ. Sci. Technol.*, 44(16), 6189-6195, doi: 10.1021/es1014423.

Kawamoto, K., P. Moldrup, P. Schjonning, B. V. Iversen, T. Komatsu, and D. E. Rolston (2006a), Gas transport parameters in the vadose zone: Development and tests of power-law models for air permeability, *Vadose Zone Journal*, 5(4), 1205-1215, doi: 10.2136/vzj2006.0030.

Kawamoto, K., P. Moldrup, P. Schjonning, B. V. Iversen, T. Komatsu, and D. E. Rolston (2006b), Gas transport parameters in the vadose zone: Development and tests of power-law models for air permeability, *Vadose Zone Journal*, 5(4), 1205-1215, doi: 10.2136/vzj2006.0030.

Kerre, B., B. Willaert, Y. Cornelis, and E. Smolders (2017), Long-term presence of charcoal increases maize yield in Belgium due to increased soil water availability, *Eur. J. Agron.*, 91, 10-15, doi: 10.1016/j.eja.2017.09.003.

Kinney, T. J., C. A. Masiello, B. Dugan, W. C. Hockaday, M. R. Dean, K. Zygourakis, and R. T. Barnes (2012), Hydrologic properties of biochars produced at different temperatures, *Biomass & Bioenergy*, 41, 34-43, doi: 10.1016/j.biombioe.2012.01.033.

Kumari, K. G. I. D., P. Moldrup, M. Paradelo, L. Elsgaard, H. Hauggaard-Nielsen, and L. W. de Jonge (2014), Effects of Biochar on Air and Water Permeability and Colloid and Phosphorus Leaching in Soils from a Natural Calcium Carbonate Gradient, *J. Environ. Qual.*, 43(2), 647-657, doi: 10.2134/jeq2013.08.0334.

Laird, D. A., R. C. Brown, J. E. Amonette, and J. Lehmann (2009), Review of the pyrolysis platform for coproducing bio-oil and biochar, *Biofuels Bioproducts & Biorefining-Biofpr*, 3(5), 547-562, doi: 10.1002/bbb.169.

Lamparter, A., M. Deurer, J. Bachmann, and W. H. M. Duijnsveld (2006), Effect of subcritical hydrophobicity in a sandy soil on infiltration and mobile water content, *Journal of Plant Nutrition and Soil Science-Zeitschrift Fur Pflanzenernahrung Und Bodenkunde*, 169, 38-46.

Lamparter, A., J. Bachmann, S. K. Woche, and M. Goebel (2014), Biogeochemical Interface Formation: Wettability Affected by Organic Matter Sorption and Microbial Activity, *Vadose Zone Journal*, 13(7), doi: 10.2136/vzj2013.10.0175.

Leelamanie, D. A. L. and J. Karube (2007), Effects of organic compounds, water content and clay on the water repellency of a model sandy soil, *Soil Sci. Plant Nutr.*, 53(6), 711-719, doi: 10.1111/j.1747-0765.2007.00199.x.

Lehmann, J. (2007), Bio-energy in the black, *Frontiers in Ecology and the Environment*, 5(7), 381-387.

Lehmann, J. and S. Joseph (2009), *Biochar for Environmental Management : Science and Technology*, Earthscan, London; Sterling, VA.

Lehmann, J., M. C. Rillig, J. Thies, C. A. Masiello, W. C. Hockaday, and D. Crowley (2011), Biochar effects on soil biota - A review RID A-2653-2011, *Soil Biol. Biochem.*, 43(9), 1812-1836, doi: 10.1016/j.soilbio.2011.04.022.

Letey, J., M. L. K. Carrillo, and X. P. Pang (2000), Approaches to characterize the degree of water repellency, *Journal of Hydrology*, 231, 61-65, doi: 10.1016/S0022-1694(00)00183-9.

Liu, H. and G. Bodvarsson (2001), Constitutive relations for unsaturated flow in a fracture network, *J. Hydrol.*, 252(1-4), 116-125, doi: 10.1016/S0022-1694(01)00449-8.

Liu, Z., B. Dugan, C. A. Masiello, R. T. Barnes, M. E. Gallagher, and H. Gonnermann (2016), Impacts of biochar concentration and particle size on hydraulic conductivity and DOC leaching of biochar-sand mixtures, *Journal of Hydrology*, 533, 461-472, doi: 10.1016/j.jhydrol.2015.12.007.

Liu, Z., B. Dugan, C. A. Masiello, and H. M. Gonnermann (2017), Biochar particle size, shape, and porosity act together to influence soil water properties, *PLoS One*, 12(6), e0179079, doi: 10.1371/journal.pone.0179079.

Luz Cayuela, M., M. Angel Sanchez-Monedero, A. Roig, K. Hanley, A. Enders, and J. Lehmann (2013), Biochar and denitrification in soils: when, how much and why does biochar reduce N<sub>2</sub>O emissions?, *Sci Rep*, 3, 1732, doi: 10.1038/srep01732.

MacDonald, L. and E. Huffman (2004), Post-fire soil water repellency: Persistence and soil moisture thresholds, *Soil Sci. Soc. Am. J.*, 68(5), 1729-1734.

Marsiello, C. A., B. Dugan, C. E. Brewer, K. A. Spokas, J. M. Novak, Z. Liu, and G. Sorrenti (2015), Biochar effects on soil hydrology, in *Biochar for Environmental Management : Science, Technology and Implementation (2nd Edition)*, edited by Johannes Lehmann and Stephen Joseph, pp. 543-562, Taylor and Francis, Florence, KY, USA.

Ma'shum, M., M. Tate, G. Jones, and J. Oades (1988), Extraction and Characterization of Water-Repellent Materials from Australian Soils, *J. Soil Sci.*, 39(1), 99-110.

Mohammadi, M. H. and M. Vanclouster (2011), Predicting the Soil Moisture Characteristic Curve from Particle Size Distribution with a Simple Conceptual Model, *Vadose Zone Journal*, 10(2), 594-602, doi: 10.2136/vzj2010.0080.

Moldrup, P., T. Olesen, J. Gamst, P. Schjonning, T. Yamaguchi, and D. Rolston (2000), Predicting the gas diffusion coefficient in repacked soil: Water-induced linear reduction model, *Soil Sci. Soc. Am. J.*, 64(5), 1588-1594.

Moldrup, P., T. Olesen, T. Komatsu, P. Schjonning, and D. Rolston (2001), Tortuosity, diffusivity, and permeability in the soil liquid and gaseous phases, *Soil Sci. Soc. Am. J.*, 65(3), 613-623.

Moldrup, P., T. Olesen, D. Rolston, and T. Yamaguchi (1997), Modeling diffusion and reaction in soils .7. Predicting gas and ion diffusivity in undisturbed and sieved soils, *Soil Sci.*, 162(9), 632-640, doi: 10.1097/00010694-199709000-00004.

Moldrup, P., T. Olesen, S. Yoshikawa, T. Komatsu, A. McDonald, and D. Rolston (2005a), Predictive-descriptive models for gas and solute diffusion coefficients in variably saturated porous media coupled to pore-size distribution: III. Inactive pore space interpretations of gas diffusivity, *Soil Sci.*, 170(11), 867-880, doi: 10.1097/01.ss.0000196770.45951.06.

Moldrup, P., T. Olesen, S. Yoshikawa, T. Komatsu, and D. Rolston (2005b), Predictive-descriptive models for gas and solute diffusion coefficients in variably saturated porous media coupled to pore-size distribution: I. Gas diffusivity in repacked soil, *Soil Sci.*, 170(11), 843-853, doi: 10.1097/01.ss.0000196769.51788.73.

Mostafid, M. E., C. Shank, P. T. Imhoff, and R. Yazdani (2012), Gas transport properties of compost-woodchip and green waste for landfill biocovers and biofilters, *Chem. Eng. J.*, 191, 314-325, doi: 10.1016/j.cej.2012.03.022.

Mualem, Y. (1976), A new model for predicting the hydraulic conductivity of unsaturated porous media, *Water Resour. Res.*, 12(3), 513-522, doi: 10.1029/WR012i003p00513.

Mukherjee, A., R. Lal, and A. R. Zimmerman (2014), Effects of biochar and other amendments on the physical properties and greenhouse gas emissions of an artificially degraded soil, *Sci. Total Environ.*, 487, 26-36, doi: 10.1016/j.scitotenv.2014.03.141.

Nanda, S., P. Mohanty, K. K. Pant, S. Naik, J. A. Kozinski, and A. K. Dalai (2013), Characterization of North American Lignocellulosic Biomass and Biochars in Terms of their Candidacy for Alternate Renewable Fuels, *BioEnergy Res.*, 6(2), 663-677, doi: 10.1007/s12155-012-9281-4.

Nemes, A. and W. Rawls (2006), Evaluation of different representations of the particle-size distribution to predict soil water retention, *Geoderma*, 132(1-2), 47-58, doi: 10.1016/j.geoderma.2005.04.018.

Novak, J. M., W. J. Busscher, D. L. Laird, M. Ahmedna, D. W. Watts, and M. A. S. Niandou (2009), Impact of Biochar Amendment on Fertility of a Southeastern Coastal Plain Soil, *Soil Sci.*, 174(2), 105-112, doi: 10.1097/SS.0b013e3181981d9a.

Ojeda, G., S. Mattana, A. Avila, J. Maria Alcaniz, M. Volkmann, and J. Bachmann (2015), Are soil-water functions affected by biochar application?, *Geoderma*, 249, 1-11, doi: 10.1016/j.geoderma.2015.02.014.

Olsson, M., J. Kjallstrand, and G. Petersson (2003), Oxidative pyrolysis of integral softwood pellets, *J. Anal. Appl. Pyrolysis*, 67(1), 135-141, doi: 10.1016/S0165-2370(02)00058-X.

Peng, S., Q. Hu, and S. Hamamoto (2012), Diffusivity of rocks: Gas diffusion measurements and correlation to porosity and pore size distribution, *Water Resour. Res.*, 48, W02507, doi: 10.1029/2011WR011098.

Pereira, R. C., J. Kaal, M. C. Arbestain, R. Pardo Lorenzo, W. Aitkenhead, M. Hedley, F. Macias, J. Hindmarsh, and J. A. Macia-Agullo (2011), Contribution to characterisation of biochar to estimate the labile fraction of carbon, *Org. Geochem.*, 42(10), 1331-1342, doi: 10.1016/j.orggeochem.2011.09.002.

Poulsen, T. G. and H. Blendstrup (2008), Predicting Air Permeability in Porous Media with Variable Structure, Bulk Density, and Water Content, *Vadose Zone Journal*, 7(4), 1223-1229, doi: 10.2136/vzj2008.0035.

Poulsen, T. G., H. Blendstrup, and P. Schjonning (2008), Air Permeability in Repacked Porous Media with Variable Structure-Forming Potential, *Vadose Zone Journal*, 7(4), 1139-1143, doi: 10.2136/vzj2007.0147.

Poulsen, T. G., P. Moldrup, S. Yoshikawa, and T. Komatsu (2006), Bimodal probability law model for unified description of water retention, air and water permeability, and gas diffusivity in variably saturated soil, *Vadose Zone Journal*, 5(4), 1119-1128, doi: 10.2136/vzj2005.0146.

Rajkai, K., S. Kabos, and M. van Genuchten (2004), Estimating the water retention curve from soil properties: comparison of linear, nonlinear and concomitant variable methods, *Soil Tillage Res.*, 79(2), 145-152, doi: 10.1016/j.still.2004.07.003.

Rawls, W., Y. Pachepsky, J. Ritchie, T. Sobecki, and H. Bloodworth (2003), Effect of soil organic carbon on soil water retention, *Geoderma*, 116(1-2), 61-76, doi: 10.1016/S0016-7061(03)00094-6.

Revell, K. T., R. O. Maguire, and F. A. Agblevor (2012), Influence of Poultry Litter Biochar on Soil Properties and Plant Growth, *Soil Sci.*, 177(6), 402-408, doi: 10.1097/SS.0b013e3182564202.

Rogovska, N., D. Laird, R. Cruse, P. Fleming, T. Parkin, and D. Meek (2011), Impact of Biochar on Manure Carbon Stabilization and Greenhouse Gas Emissions, *Soil Sci. Soc. Am. J.*, 75, 871-879.

Rondon, M. A., J. Lehmann, J. Ramirez, and M. Hurtado (2007), Biological nitrogen fixation by common beans (*Phaseolus vulgaris* L.) increases with bio-char additions, *Biol. Fertility Soils*, 43(6), 699-708, doi: 10.1007/s00374-006-0152-z.

Savage, S. (1974), Mechanism of Fire-Induced Water Repellency in Soil, *Soil Sci. Soc. Am. J.*, 38(4), 652-657.

Schaap, M. and W. Bouten (1996), Modeling water retention curves of sanely soils using neural networks, *Water Resour. Res.*, 32(10), 3033-3040, doi: 10.1029/96WR02278.

Schnitzer, M. I., C. M. Monreal, G. A. Facey, and P. B. Fransham (2007a), The conversion of chicken manure to biooil by fast pyrolysis I. Analyses of chicken manure, biooils and char by C-13 and H-1 NMR and FTIR spectrophotometry, *J. Environ. Sci. Health Part B-Pestic. Contam. Agric. Wastes*, 42(1), 71-77, doi: 10.1080/03601230601020894.

Schnitzer, M. I., C. M. Monreal, G. Jandl, P. Leinweber, and P. B. Fransham (2007b), The conversion of chicken manure to biooil by fast pyrolysis II. Analysis of chicken manure, biooils, and char by curie-point pyrolysis-gas chromatography/mass spectrometry (Cp Py-GC/MS), *J. Environ. Sci. Health Part B-Pestic. Contam. Agric. Wastes*, 42(1), 79-95, doi: 10.1080/03601230601020944.

Singh, B., B. P. Singh, and A. L. Cowie (2010a), Characterisation and evaluation of biochars for their application as a soil amendment, *Aust. J. Soil Res.*, 48(6-7), 516-525, doi: 10.1071/SR10058.

Singh, B. P., B. J. Hatton, B. Singh, A. L. Cowie, and A. Kathuria (2010b), Influence of Biochars on Nitrous Oxide Emission and Nitrogen Leaching from Two Contrasting Soils, *J. Environ. Qual.*, 39(4), 1224-1235, doi: 10.2134/jeq2009.0138.

Smetanova, A., M. Dotterweich, D. Diehl, U. Ulrich, and N. Fohrer (2013), Influence of biochar and terra preta substrates on wettability and erodibility of soils, *Zeitschrift Fur Geomorphologie*, 57, 111-134, doi: 10.1127/0372-8854/2012/S-00117.

Sohi, S. P., E. Krull, E. Lopez-Capel, and R. Bol (2010), A Review of Biochar and its use and Function in Soil, *Adv. Agron.*, 105, 47-82, doi: 10.1016/S0065-2113(10)05002-9.

Song, W. and M. Guo (2012), Quality variations of poultry litter biochar generated at different pyrolysis temperatures, *J. Anal. Appl. Pyrolysis*, 94, 138-145, doi: 10.1016/j.jaap.2011.11.018.

Spokas K.A., Koskinen W.C., Baker J.M., and Reicosky D.C. (2009), Impacts of woodchip biochar additions on greenhouse gas production and sorption/degradation of two herbicides in a Minnesota soil, *Chemosphere Chemosphere*, 77(4), 574-581.

Spokas, K. A., J. M. Novak, C. A. Masiello, M. G. Johnson, E. C. Colosky, J. A. Ippolito, and C. Trigo (2014), Physical Disintegration of Biochar: An Overlooked Process, *Environ. Sci. Technol. Lett.*, 1 (8), 326-332, doi: 10.1021/ez500199t.

Spokas, K. A. (2013), Impact of biochar field aging on laboratory greenhouse gas production potentials, *GCB Bioenergy*, 5(2), 165-176, doi: 10.1111/gcbb.12005.

Spokas, K. A. et al. (2012a), Biochar: A Synthesis of Its Agronomic Impact beyond Carbon Sequestration, *J. Environ. Qual.*, 41(4), 973-989, doi: 10.2134/jeq2011.0069.

Spokas, K. A., J. M. Novak, and R. T. Venterea (2012b), Biochar's role as an alternative N-fertilizer: ammonia capture, *Plant Soil*, 350(1-2), 35-42, doi: 10.1007/s11104-011-0930-8.

Spokas, K. A., J. M. Novak, C. E. Stewart, K. B. Cantrell, M. Uchimiya, M. G. DuSaire, and K. S. Ro (2011), Qualitative analysis of volatile organic compounds on biochar, *Chemosphere*, 85(5), 869-882, doi: 10.1016/j.chemosphere.2011.06.108.

Sun, F. and S. Lu (2014), Biochars improve aggregate stability, water retention, and pore- space properties of clayey soil, *J. Plant Nutr. Soil Sci.*, 177(1), 26-33, doi: 10.1002/jpln.201200639.

Sun, Z., P. Moldrup, L. Elsgaard, E. Arthur, E. W. Bruun, H. Hauggaard-Nielsen, and L. W. de Jonge (2013), Direct and Indirect Short-term Effects of Biochar on Physical Characteristics of an Arable Sandy Loam, *Soil Sci.*, 178(9), 465-473, doi: 10.1097/SS.0000000000000010.

Tang, P. and V. Puri (2004), Methods for minimizing segregation: A review, *Particul. Sci. Technol.*, 22(4), 321-337, doi: 10.1080/02726350490501420.

Taumer, K., H. Stoffregen, and G. Wessolek (2005), Determination of repellency distribution using soil organic matter and water content, *Geoderma*, 125(1-2), 107-115, doi: 10.1016/j.geoderma.2004.07.004.

Teixido, M., J. J. Pignatello, J. L. Beltran, M. Granados, and J. Peccia (2011), Speciation of the Ionizable Antibiotic Sulfamethazine on Black Carbon (Biochar), *Environ. Sci. Technol.*, 45(23), 10020-10027, doi: 10.1021/es202487h.

Tian, J., S. Yi, P. Imhoff, P. Chiu, M. Guo, J. Maresca, V. Beneski, and S. Cooksey (2014), Biochar-Amended Media for Enhanced Nutrient Removal in Stormwater Facilities, *American Society of Civil Engineers*, 197-208, doi: 10.1061/9780784413548.022.

Topp, G. and W. Zebchuk (1979), Determination of Soil-Water Desorption Curves for Soil Cores, *Can. J. Soil Sci.*, 59(1), 19-26.

Troeh, F., J. Jabro, and D. Kirkham (1982), Gaseous-Diffusion Equations for Porous Materials, *Geoderma*, 27(3), 239-253, doi: 10.1016/0016-7061(82)90033-7.

Tryon, E. (1948), Effect of Charcoal on Certain Physical, Chemical, and Biological Properties of Forest Soils, *Ecol. Monogr.*, 18(1), 81-115, doi: 10.2307/1948629.

U.S. EPA (2012), Sustainable Futures/ P2 Framework Manual 2012: Estimating Physical/Chemical and Environmental Fate Properties with EPI Suite, *EPA-748B12-001*, 5-1.

Uchimiya, M., K. B. Cantrell, P. G. Hunt, J. M. Novak, and S. Chang (2012), Retention of Heavy Metals in a Typic Kandudult Amended with Different Manure-based Biochars, *J. Environ. Qual.*, *41*(4), 1138-1149, doi: 10.2134/jeq2011.0115.

USEPA (Ed.) (2013), *Inventory of U.S. Greenhouse Gas Emissions and Sinks: 1990 - 2011*, vol. EPA 430-R-13-001.

Uzoma, K. C., M. Inoue, H. Andry, H. Fujimaki, A. Zahoor, and E. Nishihara (2011), Effect of cow manure biochar on maize productivity under sandy soil condition.(Report), *Soil Use Manage.*, *27*, 205-212.

Valipour, N. M., F. C. Birjandi, and J. Sargolzaei (2014), Super-non-wettable surfaces: A review, *Colloids and Surfaces A-Physicochemical and Engineering Aspects*, *448*, 93-106, doi: 10.1016/j.colsurfa.2014.02.016.

van Genuchten, M. (1980), A Closed-Form Equation for Predicting the Hydraulic Conductivity of Unsaturated Soils, *Soil Sci. Soc. Am. J.*, *44*(5), 892-898.

Wallach, R., M. Margolis, and E. R. Graber (2013), The role of contact angle on unstable flow formation during infiltration and drainage in wettable porous media, *Water Resour. Res.*, *49*(10), 6508-6521, doi: 10.1002/wrcr.20522.

Wallis, M., D. Horne, and A. Palmer (1993), Water Repellency in a New-Zealand Development Sequence of Yellow-Brown Sands, *Aust. J. Soil Res.*, *31*(5), 641-654, doi: 10.1071/SR9930641.

Webb, P. A. (2001), Volume and density determinations for particle technologists, *Micromeritics Instrument Corp.*, 2/16/2001.

Wenzel, R. N. (1936), Resistance of solid surfaces to wetting by water, *Industrial and Engineering Chemistry*, *28*, 988-994, doi: 10.1021/ie50320a024.

Wong, J. T. F., Z. Chen, C. W. W. Ng, and M. H. Wong (2016), Gas permeability of biochar-amended clay: potential alternative landfill final cover material, *Environ. Sci. Pollut. Res.*, *23*(8), 7126-7131, doi: 10.1007/s11356-015-4871-2.

Yanai, Y., K. Toyota, and M. Okazaki (2007), Effects of charcoal addition on N<sub>2</sub>O emissions from soil resulting from rewetting air-dried soil in short-term laboratory

experiments, *Soil Sci. Plant Nutr.*, 53(2), 181-188, doi: 10.1111/j.1747-0765.2007.00123.x.

Yi, S., B. Witt, P. Chiu, M. Guo, and P. Imhoff (2015), The Origin and Reversible Nature of Poultry Litter Biochar Hydrophobicity, *J. Environ. Qual.*, 44(3), 963-971, doi: 10.2134/jeq2014.09.0385.

Zabaniotou, A., G. Stavropoulos, and V. Skoulou (2008), Activated carbon from olive kernels in a two-stage process: Industrial improvement, *Bioresour. Technol.*, 99(2), 320-326, doi: 10.1016/j.biortech.2006.12.020.

Zhang, W., J. Niu, V. L. Morales, X. Chen, A. G. Hay, J. Lehmann, and T. S. Steenhuis (2010), Transport and retention of biochar particles in porous media: effect of pH, ionic strength, and particle size, *Ecohydrology*, 3(4), 497-508, doi: 10.1002/eco.160.

Zisman, W. A. (1964), Relation of the Equilibrium Contact Angle to Liquid and Solid Constitution, *Advances in Chemistry*, 43, 1-51.

**APPENDIX A:**

**THE ORIGIN AND REVERSIBLE NATURE OF POULTRY LITTER  
BIOCHAR HYDROPHOBICITY**

### A-1 Properties of poultry litter

Table A1: Properties of poultry litter prior to pyrolysis <sup>a</sup>		
Element	Total (g kg <sup>-1</sup> )	Water Extractable (g kg <sup>-1</sup> )
N	30.66 ± 9.52 <sup>b</sup>	7.65 ± 13.48 <sup>b</sup>
P	15.14 ± 0.76	2.95 ± 5.66
S	16.16 ± 7.46	8.37 ± 0.18
K	41.77 ± 12.31	27.18 ± 0.72
Na	18.64 ± 7.10	2.89 ± 0.09
Ca	43.03 ± 16.71	1.53 ± 0.27
Mg	11.06 ± 10.15	1.34 ± 0.54
Fe	0.748 ± 0.11	0.051 ± 0.01
Mn	0.705 ± 0.03	0.018 ± 0.04
Cu	0.661 ± 0.13	0.159 ± 0.07
Pb	0.002 ± 0.03	ND <sup>c</sup>
Zn	0.628 ± 0.16	0.048 ± 0.01
Cd	0.001 ± 0.00	ND
As	0.037 ± 0.03	0.03 ± 0.00
Se	0.002 ± 0.00	0.002 ± 0.00

<sup>a</sup> Data obtained from [Song and Guo, 2012]

<sup>b</sup> 95% confidence interval

<sup>c</sup> Water extractable properties were made on solution prepared with 1:10 solid/water ratio of poultry litter to deionized water shaken for 24 hr at room temperature

ND= none detected

## **A-2 Contact angle stability**

Figure A1 demonstrates that contact angles measured on poultry litter biochars (PLBC) pyrolyzed at 300°C (PLBC300) and 600°C (PLBC600) mounted on a microscope slide were stable up to 60 s. There was a small downward trend in contact angles measured for PLBC300 biochar between 60-100 s. The contact angles measured between 0-60 s are reported in this work and thus not influenced by transient effects. Contact angle measurements over 0-60 s are consistent with other published procedures [Bachmann *et al.*, 2000].

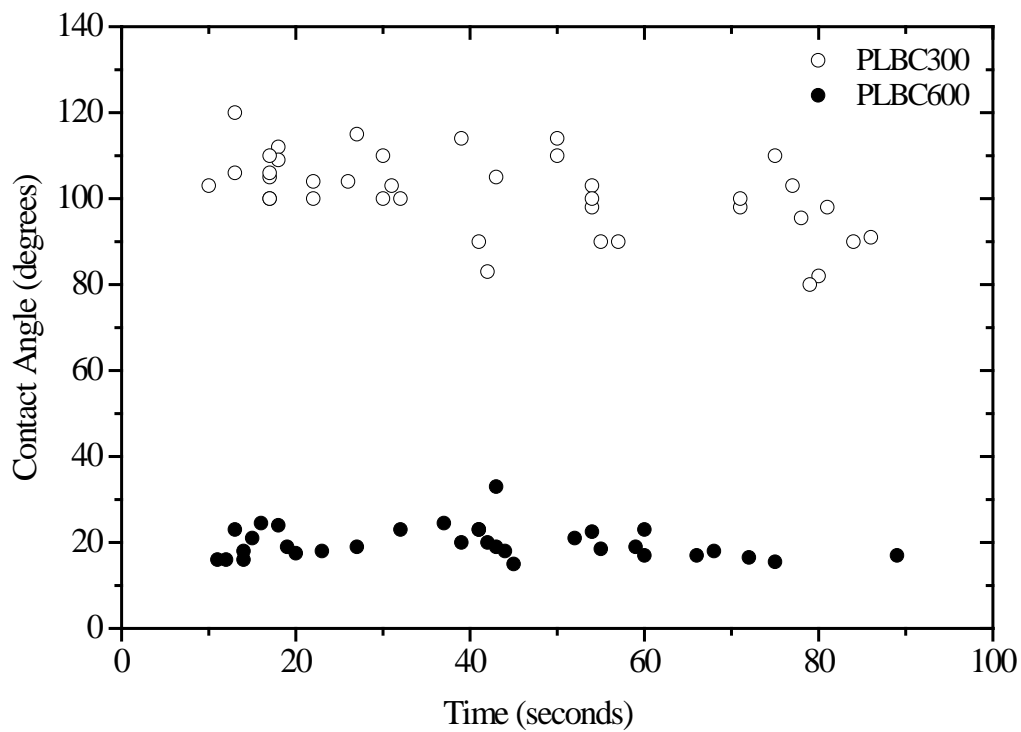


Figure A1: Time-dependent contact angle of water droplets placed on PLBC300 and PLBC600.

### **A-3 Effect of leached compounds on air-water interfacial tension**

Changes in the air-water interfacial tension would alter the contact angle (CA) of water droplets on biochar surfaces. To assess the impact of leached compounds from PLBC on air-water interfacial tension three solutions were analyzed: a reference DI water, and two water extraction solutions prepared with a hydrophobic PLBC. Here, PLBC pyrolyzed at 400°C (PLBC400) was used. Based on water drop penetration time tests, this biochar was hydrophobic but after rinsing in DI water for 24 h became hydrophilic (see manuscript).

Solution 1 was prepared by adding 5 g of PLBC400 to 100 mL DI water and mixing the solution on a mechanical shaker at 200 rpm for 24 h. Solution 2 was identical to the first, except that a higher concentration of PLBC400 was selected: 25 g of PLBC400 was mixed with 75 mL DI water. After mixing for 24 h, PLBC400 was separated from the rinsate of both solutions by settlement. The air-water interfacial tension was then measured 5-10 times on each water sample using a CSC Scientific DuNouy Interfacial Tensiometer (model 70545, Fairfax, VA) following standard measurement procedures described in the instrument's user manual.

The air-water interfacial tensions of DI water and PLBC400 rinsate solutions are reported in Table A2. Measurements of the interfacial tension of DI on different sampling days likely varied because of differences in room temperature and possibly the orientation/alignment of the circular platinum ring used in the interfacial tension measurement, which may change slightly with use. Interfacial tensions of DI water and Solution 1 differed (t-test,  $p < 0.05$ ), but those for DI water and Solution 2, the more concentrated PLBC400 mixture, were not significantly different (t-test,  $p = 0.706$ ). The difference in interfacial tension between DI water and Solution 1 was small. At a 95%

confidence level, interfacial tensions of DI water and Solution 1 and Solution 2 differed by less than 0.2 dynes/cm (t-test,  $p < 0.05$ ), which is  $< 0.3\%$  of the mean interfacial tension. Thus, while there is some effect of leached compounds from PLBC400 on air-water interfacial tension, the magnitude of this effect is small.

It is unlikely that compounds leached from PLBC affected CAs reported in Figures 1, 2, and 4 in the manuscript. Considering that leached compounds from PLBC can slightly alter air-water interfacial tension, transient changes might occur as dissolved organic compounds are transported to the air-water interface and modified surface tension and CAs. However, no such changes were observed in CAs over the 60 s measurement period (Figure A1), and therefore, the influence on measured CAs is considered negligible within 60 s in this study.

Table A2: Air-water interfacial tensions of water solutions mixed with PLBC400 and t-test results

<b>Date</b>	<b>Sample</b>	<b>Temp (°C)</b>	<b>IFT (dynes/cm)</b>	<b>Null Hypothesis</b>	<b>t-Test p Value</b>
7/15/2011	DI water 1	21	76.9 ± 0.4 (5) <sup>a</sup>	$\mu_{DI1} = \mu_{S1}$	0.021 (two-tailed)
	Solution 1		76.3 ± 0.4 (10)	$\mu_{DI1} - \mu_{S1} = 0.2$	0.003 (one-tailed)
7/21/2011	DI water 2	22	76.0 ± 0.4 (10)	$\mu_{DI2} = \mu_{S2}$	0.706 (two-tailed)
	Solution 2		75.9 ± 0.1 (10)	$\mu_{DI2} - \mu_{S2} = 0.2$	0.038 (one-tailed)

<sup>a</sup>mean ± one standard deviation. Number of samples in parentheses.

#### A-4 Rinsate analyses

The biochars produced at 300 and 600°C (PLBC300 and PLBC600), and biochar produced at 300°C heated for 12 h at 105°C (HT-PLBC300) were rinsed according to procedures described in the manuscript, and precipitates from the rinsates were analyzed using FTIR. Spectra are shown in Figure B2 for the three biochars. Although FTIR spectra differ between biochar type, peaks occur at many of the same wave numbers indicating the same functional groups, which is expected since PL is the common source material. The small peaks between 3020 - 2800  $\text{cm}^{-1}$  from PLBC300 indicate C-H stretching from alkyl groups that correlated well with hydrophobicity of plant-derived biochars [Kinney *et al.*, 2012]. Ellerbrock *et al.* [Ellerbrock *et al.*, 2005] suggested that for soil organic matter the most important functional groups controlling soil wettability are the hydrophobic CH-groups, which occur between 3020-2800  $\text{cm}^{-1}$ . The alkyl peaks in region 3020-2800  $\text{cm}^{-1}$  were much smaller for precipitates from hydrophilic PLBC600 and HT-PLBC300, though. Thus, the presence (PLBC300) or absence (PLBC600 and HT-PLBC300) of the hydrophobic CH-groups in the 3020 - 2800  $\text{cm}^{-1}$  wavelength range is consistent with CAs (Figures 1 and 2 in manuscript) measured for PLBC300, PLBC600, and HT-PLBC300. This suggests that alkyl compounds found in the OC coating on PLBC300 were the cause of hydrophobicity.

Biochar sample rinsates were also analyzed using GS-MS following procedures described in the manuscript, and spectra are shown for PLBC300 and PLBC600 rinsates in Figure A3. All spectra were baseline corrected using a sample blank and stability was reached after 15 minutes of elution time. The peaks measured below an absorbance of 3000 were neglected from compound characterization. More peaks were measurable on samples prepared using PLBC pyrolyzed at 300°C than those prepared with PLBC

pyrolyzed at 600°C. Compounds identified are shown in Table A3 and A4 for PLBC300 and PLBC600, respectively. Using U.S. Environmental Protection Agency's Estimation Program Interface (EPI) Suite, the physical properties of these compounds were estimated using MPBPWIN v1.43 to obtain water solubility, boiling point, melting point, vapor pressures at 25 and 105°C [Boethling, Robert S, Mackay, Donald, Sheppard, Steve, 2001; U.S. EPA, 2012]. The results are reported in the Tables A3 and A4. The vapor pressures of all organic molecules are below that of water, indicating that these compounds will vaporize at lower temperatures and pressures than water. Therefore, if heated to 105°C for long periods, these compounds covering biochar surfaces might be removed.

Table A3: Properties of water extractable organic carbons detected from PLBC300 rinsate using GC-MS

<b>Retention Time (min)</b>	<b>Compound</b>	<b>% Match from GC</b>	<b>Vapor Pressure<sup>a</sup> (mm Hg at 25°C)</b>	<b>Water Solubility<sup>a</sup> (mg/L at 25°C)</b>	<b>Melting Point<sup>a</sup> (°C)</b>	<b>Boiling Point<sup>a</sup> (°C)</b>	<b>Vapor Pressure<sup>a</sup> (mm Hg at 105°C)</b>
21.241-21.3	1,3-bis(1,1-dimethylethyl)-benzene	95	7.97E-02	5.33E-01	19.29	229.63	1.22E+01
22.305-22.325	Tetradecane	97	3.69E-02	9.19E-03	1.36	243.20	6.45E+00
25.636-25.707	2,5-bis(1,1-dimethylethyl)-phenol	95	6.18E-04	4.32E+00	76.96	281.15	1.53E+00

<sup>a</sup>values obtained from EPI Suite [*U.S. EPA, 2012*]

Table A4: Properties of water extractable organic compounds from PLBC600 rinsate using GC-MS							
<b>Retention Time</b> (min)	<b>Compound</b>	<b>% Match from GC</b>	<b>Vapor Pressure<sup>a</sup></b> (mm Hg at 25°C)	<b>Water Solubility<sup>a</sup></b> (mg/L at 25°C)	<b>Melting Point<sup>a</sup></b> (°C)	<b>Boiling Point<sup>a</sup></b> (°C)	<b>Vapor Pressure<sup>a</sup></b> (mm Hg at 105°C)
~22	1,3-bis(1,1-dimethylethyl)-benzene	95	7.97E-02	0.5327	19.29	229.63	12.2
~26	2,5-bis(1,1-dimethylethyl)-phenol	95	6.18E-04	4.316	76.96	281.15	1.53
~28.5	Octacosane	90	3.24E-03	2.94E-04	133.98	427.25	

<sup>a</sup>values obtained from EPI Suite [*U.S. EPA*, 2012]

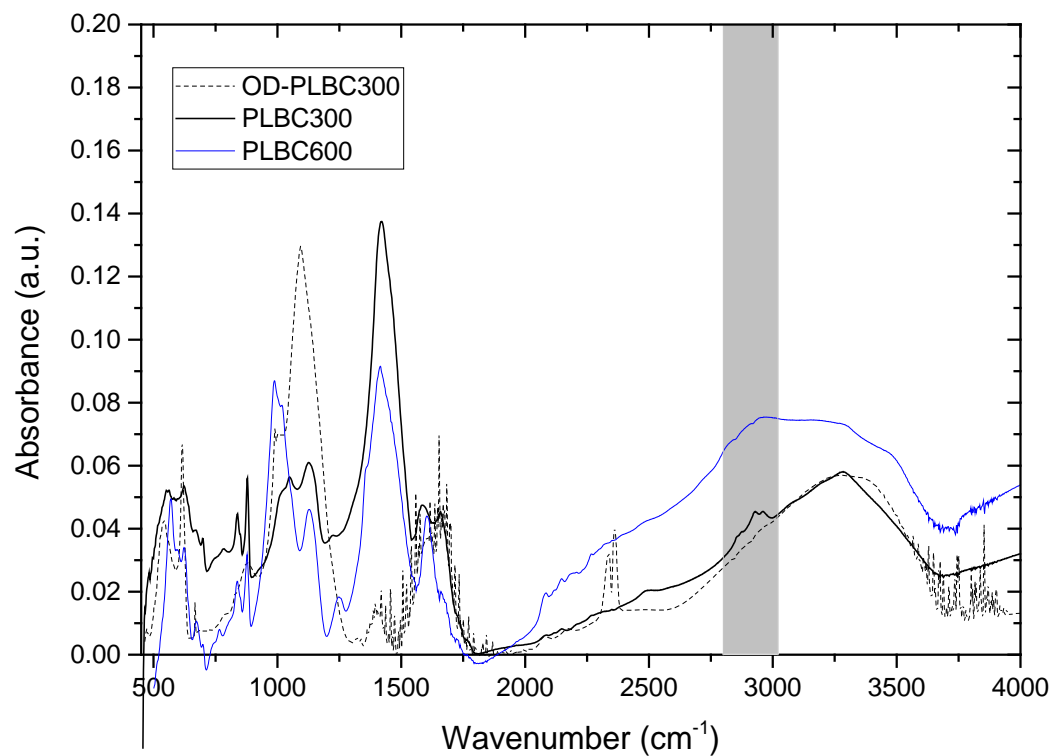


Figure A2: FTIR spectra of water extractable compounds from PLBC at 300°C (PLBC300), PLBC at 300°C heated for 12 h at 105°C (HT-PLBC300), and PLBC at 600°C (PLBC600). Highlighted region is spectral region 2800 - 3020 cm<sup>-1</sup>.

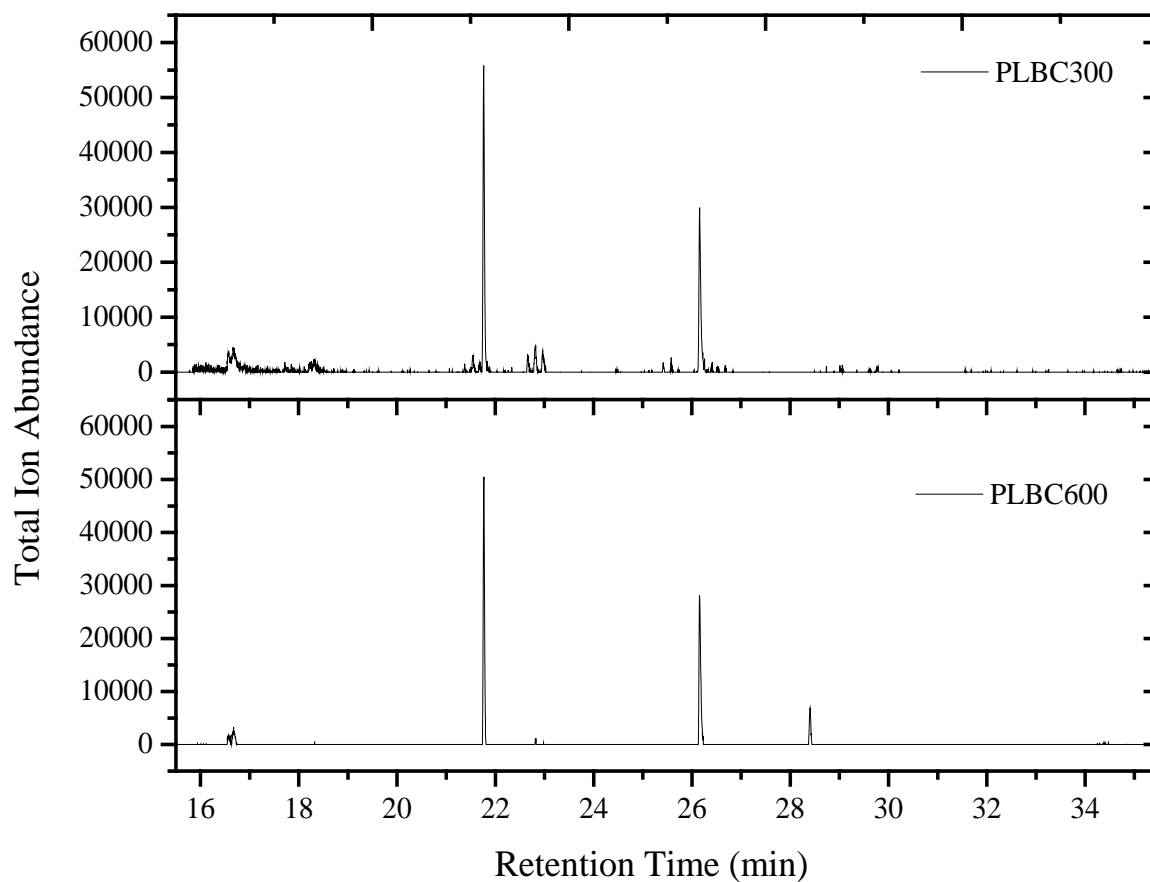


Figure A3: Baseline corrected GCMS spectrogram of water extractable organic compounds from biochar produced at pyrolysis temperatures 300°C and 600°C (PLBC300 and PLBC600, respectively). Peaks below the absorbance of 3000 were ignored for chemical identification.

**APPENDIX B:**

**SOIL-WATER RETENTION CURVE MODELS FOR BIOCHAR AMENDED  
SOILS**

## B-1 Sample information and uncertainty

Table B1: The number of data collected per individual sample using WP4C to obtain water sorption data

Sample type <sup>a</sup>	Adsorption isotherm			Desorption isotherm		
	# of individual samples	# of measurements per sample cup	Total data	# of individual samples	# of measurements per sample cup	Total data
100% PLBC <sup>a</sup>	10	1 to 4	13	8	2 to 43	82
100% SRBC <sup>b</sup>	9	1 to 12	20	7	2 to 9	34
2% PLBC-Sand <sup>c</sup>	3	1 to 3	11	2	4 to 8	12
7% PLBC-Sand	3	2 to 3	9	2	5 to 9	8
2% PLBC-SL	40	1 to 5	80	2	2 to 3	5
7% PLBC-SL	47	1 to 2	51	2	2	4
2% SRBC-Sand	17	1 to 5	33	6	1 to 5	8
7% SRBC-Sand	27	1 to 2	37	8	2 to 5	10
2% SRBC-SL	15	1 to 8	18	5	1 to 5	27
7% SRBC-SL	24	1 to 7	56	3	3 to 5	14

<sup>a</sup>PLBC = poultry litter biochar,

<sup>b</sup>SRBC = Soil Reef biochar,

<sup>c</sup>2% PLBC Sand = 30/40 Accusand, SL = sandy loam, 2% and 7% by weight

Table B2: Estimates of uncertainty of biochar in sand samples used in soil-water retention characteristic curves

Method	$pF$	Sand		2%PLBC-Sand <sup>c</sup>		7%PLBC-Sand <sup>d</sup>		2%SRBC-Sand <sup>e</sup>		7%SRBC-Sand <sup>f</sup>	
		Standard error Mass, g	Standard error Volume, mL	Standard error Mass, g	Standard error Volume, mL	Standard error Mass, g	Standard error Volume, mL	Standard error Mass, g	Standard error Volume, mL	Standard error Mass, g	Standard error Volume, mL
TT <sup>a</sup>	0.8	0.001	0.003	0.001	0.003	0.001	0.004	0.001	0.004	0.001	0.004
TT	1.1	0.001	0.003	0.001	0.003	0.001	0.003	0.001	0.003	0.001	0.004
TT	1.2	0.002	0.003	0.001	0.003	0.001	0.003	0.001	0.003	0.001	0.003
TT	1.3	0.004	0.002	0.002	0.002	0.003	0.002	0.002	0.002	0.002	0.002
TT	1.4	0.102	3.28E-04	0.034	0.001	0.013	0.001	0.019	0.001	0.004	0.001
TT	1.6	0.119	3.05E-04	0.085	3.47E-04	0.026	0.001	0.053	4.29E-04	0.006	0.001
TT	1.8	0.114	3.11E-04	0.044	4.81E-04	0.018	0.001	0.033	5.37E-04	0.007	0.001
PPE <sup>b</sup>	2.1	0.190	2.44E-04	0.075	3.68E-04	0.025	0.001	0.041	4.83E-04	0.006	0.001
PPE	2.4	0.519	1.55E-04	0.222	2.19E-04	0.040	4.85E-04	0.061	3.99E-04	0.008	0.001
PPE	2.6	9.451	6.91E-05	0.435	1.62E-04	0.056	4.07E-04	0.082	3.46E-04	0.009	0.001
PPE	2.7	14.498	6.62E-05	0.798	1.26E-04	0.070	3.66E-04	0.093	3.25E-04	0.009	0.001
PPE	2.9	131.669	6.11E-05	0.885	1.21E-04	0.078	3.47E-04	0.146	2.61E-04	0.008	0.001
PPE	3.1	61.102	6.19E-05	0.910	1.20E-04	0.115	2.88E-04	0.211	2.20E-04	0.013	0.001
PPE	3.5	26.236	6.37E-05	1.101	1.11E-04	0.140	2.62E-04	0.292	1.89E-04	0.014	0.001
PPE	3.8	12.172	6.73E-05	1.025	1.14E-04	0.153	2.51E-04	0.545	1.44E-04	0.021	0.001

<sup>a</sup>TT = tension table<sup>b</sup>PPE = pressure plate extractor<sup>c</sup>2%PLBC-Sand = 2% (w/w) of rinsed/oven-dried/sieved poultry litter biochar (PLBC) in 30/40 Accusand<sup>d</sup>7%PLBC-Sand = 7% (w/w) PLBC in Sand<sup>e</sup>2%SRBC-Sand = 2% (w/w) of rinsed/oven-dried/sieved Soil Reef™ biochar (SRBC) in Sand<sup>f</sup>7%SRBC-Sand = 7% (w/w) SRBC in Sand

Table B3: Estimates of uncertainty of biochar in sandy loam (SL) samples used in soil-water retention characteristic curves

Method	$pF$	SL	2%PLBC-SL		7%PLBC-SL		2%SRBC-SL		7%SRBC-SL		
		Standard error Mass, g	Standard error Volume, mL	Standard error Mass, g	Standard error Volume, mL	Standard error Mass, g	Standard error Volume, mL	Standard error Mass, g	Standard error Volume, mL	Standard error Mass, g	Standard error Volume, mL
TT	0.8	0.002	0.004	0.002	0.004	0.002	0.004	0.002	0.004	0.001	0.005
TT	1.3	0.002	0.004	0.002	0.004	0.002	0.004	0.002	0.004	0.001	0.005
PPE	1.8	0.002	0.004	0.002	0.004	0.002	0.004	0.002	0.004	0.002	0.004
PPE	2.4	0.002	0.004	0.002	0.003	0.002	0.004	0.002	0.004	0.002	0.004
PPE	2.7	0.002	0.003	0.003	0.003	0.002	0.003	0.002	0.003	0.002	0.003
PPE	3.0	0.004	0.003	0.005	0.002	0.004	0.002	0.004	0.002	0.003	0.003
PPE	3.2	0.004	0.002	0.006	0.002	0.004	0.002	0.005	0.002	0.003	0.003
PPE	3.3	0.007	0.002	0.009	0.002	0.006	0.002	0.009	0.002	0.006	0.002
PPE	3.7	0.017	0.001	0.015	0.001	0.010	0.001	0.020	0.001	0.015	0.001
PPE	4.0	0.045	0.001	0.028	0.001	0.013	0.001	0.024	0.001	0.019	0.001

<sup>a</sup>TT = tension table

<sup>b</sup>PPE = pressure plate extractor

<sup>c</sup>2%PLBC-Sand = 2% (w/w) of rinsed/oven-dried/sieved poultry litter biochar (PLBC) in 30/40 Accusand

<sup>d</sup>7%PLBC-Sand = 7% (w/w) PLBC in Sand

<sup>e</sup>2%SRBC-Sand = 2% (w/w) of rinsed/oven-dried/sieved Soil Reef™ biochar (SRBC) in Sand

<sup>f</sup>7%SRBC-Sand = 7% (w/w) SRBC in Sand

## B-2 Total water potential of WP4C and osmotic potential

It was observed during the WP4C measurements that the interpores of the biochars started filling and saturating the samples beyond moisture content (MC) above 0.4. There was a lot of uncertainty in the data and osmotic effects were present and needed correction. Figure B1 (a) plots all the data and revealed that between  $MC > 0.3$ , the total water potential becomes linear from assuming that water on PLBC surfaces flattened out and lost concavity when water started to fill the voids. When osmotic effects dominate, the total potential should be linearly related to the moisture content from the dilution effects. The water films have no curvature; therefore, a solid red line was drawn to indicate the region where osmotic effects dominate the total potential. The data that lies on the linear line represents data that needed correction by removing the osmotic potential in Figure B1(a).

The PLBC data were linearly regressed with  $MC \geq 0.40$  to obtain an equation to correct for the osmotic effects in Figure B1(b). The data were also regressed with  $MC \geq 0.3$  and showed a similar equation, therefore, not shown. It is recommended to regress the data at various MC and use both equations to correct for osmotic effects to see the influence on the results. In this case we used MC of 0.4 and 0.3.

The regression was applied on the data to correct for the osmotic potential and filtered for  $pF > 3.85$ . The corrected data with high MC was removed since as MC increases,  $pF$  must get small as the water has no more curvature. The data was also filtered using a restraint of  $pF > 3.85$  and  $MC < 0.3$ . These results are shown in Figure B1(c). These data and the fittings were used to estimate the  $pF$ -MC relationship for

PLBC for the matric potential. The equation in Figure B1(c) from  $0 < MC < 0.35$  was used to predict the  $pF$ -MC relationships for 2% and 7% PLBC in sand and sandy loam.

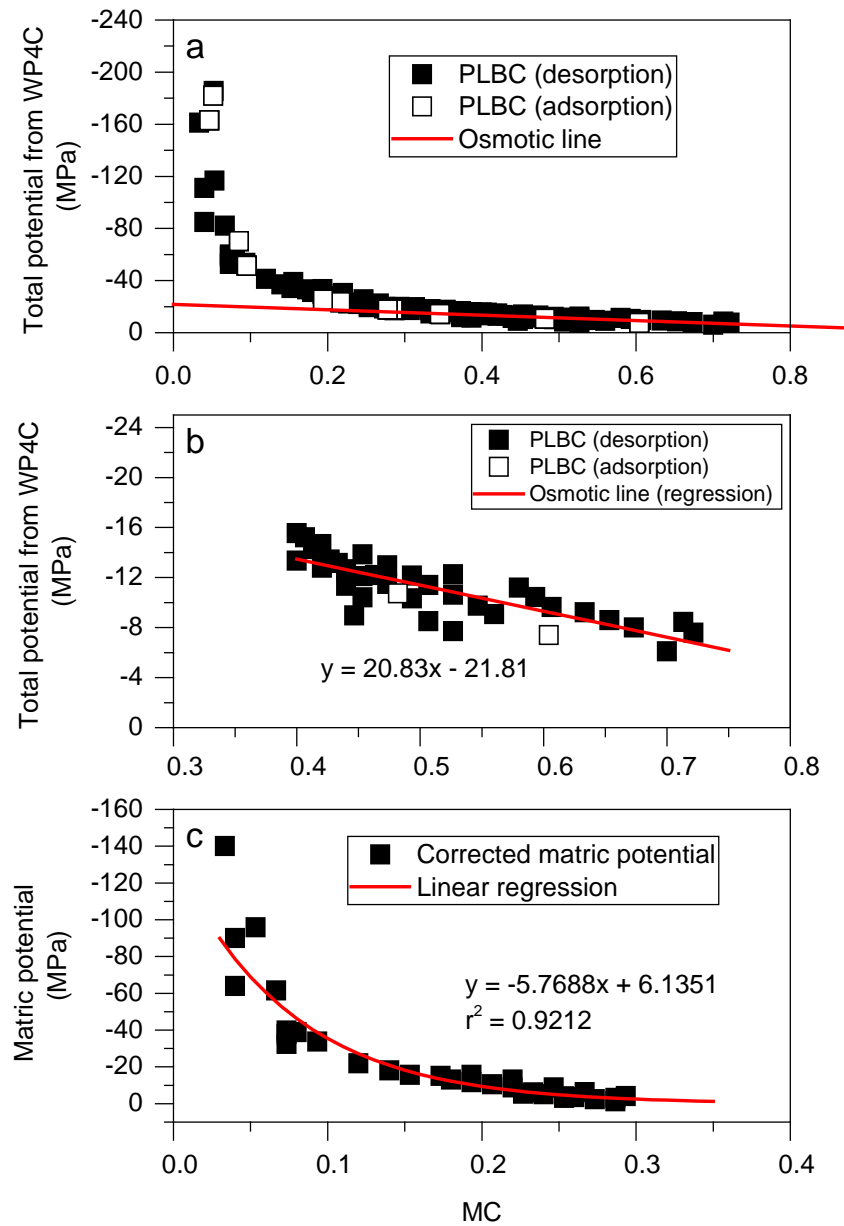


Figure B1: (a) Total water potential versus gravimetric moisture content (MC) of PLBC. Solid line indicates where osmotic effects dominate total potential. (b) PLBC data linearly regressed for  $MC \geq 0.40$ . (c) Corrected water potential of PLBC for  $pF > 3.85$  at  $MC < 0.3$ .

### B-3 Biochar SEM images

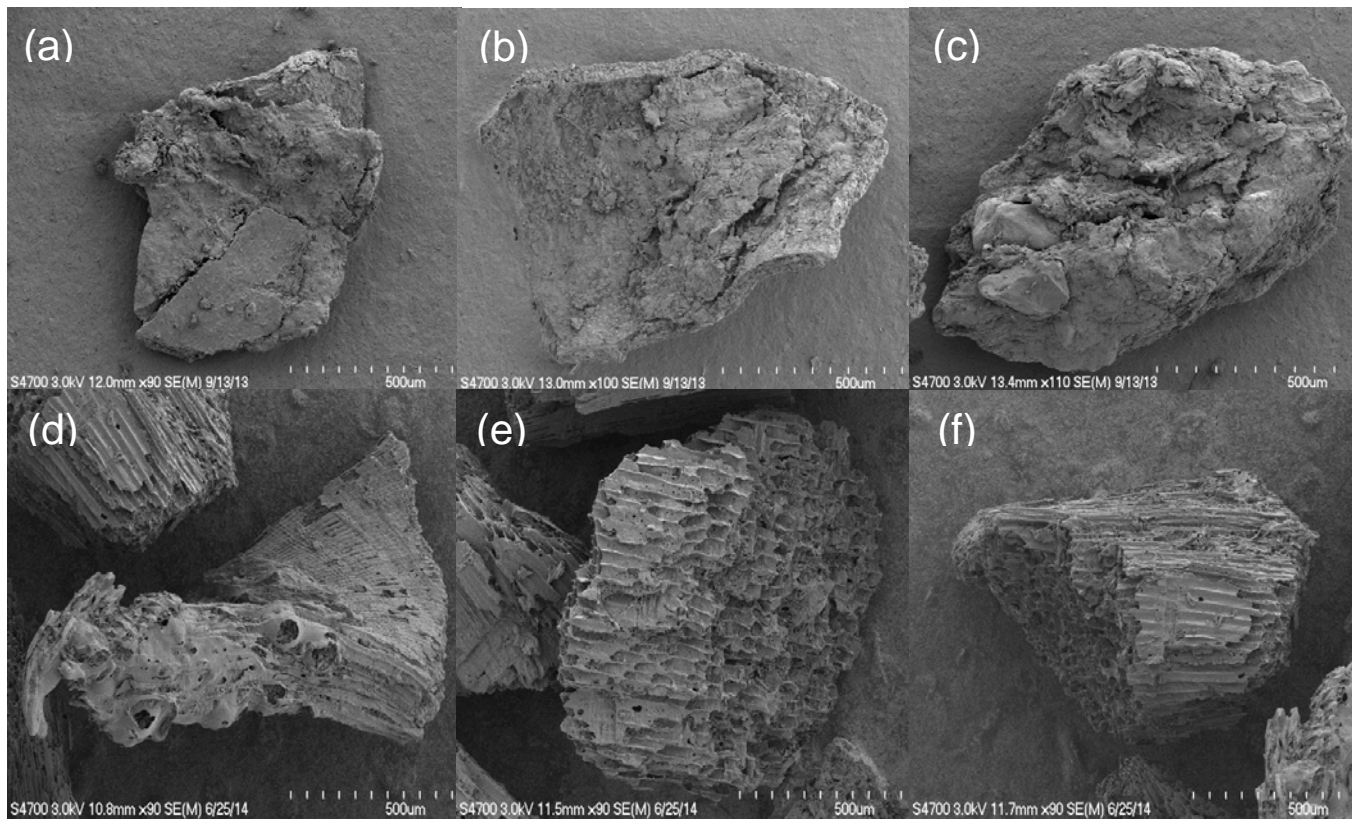


Figure B2: SEM images of rinsed PLBC (a, b, and c) and SEM images of rinsed SRBC (d, e, and f)

### B-4 Soil water retention data

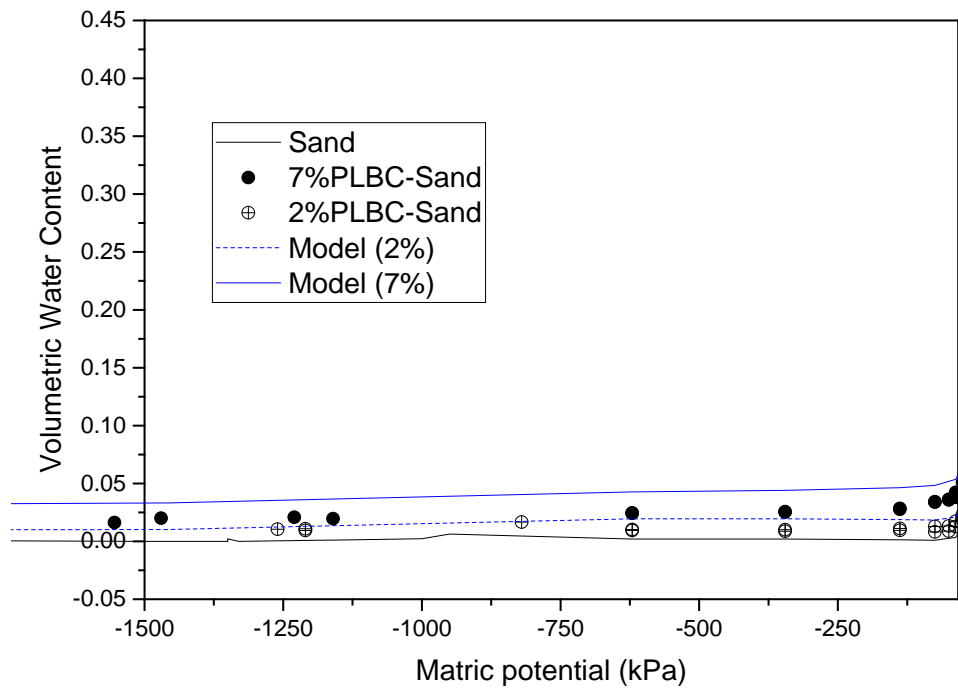


Figure B3: Soil water retention data and Model 3 prediction of PLBC in Sand at 2% and 7%

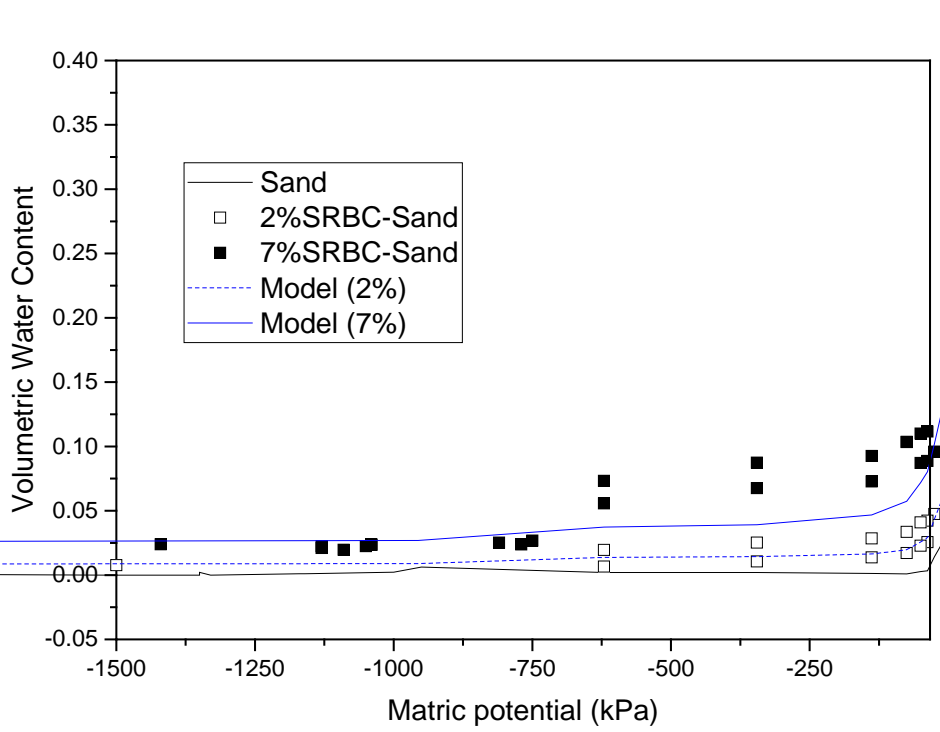


Figure B4: Soil water retention data and Model 3 prediction of SRBC in Sand at 2% and 7%

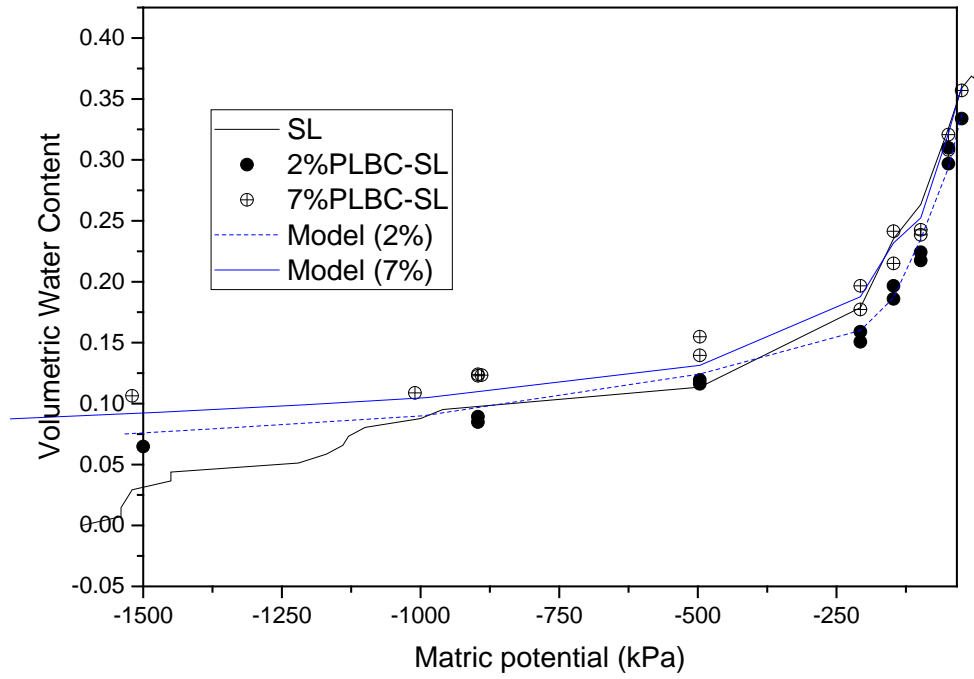


Figure B5: Soil water retention data and Model 4 prediction of PLBC in sandy loam (SL) at 2% and 7%

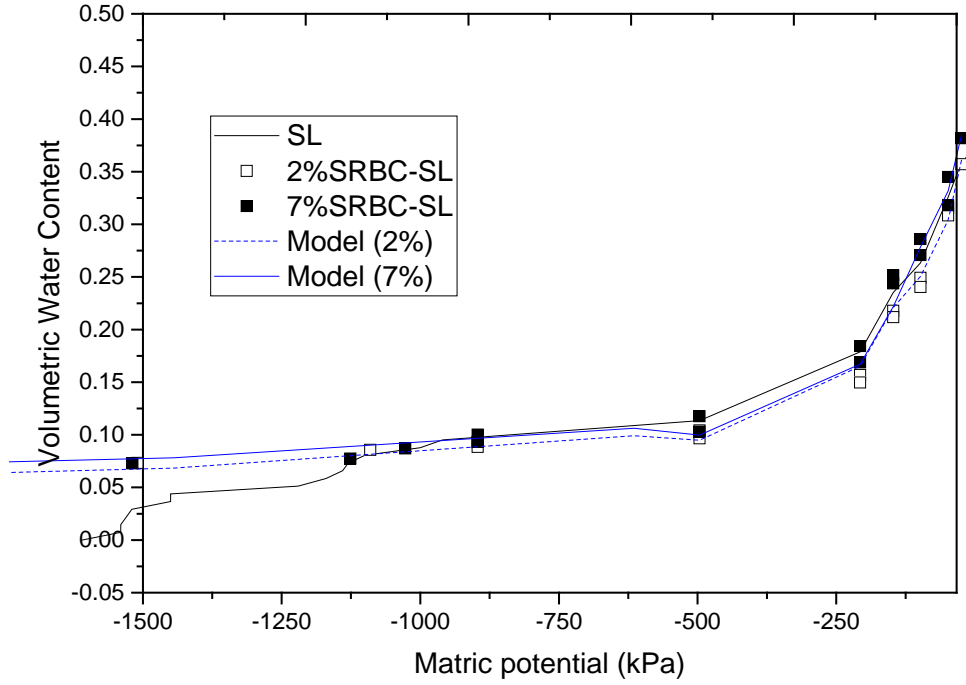


Figure B6: Soil water retention data and Model 4 prediction of SRBC in sandy loam (SL) at 2% and 7%

#### B-4 Nomenclature

$h_c$  = capillary pressure in cm-H<sub>2</sub>O

$MC$  = moisture content

$M_{s_{1i}}$  = mass of particle class 1 collected on sieve  $i$

$M_{s_{2i}}$  = mass of particle class 2 collected on sieve  $i$

$M_t$  = total mass of particles on all sieves, for both particle classes

$M_{w,i}$  = mass of water at each step  $i$

$n$  = total porosity

$n_i$  = number of spherical particles

$r_i$  = pore radius

$R_i$  = mean particle radius

$$S_w = \frac{n}{\theta_w \text{ at } pF \sim 1.0}$$

$V_v$  = Volume of voids

$V_s$  = Volume of solids

$V_t$  = Total Volume

$V_{s_{1i}}$  = volume of particle class 1 collected on sieve  $i$

$V_{s_{2i}}$  = volume of particle class 2 collected on sieve  $i$

$w_i$  = fraction of solid mass

$\Delta Adsorbed\ water_i$  = change or increase in adsorbed water because of biochar addition  
at pressure step  $i$

$\epsilon$  = void ratio

$\theta_w$  = volumetric water content

$\theta_{v_i}$  = volumetric water content evaluated using Arya et al. (1999) model

$\theta$  = contact angle, assume =  $0^0$ ,  $\cos \theta = 1$

$\Delta\theta_{v_i}|_{Arya\ Model}$  = change in  $\theta_{v_i}$  as computed from Arya et al. (1999) model between the native reference soil and this reference soil amended with biochar at pressure step  $i$

$\rho_{s_1}$  = envelope density of particle class 1

$\rho_{s_2}$  = envelope density of particle class 2

$\overline{\rho}_{s_i}$  = particle density based on volume, not mass

$\sigma$  = surface tension at air – water interface

$$\Phi = \frac{\epsilon}{1 + \epsilon}$$

= Interparticle porosity of sample (not total porosity as suggested by Arya, 1999)

### B-5 Arya model derivation

- 1) Computing weighted particle density by volume, not mass, collected on sieve  $i$

$$\bar{\rho}_{s_i} = \frac{V_{s_{1i}} \rho_{s_1} + V_{s_{2i}} \rho_{s_2}}{V_{s_{1i}} + V_{s_{2i}}} \quad [1]$$

Because,

$$V_{s_1} = \frac{M_{s_1}}{\rho_{s_1}} \text{ and } V_{s_2} = \frac{M_{s_2}}{\rho_{s_2}} \quad [2]$$

Substitute [2] into [1],

$$\bar{\rho}_{s_i} = \frac{\frac{M_{s_{1i}}}{\rho_{s_{1i}}} \rho_{s_{1i}} + \frac{M_{s_{2i}}}{\rho_{s_{2i}}} \rho_{s_{2i}}}{\frac{M_{s_{1i}}}{\rho_{s_1}} + \frac{M_{s_{2i}}}{\rho_{s_2}}} = \frac{M_{s_{1i}} + M_{s_{2i}}}{\frac{M_{s_{1i}}}{\rho_{s_1}} + \frac{M_{s_{2i}}}{\rho_{s_2}}} \quad [3]$$

- 2) Void ratio,  $\epsilon$

$$\epsilon = \frac{V_v}{V_s} = \frac{\bar{\rho}_s - \rho_b}{\rho_b} \quad [4]$$

- 3) Use equation [1] in Arya et al. (1994) to determine volume of solids,  $V_{s_i}$ , for each sieve fraction  $i$

$$V_{s_i} = \left( \frac{M_{s_{1i}}}{\rho_{s_1}} + \frac{M_{s_{2i}}}{\rho_{s_2}} \right) \frac{e}{M_t} \quad [5]$$

- 4) Use equation [3] in Arya et al. (1999) to determine the volumetric water content for each particle class,  $\theta_{v_i}$ . This is the water in interpores. The mass fraction,  $w_i$ , in Arya's model was replaced with a solid volume fraction,  $v_i$ .

$$\theta_{v_i} = (\Phi S_w) \sum_{j=1}^i \left( \frac{M_{s_{1j}}}{\rho_{s_1}} + \frac{M_{s_{2j}}}{\rho_{s_2}} \right) \frac{\bar{\rho}_s}{M_t} \quad [6]$$

- 5) From equation [6], compute the volumetric water content for each sieve size. Then assign a capillary pressure to each sieve size.

The key is everywhere  $\rho_s$  appears in Arya's derivation, replace it with  $\bar{\rho}_s$  in equation [3] above. Everywhere  $w_i$  appears, replace it with  $v_i$

$$V_i = \left( \frac{M_{s_{1j}}}{\rho_{s_1}} + \frac{M_{s_{2j}}}{\rho_{s_2}} \right) \frac{\bar{\rho}_s}{M_t} \quad [7]$$

To find the capillary pressure for each sieve size  $i$ , use:

$$n_i = \frac{3w_i}{4\pi\bar{\rho}_{s_i}R_i^3} \quad [8]$$

Then use equation [9] from Arya & Heitman (2015) to obtain  $r_i$ ,

$$r_i = \sqrt{\frac{0.0717 \Phi \frac{w_i}{\rho_b}}{n_i^{4/3} R_i}} \quad [9]$$

$$w_i = M_{s_{1i}} + M_{s_{2i}}$$

Finally the capillary pressure ( $h_c$ ) is computed:

$$h_c = \frac{2\sigma\cos\theta}{r_i} \quad [10]$$

$$\Delta\theta_{v_i}|_{Arya\ Model} = \theta_{v_i}|_{biochar-reference\ soil} - \theta_{v_i}|_{reference\ soil} \quad [11]$$

At  $pF \approx 1.0$ ,

1)

$$\begin{aligned} \Delta\theta_{v_i}|_{Arya\ Model} &= \theta_{v_i}|_{biochar-reference\ soil} - \theta_{v_i}|_{reference\ soil} \\ &= (\Phi S_w) \sum_{j=1}^i V_i \end{aligned}$$

$\Phi S_w$  = measured volumetric water content at  $pF \approx 1$  = change or increase in total adsorbed water because of biochar addition to sample

2) For the largest sieve,  $\sum_{j=1}^i V_i = 1.0$

a. Arya model for the reference soil:

$$\theta_{v_i}|_{reference\ soil} = (\Phi S_w) * 1.0$$

b. Arya model for the biochar-amended reference soil:

$$\theta_{v_i}|_{biochar-reference\ soil} = (\Phi S_w) * 1.0$$

- 3) If this approach is followed, the model should fit data at  $\text{pF} \approx 1$  almost perfectly for  $\theta_{wai}$

## B-6 SWRC Model

Model 1

$$\theta_{w_i} = \theta_{w_i}|_{ref\ soil}$$

Model 2

$$\theta_{w_i} = \theta_{w_i}|_{ref\ soil} + \frac{\Delta Adsorbed\ water_i}{V_t}$$

Model 3

$$\theta_{w_i} = \theta_{w_i}|_{ref\ soil} + \frac{intraparticle\ PV_i}{V_t} + \frac{\Delta Adsorbed\ water_i}{V_t}$$

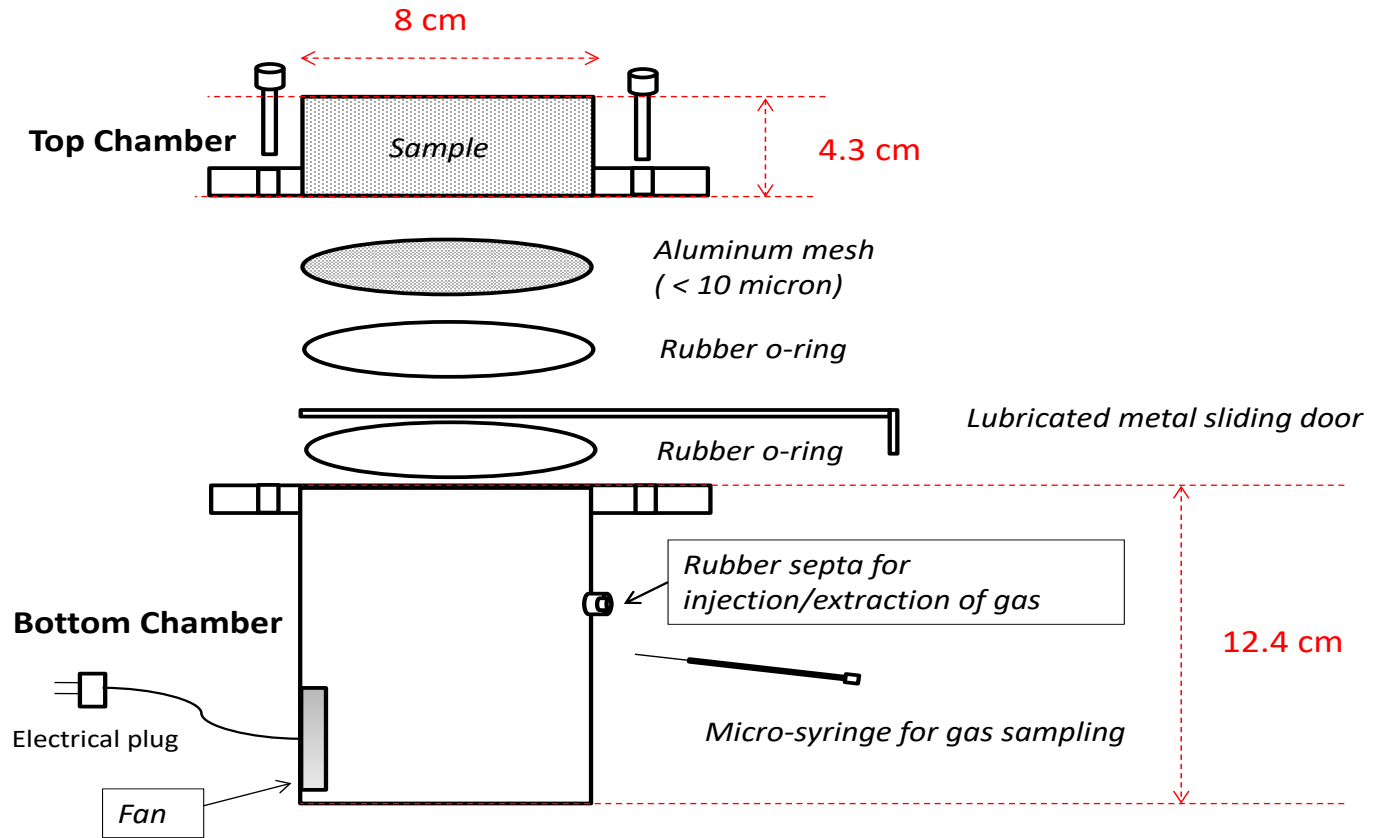
Model 4

$$\theta_{w_i} = \theta_{w_i}|_{ref\ soil} + \Delta\theta_{v_i}|_{Arya\ Model} + \frac{intraparticle\ PV_i}{V_t} + \frac{\Delta Adsorbed\ water_i}{V_t}$$

**APPENDIX C:**

**THE EFFECTS OF BIOCHAR ON GAS TRANSPORT IN VARIABLY  
SATURATED SAND AND SANDY LOAM SOIL**

C-1 Schematic of diffusion apparatus



171

Figure C1: Schematic of diffusion apparatus

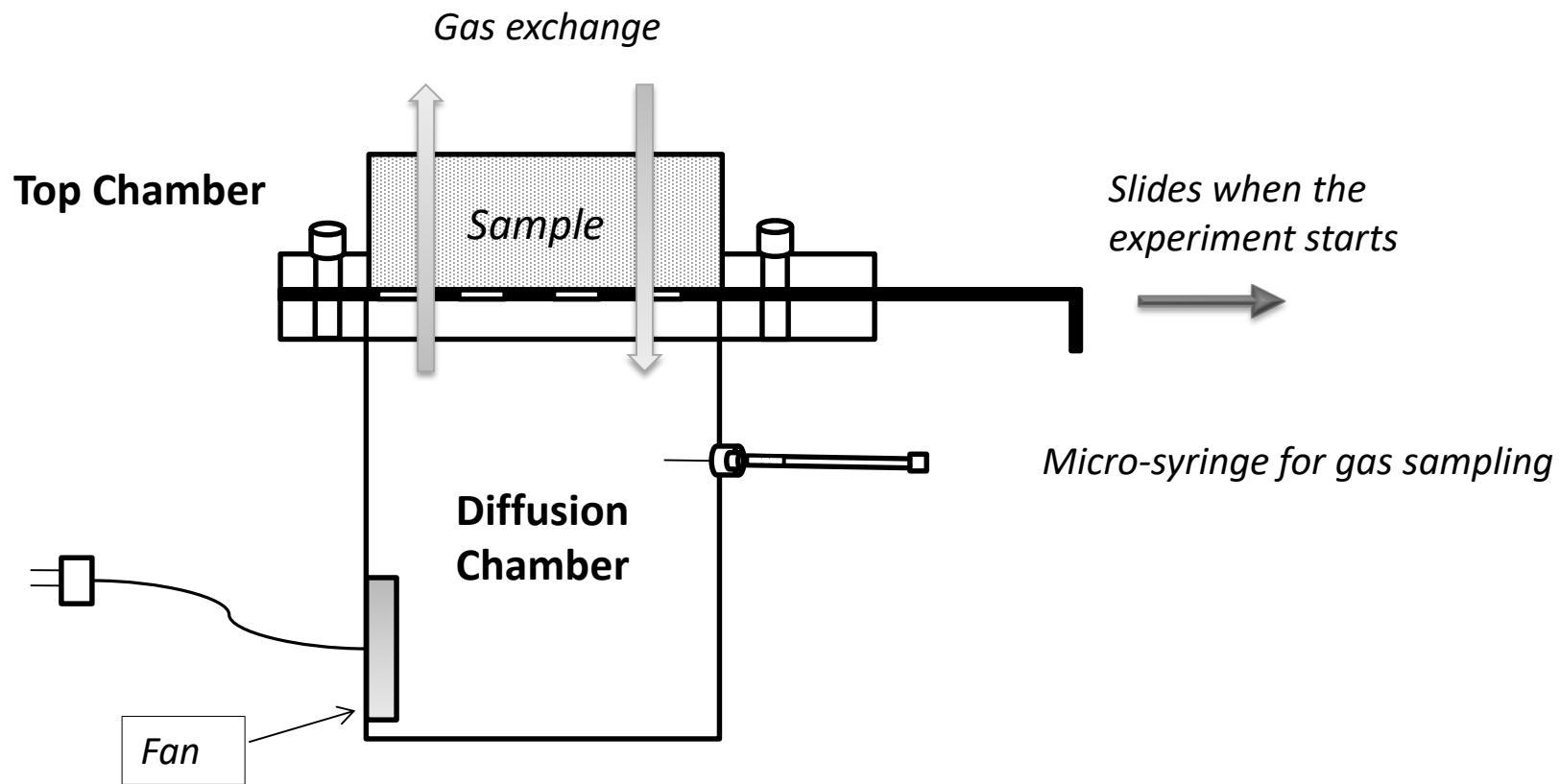


Figure C2: Schematic of diffusion apparatus intact

### C-2 Schematic of air permeability apparatus

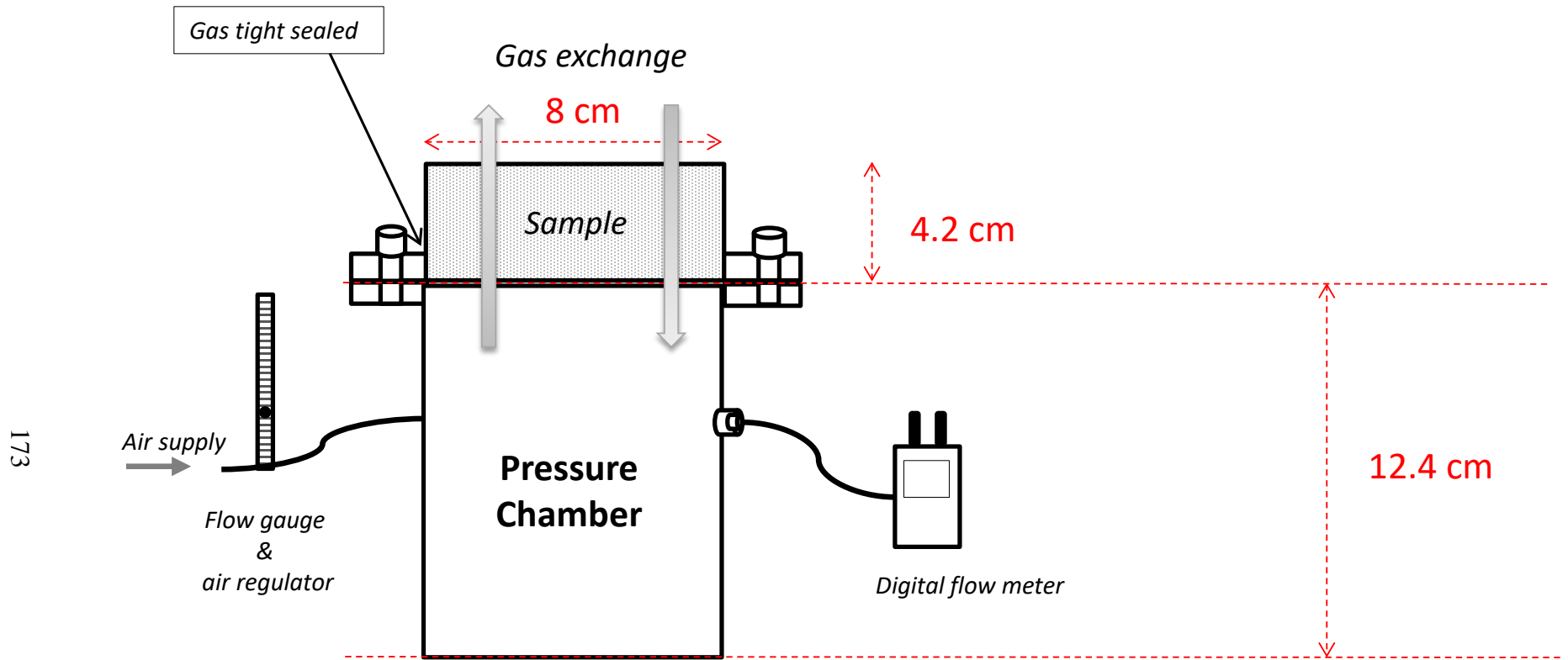


Figure C3: Schematic of air permeability apparatus intact

### C-3 Photographs of biochars

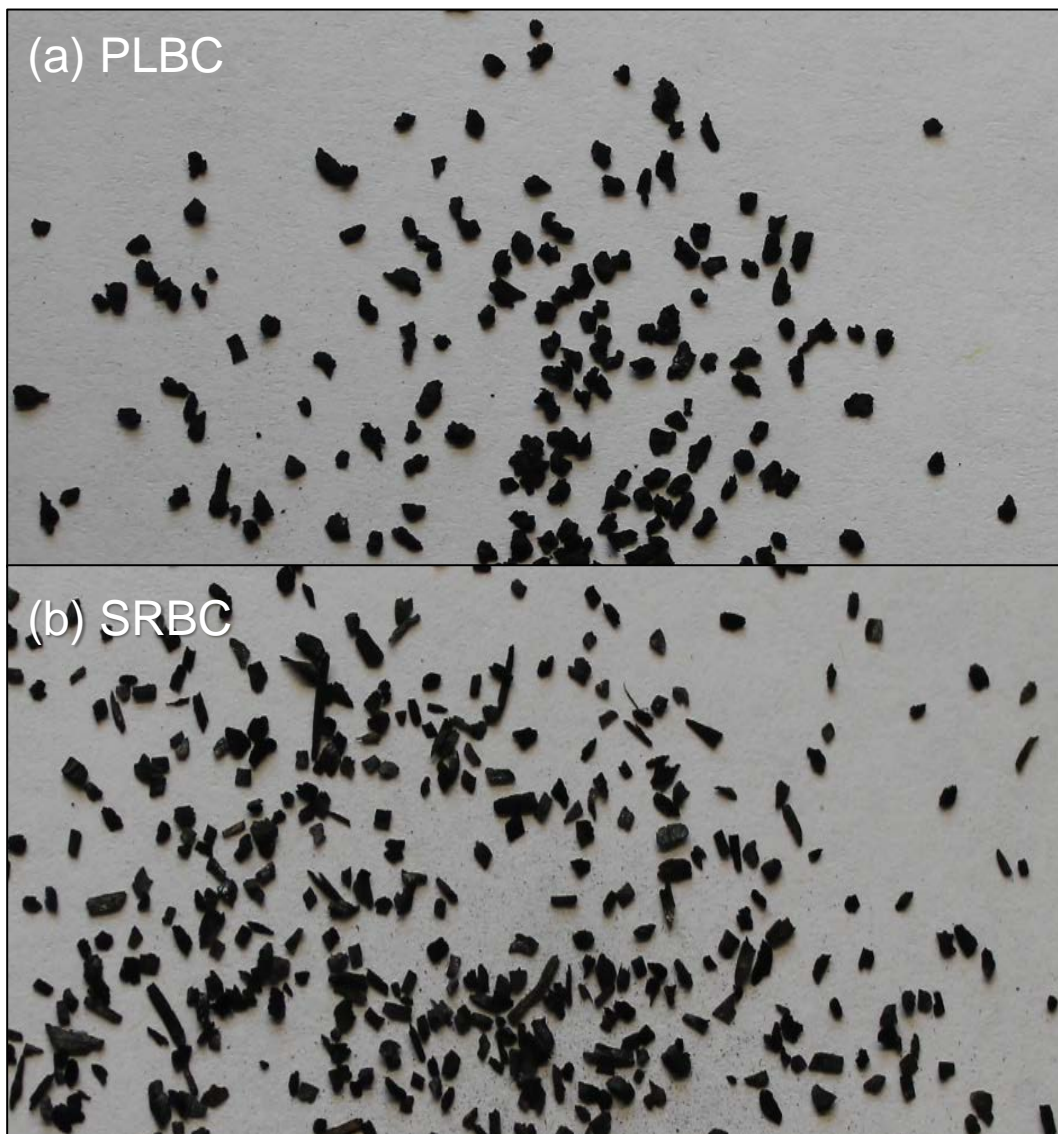


Figure C4: Photographs of rinsed and sieved biochars where (a) is poultry litter biochar (PLBC) and (b) is Soil Reef biochar (SRBC)

**APPENDIX D:**

**PERMISSIONS**

**American Society of Agronomy Inc. LICENSE  
TERMS AND CONDITIONS**

May 06, 2018

---

This is a License Agreement between Susan Yi ("You") and American Society of Agronomy Inc. ("American Society of Agronomy Inc.") provided by Copyright Clearance Center ("CCC"). The license consists of your order details, the terms and conditions provided by American Society of Agronomy Inc., and the payment terms and conditions.

**All payments must be made in full to CCC. For payment instructions, please see information listed at the bottom of this form.**

License Number	4343161381278
License date	May 06, 2018
Licensed content publisher	American Society of Agronomy Inc.
Licensed content title	Journal of environmental quality
Licensed content date	Jan 1, 1972
Type of Use	Thesis/Dissertation
Requestor type	Academic institution
Format	Print, Electronic
Portion	chapter/article
The requesting person/organization is:	Susan Yi/University of Delaware
Title or numeric reference of the portion(s)	Chapter 2
Title of the article or chapter the portion is from	The Origin and Reversible Nature of Poultry Litter Biochar Hydrophobicity
Editor of portion(s)	N/A
Author of portion(s)	Susan Yi
Volume of serial or monograph.	Vol. 44 No. 3, p. 963-971
Page range of the portion	
Publication date of portion	April 27, 2015
Rights for	Main product
Duration of use	Current edition and up to 5 years

---

---

Creation of copies for the disabled	yes
With minor editing privileges	no
For distribution to	United States
In the following language(s)	Original language of publication
With incidental promotional use	no
The lifetime unit quantity of new product	Up to 499
Title	The Origin and Reversible Nature of Poultry Litter Biochar Hydrophobicity
Instructor name	Paul T. Imhoff
Institution name	University of Delaware
Expected presentation date	May 2018
Billing Type	Credit Card
Credit card info	Visa ending in 0203
Credit card expiration	06/2018
Total (may include CCC user fee)	183.50 USD
Terms and Conditions	

---

## TERMS AND CONDITIONS

The following terms are individual to this publisher:

None

### Other Terms and Conditions:

#### STANDARD TERMS AND CONDITIONS

1. Description of Service; Defined Terms. This Republication License enables the User to obtain licenses for republication of one or more copyrighted works as described in detail on the relevant Order Confirmation (the "Work(s)"). Copyright Clearance Center, Inc. ("CCC") grants licenses through the Service on behalf of the rightsholder identified on the Order Confirmation (the "Rightsholder"). "Republication", as used herein, generally means the inclusion of a Work, in whole or in part, in a new work or works, also as described on the Order Confirmation. "User", as used herein, means the person or entity making such republication.

2. The terms set forth in the relevant Order Confirmation, and any terms set by the Rightsholder with respect to a particular Work, govern the terms of use of Works in connection with the Service. By using the Service, the person transacting for a republication license on behalf of the User represents and warrants that he/she/it (a) has been duly authorized by the User to accept, and hereby does accept, all such terms and conditions on behalf of User, and (b) shall inform User of all such terms and conditions. In the event such person is a "freelancer" or other third party independent of User and CCC, such party shall be deemed jointly a "User" for purposes of these terms and conditions. In any event, User shall be deemed to have accepted and agreed to all such terms and conditions if User republishes the Work in any fashion.

#### 3. Scope of License; Limitations and Obligations.

3.1 All Works and all rights therein, including copyright rights, remain the sole and exclusive property of the Rightsholder. The license created by the exchange of an Order Confirmation (and/or any invoice) and payment by User of the full amount set forth on that document includes only those rights expressly set forth in the Order Confirmation and in these terms and conditions, and conveys no other rights in the Work(s) to User. All rights not expressly granted are hereby reserved.

3.2 General Payment Terms: You may pay by credit card or through an account with us payable at the end of the month. If you and we agree that you may establish a standing account with CCC, then the following terms apply: Remit Payment to: Copyright Clearance Center, 29118 Network Place, Chicago, IL 60673-1291. Payments Due: Invoices are payable upon their delivery to you (or upon our notice to you that they are available to you for downloading). After 30 days, outstanding amounts will be subject to a service charge of 1-1/2% per month or, if less, the maximum rate allowed by applicable law. Unless otherwise

specifically set forth in the Order Confirmation or in a separate written agreement signed by CCC, invoices are due and payable on “net 30” terms. While User may exercise the rights licensed immediately upon issuance of the Order Confirmation, the license is automatically revoked and is null and void, as if it had never been issued, if complete payment for the license is not received on a timely basis either from User directly or through a payment agent, such as a credit card company.

3.3 Unless otherwise provided in the Order Confirmation, any grant of rights to User (i) is “one-time” (including the editions and product family specified in the license), (ii) is non-exclusive and non-transferable and (iii) is subject to any and all limitations and restrictions (such as, but not limited to, limitations on duration of use or circulation) included in the Order Confirmation or invoice and/or in these terms and conditions. Upon completion of the licensed use, User shall either secure a new permission for further use of the Work(s) or immediately cease any new use of the Work(s) and shall render inaccessible (such as by deleting or by removing or severing links or other locators) any further copies of the Work (except for copies printed on paper in accordance with this license and still in User's stock at the end of such period).

3.4 In the event that the material for which a republication license is sought includes third party materials (such as photographs, illustrations, graphs, inserts and similar materials) which are identified in such material as having been used by permission, User is responsible for identifying, and seeking separate licenses (under this Service or otherwise) for, any of such third party materials; without a separate license, such third party materials may not be used.

3.5 Use of proper copyright notice for a Work is required as a condition of any license granted under the Service. Unless otherwise provided in the Order Confirmation, a proper copyright notice will read substantially as follows: “Republished with permission of [Rightsholder’s name], from [Work's title, author, volume, edition number and year of copyright]; permission conveyed through Copyright Clearance Center, Inc. ” Such notice must be provided in a reasonably legible font size and must be placed either immediately adjacent to the Work as

used (for example, as part of a by-line or footnote but not as a separate electronic link) or in the place where substantially all other credits or notices for the new work containing the republished Work are located. Failure to include the required notice results in loss to the Rightsholder and CCC, and the User shall be liable to pay liquidated damages for each such failure equal to twice the use fee specified in the Order Confirmation, in addition to the use fee itself and any other fees and charges specified.

3.6 User may only make alterations to the Work if and as expressly set forth in the Order Confirmation. No Work may be used in any way that is defamatory, violates the rights of third parties (including such third parties' rights of copyright, privacy, publicity, or other tangible or intangible property), or is otherwise illegal, sexually explicit or obscene. In addition, User may not conjoin a Work with any other material that may result in damage to the reputation of the Rightsholder. User agrees to inform CCC if it becomes aware of any infringement of any rights in a Work and to cooperate with any reasonable request of CCC or the Rightsholder in connection therewith.

4. Indemnity. User hereby indemnifies and agrees to defend the Rightsholder and CCC, and their respective employees and directors, against all claims, liability, damages, costs and expenses, including legal fees and expenses, arising out of any use of a Work beyond the scope of the rights granted herein, or any use of a Work which has been altered in any unauthorized way by User, including claims of defamation or infringement of rights of copyright, publicity, privacy or other tangible or intangible property.

5. Limitation of Liability. UNDER NO CIRCUMSTANCES WILL CCC OR THE RIGHTSHOLDER BE LIABLE FOR ANY DIRECT, INDIRECT, CONSEQUENTIAL OR INCIDENTAL DAMAGES (INCLUDING WITHOUT LIMITATION DAMAGES FOR LOSS OF BUSINESS PROFITS OR INFORMATION, OR FOR BUSINESS INTERRUPTION) ARISING OUT OF THE USE OR INABILITY TO USE A WORK, EVEN IF ONE OF THEM HAS BEEN ADVISED OF THE POSSIBILITY OF SUCH DAMAGES. In any event, the total liability of the Rightsholder and CCC (including their respective employees and directors) shall not exceed the total amount actually paid by User for this license. User assumes full liability for the actions and omissions of its principals, employees, agents, affiliates, successors and assigns.

6. Limited Warranties. THE WORK(S) AND RIGHT(S) ARE PROVIDED "AS IS". CCC HAS THE RIGHT TO GRANT TO USER THE RIGHTS GRANTED IN THE ORDER CONFIRMATION DOCUMENT. CCC AND THE RIGHTSHOLDER DISCLAIM ALL OTHER WARRANTIES RELATING TO THE WORK(S) AND RIGHT(S), EITHER EXPRESS OR IMPLIED, INCLUDING WITHOUT LIMITATION IMPLIED WARRANTIES OF MERCHANTABILITY OR FITNESS FOR A PARTICULAR PURPOSE. ADDITIONAL

ABSTRACTS, INSERTS OR OTHER PORTIONS OF THE WORK (AS OPPOSED TO THE ENTIRE WORK) IN A MANNER CONTEMPLATED BY USER; USER UNDERSTANDS AND AGREES THAT NEITHER CCC NOR THE RIGHTSHOLDER MAY HAVE SUCH ADDITIONAL RIGHTS TO GRANT.

7. Effect of Breach. Any failure by User to pay any amount when due, or any use by User of a Work beyond the scope of the license set forth in the Order Confirmation and/or these terms and conditions, shall be a material breach of the license created by the Order Confirmation and these terms and conditions. Any breach not cured within 30 days of written notice thereof shall result in immediate termination of such license without further notice. Any unauthorized (but licensable) use of a Work that is terminated immediately upon notice thereof may be liquidated by payment of the Rightsholder's ordinary license price therefor; any unauthorized (and unlicensable) use that is not terminated immediately for any reason (including, for example, because materials containing the Work cannot reasonably be recalled) will be subject to all remedies available at law or in equity, but in no event to a payment of less than three times the Rightsholder's ordinary license price for the most closely analogous licensable use plus Rightsholder's and/or CCC's costs and expenses incurred in collecting such payment.

#### 8. Miscellaneous.

8.1 User acknowledges that CCC may, from time to time, make changes or additions to the Service or to these terms and conditions, and CCC reserves the right to send notice to the User by electronic mail or otherwise for the purposes of notifying User of such changes or additions; provided that any such changes or additions shall not apply to permissions already secured and paid for.

8.2 Use of User-related information collected through the Service is governed by CCC's privacy policy, available online here:

<http://www.copyright.com/content/cc3/en/tools/footer/privacypolicy.html>

8.3 The licensing transaction described in the Order Confirmation is personal to User. Therefore, User may not assign or transfer to any other person (whether a natural person or an organization of any kind) the license created by the Order Confirmation and these terms and conditions or any rights granted hereunder; provided, however, that User may assign such license in its entirety on written notice to CCC in the event of a transfer of all or substantially all of User's rights in the new material which includes the Work(s) licensed under this Service.

8.4 No amendment or waiver of any terms is binding unless set forth in writing and signed by the parties. The Rightsholder and CCC hereby object to any terms contained in any writing prepared by the User or its principals, employees, agents or affiliates and purporting to govern or otherwise relate to the licensing transaction described in the Order Confirmation, which terms are in any way inconsistent with any terms set forth in the Order Confirmation and/or in these terms and conditions or CCC's standard operating procedures, whether such writing is

prepared prior to, simultaneously with or subsequent to the Order Confirmation, and whether such writing appears on a copy of the Order Confirmation or in a separate instrument.

8.5 The licensing transaction described in the Order Confirmation document shall be governed by and construed under the law of the State of New York, USA, without regard to the principles thereof of conflicts of law. Any case, controversy, suit, action, or proceeding arising out of, in connection with, or related to such licensing transaction shall be brought, at CCC's sole discretion, in any federal or state court located in the County of New York, State of New York, USA, or in any federal or state court whose geographical jurisdiction covers the location of the Rightsholder set forth in the Order Confirmation. The parties expressly submit to the personal jurisdiction and venue of each such federal or state court. If you have any comments or questions about the Service or Copyright Clearance Center, please contact us at 978-750-8400 or send an e-mail to [info@copyright.com](mailto:info@copyright.com).

v 1.1

**Questions? [customer care@copyright.com](mailto:customer care@copyright.com) or +1-855-239-3415 (toll free in the US) or +1-978-646-2777.**